NASA Contractor Report 3491

A Study of Flight Control Requirements for Advanced, Winged, Earth-to-Orbit Vehicles With Far-Aft Center-of-Gravity Locations

Andrew K. Hepler, Howard Zeck,
William H. Walker, and Alexander Polack

NASA

NASA Contractor Report 3491

A Study of Flight Control Requirements for Advanced, Winged, Earth-to-Orbit Vehicles With Far-Aft Center-of-Gravity Locations

Andrew K. Hepler, Howard Zeck,
William H. Walker, and Alexander Polack
Boeing Aerospace Company
Kent, Washington

N/\S/

National Aeronautics
and Space Administration

Scientific and Technical
Information Branch

1982

CONTENTS .

SUMMARY

Recent studies of advanced space transportation vehicles have indicated potential cost/performance benefits of using a control configured vehicle (CCV) design approach for the vertical-take-off (VTO) single-stage-to-orbit (SSTO) concept. The present study is a follow-on of the original (Ref. 1) CCV study which identified a critical stability and control problem for aft center-of-gravity locations that are a characteristic of this class of vehicles.

A baseline CCV configuration, derived from the original study, was selected to determine and evaluate aerodynamic stability and control characteristics. Evaluations were made to determine dynamic stability boundaries, time responses, trim control, operational center-of-gravity limits, and flight control subsystem design requirements. The analyses included: ascent course error and gimbal requirements with winds, gust analysis, aerodynamic configuration trade-offs, landing approach analysis with conventional and wing tip fin controllers comparisons, and the effect of vehicle size with large increases in payload on flight control characteristics. Based on the study results, a brief technical assessment was made to identify critical technologies pertinent to CCV designs and to outline types of programs required to develop these technologies.

SYMBOLS

a	Speed of Sound
A. C.	Aerodynamic Center, Measured from Nose Reference
a_z	Normal Acceleration
b	Wing Span
CCV	Control Configured Vehicle
C. P.	Center of Pressure, Measured from Nose Reference
C_{L_α}	Slope of Lift Coefficient
C_L	Lift Coefficient
C. G.	Center of Gravity, Measured from Nose Reference
EASY	Flight Control Dynamic Analysis Program
GLOW	Gross Lift-Off Weight
I	Moment of Inertia

SYMBOLS

L_B	Reference Body Length
L_V	Vertical Tail Moment Arm
M	Mach Number, V/a
P	Roll Rate
q	Dynamic Pressure
RSI	Reusable Surface Insulator
S	Complex Frequency
S_{REF}	Reference Wing Area
S_T	Vertical Tail Area
T	Thrust
TPS	Thermo Protection System
V	Velocity
$\overline{V}$	Tail Volume Coefficient, $L_T S_T/b S_{REF}$
α	Angle of Attack
$\triangle\alpha$	Pitch Angle Increment
β	Angle of Sideslip
δ	Control Surface Deflection
$\triangle\phi$	Roll Angle Increment
ρ	Atmospheric Density
σ	Real Part of Complex Frequency
$j\omega$	Imaginary Part of Complex Frequency

Subscripts:

A	Aileron
R	Rudder
e	Elevon
BF	Body Flap

2

INTRODUCTION

The background for this study is contained in References 1, 2, 3, and 4 in which the technique of control configured vehicle design approach is applied to VTO single-stage-to-orbit configurations. Supported by other in-house NASA studies, a continuing problem for these types of vehicles is the far-aft center-of-gravity (C. G.) locations. Aft C. G. locations, in general, degrade the static stability characteristics and could result in an uncontrollable vehicle. The basic contributor to an aft C. G. location is the large amount of rocket engines at the rear of the body that are required for lift-off of the VTO vehicle. Thus, the main purpose of this study is to examine the design and flight control problems of CCV configurations with far-aft C. G. locations and to define plausible solutions. Specific objectives include:

- Analyses of the characteristics of a (CCV) baseline configuration supplied by NASA to identify critical stability and control problems.

- Determination of flight control characteristics and trade-offs for the baseline configuration in both ascent and entry modes as functions of C. G. variations and vehicle size.

- Assessment of critical technologies applicable to enhance VTO CCV designs.

The scope of this study included the necessary engineering studies, analyses, trade-offs, special investigations, and planning to accomplish the objectives of this study consistent with the guidelines and constraints. Midway through the study additional funds were made available to analyze in more detail the flight control characteristics during the approach and landing phase of the entry flight profile (nominally referred to as the "add-on" study). The add-on analysis has been integrated with the main body of the study.

VEHICLE DESCRIPTION

Baseline (CCV) vehicle characteristics were supplied by NASA for the flight control analysis studies. These characteristics were based on the Mod I configuration of the original CCV study (Ref. 1) with minor updates. The vehicle is basically a VTO configuration with a relatively high entry planform loading. The reference wing area is 557.4 square meters (6000 ft^2) with an overall reference

body length of 66.8 meters (219.2 ft.). A schematic layout of the baseline configuration is shown in Figure 1. The LH_2/LO_2 rocket main engines consist of three fixed expansion engines inboard and three two position nozzle engines outboard at the aft end of the body. Locations of the LH_2 and LO_2 propellant tanks and other main subsystems are also indicated in Figure 1. An alternate configuration utilizing small wing tip fins in place of the baseline vertical tail (Figure 2 and Reference 4) was also investigated in some depth to determine its flight control characteristics. More structural details of the baseline tip fins are given in Figure 3. A proposed growth tip fin (twice the area as shown in Figure 4) was also briefly studied.

STUDY APPROACH

The general approach for this study was similar to that used in the first CCV study, Reference 1. The baseline configuration (supplied by NASA) essentially was the Mod I configuration of Reference 1 with updated mass properties and moments of inertia. Additional wind-tunnel test data of this baseline configuration was also supplied by NASA for use in the aerodynamic and flight control analyses of this study. For the flight control investigations, five fixed design points were selected for analysis and determination of their stability and time trajectory range from hypersonic to subsonic speeds. (See Figure 2.) This design point approach allows detailed insights of flight control stability properties at various points along the entry trajectory which are essential before a complete entry 6D simulation is undertaken. An analysis of the ascent mode utilizing rocket engine gimbaling for control and course heading error corrections because of wind shears was also briefly studied. Additional studies of the flight control dynamics during the approach and landing phase were also performed as an "add on" to the scope of the original study contract.

Study Guidelines

Vehicle Definition.-The baseline configuration supplied by NASA is a vertical-take-off (VTO), horizontal-landing, single-stage-to-orbit (SSTO) vehicle.

4

Mission Requirements.-The payload is 29,500 kg (65,000 lb) delivered to a 185 km (100 n.m.) orbit. The entry flight profile included a 1853 km (1100 n.m.) cross range (supplied by NASA). The payload bay size is 4.6 X 18.3 m (15 X 60 ft).

Landing Conditions.-Landing speed should not exceed 85 m/sec (165 knots) at an angle of attack no greater than 15 degrees.

Vehicle Center of Gravity (C. G.).-Baseline value is 0.715 of body length.

Longitudinal Control Limits.-Total elevon deflection is limited to -40 to 20 degrees. (Note: Aerodynamic heating and TPS requirements could further limit these deflections.)

TPS Limits.-During the course of the study, NASA specified a TPS temperature limit for repeated use of 1812 K (2800°F).

Lateral-Directional Stability and Control.-The baseline configuration with a conventional centerline vertical tail and an alternate configuration with a tip fin controller are to be investigated and compared for their flight control characteristics.

Fixed Design Points (Selected for Flight Control Analyses).-

Design Point	Mach	Altitude km	Angle of Attack Deg
1	0.3	Sea Level	12
2	0.6	9.5	10
3	1.2	15.8	7
4	3.5	30.5	12
5	8.0	52.6	36

The first Task (I) was to analyze the baseline configuration in sufficient detail to identify critical stability and control problems and to emphasize the overall vehicle system aspects (i.e., flight control, aerodynamics, heating and subsystems) for determining operational center-of-gravity and control limits. This was accomplished by "6D" flight control simulations, aerodynamic assessments, subsystem trades, and control system design investigations.

Upon completion of this phase of the study, Task II was identified as an aft C. G. study in which the baseline C. G. was moved aft to the Task I operational limit and further investigated. The impacts of the aft C. G. on requirements for very large control surface deflections and rates and subsequent hardware subsystems requirements was assessed, and total actuator weights were estimated and compared to the baseline vehicle. Also, for Task II, an alternate configuration with the baseline vertical tail replaced by a pair of small tip fin control effectors on the wing was investigated at the various flight control design points. Finally, for the Task II configuration, changes were proposed to extend the aft C. G. hypersonic trim limits.

Task III was called a payload size study in which the effects of large increases in vehicle mass and moments of inertia on flight control responses and subsystem design were assessed for potential problems and design requirements.

Task IV identified technology improvements needed to enable operation of SSTO vehicles at aft C. G. locations. Critical technologies were identified along with suggested development programs.

RESULTS AND DISCUSSION

The general format for discussing the study results is along technical discipline lines of aerodynamics, flight control, configuration structural design and subsystems. The section concludes with summary configuration trades and comparisons followed by the Task IV technology assessment.

Aerodynamics and Performance

Aerodynamic characteristics are based upon wind-tunnel test data (unpublished NASA test data) of the baseline CCV configuration. Where additional test data did not exist on elevon and body flap control effectiveness, estimates were made using combinations of in-house, Shuttle, and DATCOM analysis techniques. A representative set of aerodynamic data used for the various five design points is presented in Appendix A.

The aerodynamic analyses include: subsonic stability, trim, and landing speeds; hypersonic trim; operational C. G. limits; and aerodynamic configuration trade-offs.

Subsonic Aerodynamics.-The variation of trimmed angle of attack with subsonic speed is presented in Figure 5 for the indicated landing weight. For Design Point 1, a Mach Number of 0.3 is used which results in a level flight trimmed angle of attack of 12.5 degrees. At this angle of attack, the trimmed lift coefficient is 0.59 for a C. G. location of 0.715 body length (See Figure 6.) This plot shows that the baseline configuration has the capability of performing a maximum pull-up of only 1.25 g's at an angle of attack of 20 degrees. This is somewhat below the originally desired value of 1.5 g's. The original configuration (Mod I of Reference 1) had this capability with a subsonically deployed canard surface which was removed for the current baseline configuration. Thus, for Design Point 1 flight control analysis, the normal acceleration maneuver commands were reduced from 1.5 g's to 1.15 g's. As a Reference, the nominal shuttle landing flares use 1.5 to 1.2 g's. The main implication of the reduced normal g's is a greater loss in altitude during the flare maneuver (which is undesirable but not critical). Subsonic pitching moments for the baseline configuration are given in Figure 7.

Transonic Aerodynamics.-Flight control analysis of Design Point III (i.e., M = 1.2) required extrapolated/additional aerodynamic control effectiveness input data beyond the available wind tunnel test data of the baseline configuration. The effects of the elevon deflections (both measured and extrapolated) on the pitching-moment coefficient are compared with shuttle values in Figure 8. Control effectiveness significantly decreases for up elevon deflections beyond deflection angles of -20 degrees.

As part of the analysis to determine the operational C. G. limits, additional body flap up deflection characteristics had to be estimated as shown in Figure 9. (See Appendix A, Figure 98 for additional data.)

Hypersonic Aerodynamics.-Wind-tunnel data at a Mach Number of 20 was available for various elevon and body flap deflections. The pitching-moment data were referenced to a point 0.715 of body length for the baseline configuration. To obtain data at other C. G. locations and control deflections, estimates were made using an in-house computer program called "Hyperez". The good agreement of computed values with test data is illustrated in Figure 10. This program was also used for the aerodynamic configuration trade-offs. From the computer results, the trim characteristics over the usable hypersonic angle-of-attack range were

determined as shown in Figure 11. The selected values for elevon and body flap deflections were based upon the aerodynamic heating analysis limits for TPS utilizing RSI (presented in following section). With down elevons limited to 10 degrees, the aft C. G. is about 0.725 of body length as indicated in Figure 12.

Aerodynamic Heating.-Brief aerothermal analyses were made to estimate equilibrium temperatures for the elevon and body flap control surfaces (also, later for tip fin studies). RSI was selected for the control surface TPS. In concurrence with NASA, a maximum reuse temperature of 1812 K (2800°F) was assumed. This resulted in limits of down deflections of 10 degrees for the elevon and 14 degrees for the body flap as shown in Figure 12.

Operational C. G. Limits.-Initially, an entry profile was supplied by NASA for input trim and control deflections to assist in determining operational C. G. limits. However, with these values no range of C. G. travel was possible for the baseline configuration. (See Figure 13.) The problem area was the forward C. G. limit with up elevons. A maximum up deflection limit of -20 was selected to allow for control maneuvers and gust allowances. To open the forward C. G. limit, control surface/alpha/C. G., tradeoffs were determined as shown in Figure 14. By selecting a lower angle of attack of 7 deg and an increased up body flap deflection of -14 deg, the C. G. was moved forward from 0.745 to 0.715 of body length. With these new control deflection values, the final operational C. G. limits were established from 0.715 to 0.725 of body length for the baseline configuration (Figure 15). This allowable C. G. travel was marginal, and further configuration tradeoffs were made to improve the C. G. range. By drooping the nose of the body and adding a transonic canard surface (similar to the subsonic canard of Reference 1), the operational C. G. travel and range was very favorably moved to between 0.73 and 0.76 of body length (Fig. 16). The effect of these configuration changes on landing speed are shown in Figure 24. Further trade-offs are given in the next section.

Configuration Trade-Offs.-Since it became evident that the aerodynamic configuration was the principal parameter in establishing operational C. G. Limits, a series of configuration trade-offs were investigated. The trade-offs were analyzed at hypersonic speeds for pitch trim and subsonic speeds for directional stability. A schematic and definition of the body configuration trades and, qualitatively, their relative hypersonic C. P. trends are shown in Figure 17. A ground rule for these trades was to keep the overall body volume approximately constant (i.e.,

equal to the baseline configuration) for each parametric body change. The actual hypersonic trade-offs shown in Figure 18 illustrate the prime importance of nose camber on establishing the configuration center-of-pressure (C. P.) location. These trade-offs support the final summary results presented near the end of this study report.

Directional Stability.-Variations of static directional stability (i.e., Cn_β) with Mach Number are presented in Figure 19 for both the vertical tail on and off and the tip fins on. For comparison, the tail-on Shuttle characteristics are also shown. The CCV configurations are statically unstable throughout the entire speed range. Figure 20 is presented to size the tails subsonically by the use of a tail volume coefficient (as defined in Figure 20). This plot also illustrates, because of the aft C. G., how much more unstable the CCV configurations are relative to the Shuttle configuration. Notice, the Shuttle with small tip fins is not as unstable as the CCV baseline with a relatively large vertical tail. The CCV configuration with tip fins is unstable, and the fins adversely affect crosswind landing characteristics discussed in later sections.

Crosswind Landing Approach.-As a prologue to the flight control approach dynamic analysis, a static trim control analysis in crosswind approaches provides some insights to potential problem areas. The control deflections required to trim in crosswinds is presented in Figure 21 for both the baseline vertical tail and tip fins. The vehicle is allowed to crab into the wind 4 degrees for increased capability (i.e., landing gears usually have a designed in allowable for this angle). For 10.3 m/sec (20 knots) of crosswind, the rudder for the vertical tail has to deflect only a few degrees, whereas the tip fin deflections are greater than 50 degrees. Figure 22 shows the increase in control surface areas required to reduce the tip fin deflections to reasonable values (i.e., less than 40 degrees) for a 10.8 m/sec (21-knot) crosswind. These high deflections for the tip fins also show up unfavorably for the dynamic crosswind analysis results presented in later paragraphs.

Trade-Offs Summary.-Most of the body configuration alternatives affected both the hypersonic trim and subsonic directional stability parameters. As illustrated in Figure 23, some of the body alternatives result in a definite interplay on both parameters, whereas other body variations affect only one parameter. An objective of these trade-offs is to move the subsonic Cn_β and hypersonic trimmed C. P. to the desired regions indicated (i.e., subsonic neutral static directional stability

9

and hypersonic trim for a C. G. location back to 0.75 of body length). No single
configuration change seems to accomplish this objective. For example, a high
and narrow (required for constant body volume) body relative to the baseline con-
figuration favorably moves the hypersonic trim aft but significantly makes the
body much more directionally unstable at subsonic speeds. The size of the tail
surface to counter this instability would have to more than double as indicated
in the accompanying plot utilizing tail volume coefficient.

In addition to these aspects of the trade-offs, the impact of some of the
configuration alternates on landing speed is summarized in Figure 24. Aft C. G.
locations require down elevons for trim which result in the reduction in landing
speeds. The alternate shown is a configuration with increased nose droop.

In summary, a strategy to obtain the desired values of the above stability
and trim parameters could be to alter the body shape as follows:

. Round the bottom for nose forward of wing
. Shorten and widen body planform
. Increase nose droop

Payload Scaling.-The impact of larger payloads (i.e., larger vehicle sizes)
on the C. G./stability and control problems was briefly assessed. The baseline
vehicle was generically scaled to have the capability of injecting payloads of
80 and 160 metric tons into low Earth orbit. It is noted that the objective of
this effort was not to determine mass properties of the vehicle system but simply
to identify any unique aerodynamic/flight control characteristics or problems
that result from a large scale-up of the baseline vehicle size and payload. In
accomplishing the scaling, the following parameters were held approximately
constant:

. Landing speed   . Liftoff thrust/GLOW
. Ascent/entry trajectory   . Payload density
. Aerodynamic configuration   . Structural concept

To satisfy the landing speed and trajectory requires that the wing loading
(weight/reference area) remains constant. Dimensional scaling analysis involves
the square-cube relationship and results in a larger wing planform relative to
the body planform.

The overall scaling of the baseline vehicle to larger payload mass was accomplished by the use of preliminary design techniques employing mass fraction (λ) data based upon past in-house experience of scaling booster vehicles. (See Figure 25.) Some of the basic performance relationships used are as follows:

(Ideal) $\Delta V = $ (Actual)$\Delta V + \Delta V_{Loss}$ ΔV = Velocity Increment

(Ideal) $\Delta V = g \, I_{Eff} \, L_n \left(\frac{1}{1-\zeta}\right)$, where I_{Eff} = Effective Specific Impulse

$PL/GLOW = (1 - \zeta/\lambda)$ ζ = Propellant Loading

$GLOW = WT_{PROP} + WT_{INERT} + PL$ $= $ Weight Propellant/GLOW

$$\lambda = \frac{\text{Weight Propellant}}{(Wt_{Prop} + Wt_{Inert})}$$

PL = Payload

GLOW = Gross Lift-Off Weight

Now, for fixed rocket engine characteristics (I_{SP}, thrust loading, etc.) and trajectory, the propellant loading (ζ) and ideal ΔV are approximately constant. This results in the PL/GLOW ratios then becoming mainly only a first-order function of the mass fraction (λ). Thus, by specifying a payload, the GLOW can be determined and, hence, the propellant weights. Volumes, areas and length of the body and wing of the scaled-up vehicles can then be determined, as shown in Figure 26. Moment of inertias were scaled using dimensional analysis with allowances for the changes in relative wing/body areas. These scaled vehicle geometric and weight characteristics were then analyzed to determine hypersonic trim and time-response characteristics.

Increasing the payload mass from 17 to 160 metric tons resulted in a very favorable movement of the hypersonic trim aft C. G. limits from 0.715 to 0.775 of body length. For a fixed C. G. location, the vehicle would trim for elevons deflected in an up direction with a subsequent reduction in elevon lower surface entry temperatures. This trend (See Figure 27) was a result of the relatively larger wing planform area compared to body planform area as the payload mass increased. The effects of payload mass on flight control time responses are presented in the following section.

Flight Control

Ascent Analysis.-An in-house "Ascent Wind Shear Loads Program" was used to perform the ascent flight simulations using simplified control system models shown in Figure 28. The program is intended primarily to determine vehicle loads and trajectory characteristics for the high dynamic pressure, high wind shear phase of ascent. A flat, nonrotating earth and open-loop guidance are used for this simulation. Inputs to the program included the variations in C. G. location and moments of inertia as propellant is expended during ascent. The estimated variations are given in Figure 29 (end points at lift-off and burnout were supplied by NASA).

The first 85 seconds of the flight were simulated, reaching an altitude of 20,000 km (66,000 ft.) at a Mach Number of 2.4. Maximum dynamic pressure occurred at 63 seconds. The pitch command was the pitch time history computed from a "3D Post" no wind flight simulation supplied by NASA. Time histories of flight parameters including altitude, velocity, dynamic pressure, Mach Number, Euler and flight path angles; TVC angles, load acceleration parameters, and hinge moments were determined for two control system representations. No wind, head wind, and crosswind simulations were run using ETR (Cape Kennedy) synthetic wind profiles based on 99 percent wind shears. The final control system employed a lateral acceleration feedback in the yaw plane with the addition of a low gain heading error feedback simulating the guidance loop.

Ascents through ten wind profiles were simulated to determine load parameters and trajectory dispersions during the critical early phases of flight. Heading errors in all cases were less than 8 degrees, decreasing to less than 4 degrees by the time a Mach Number of 2.4 was reached; and rocket engine gimbal angles in the yaw plane did not exceed 6 degrees (Figure 30). For yaw gimbaling, the outboard engine nozzles were used, and for pitch the inboard engines were used. Figure 31 summarizes the results for each wind profile in terms of maximum values of load parameters, flight-path-angle errors, and heading errors. These maximum values are the ascent design conditions since they would not have been exceeded if the simulation had been extended to higher speeds approaching orbital conditions.

Design Point Analysis of Baseline Configuration.-The flight control part of the study concentrated on several design configurations of a government-supplied baseline vehicle with relaxed static stability. The penalties for a far-aft center-of-gravity design that are associated with flight control dynamics can be related to the hinge moment and actuator-rate requirements generated by the unstable vehicle. These requirements determine the weight and size of the control surface actuators and the horsepower required of the hydraulic supply system.

During the early phase of the study, it was determined that five design points would be analyzed rather than the complete trajectory. These five design points covered the entire entry trajectory range from hypersonic Mach = 8.0 to subsonic Mach = 0.3 (See study guidelines and Figure 32.)

For each design point, longitudinal and lateral-directional autopilots were designed. In selecting the autopilot gains, the Shuttle response time-history envelopes were selected as a criterion. Several configuration size and C. G. location variations were examined. For each variation, the autopilot gains were tuned to produce transient responses to the maneuver commands that were as nearly identical (for normal acceleration or angle of attack and roll angle) as possible. A simultaneous pitch-up and roll was selected for the maneuver. The control surface deflections, rates, and hinge moments were recorded and compared with each other. Those data provided the basis for estimating actuation systems weight penalties for different variations.

Subsonic - The following mass properties and inertias have been used for all of the entry dynamic analyses:

$$I_{xx} = 9.33 \times 10^6 \text{ kg - m}^2$$

$$I_{yy} = 39.54 \times 10^6 \text{ kg - m}^2$$

$$I_{zz} = 43.47 \times 10^6 \text{ kg - m}^2$$

$$P_{xz} = 0.754 \times 10^6 \text{ kg - m}^2$$

Mass = 187,537 kg

Together with NASA supplied stability derivatives and coefficients, these properties result in vehicle dynamics that can be represented by the pole locations of the characteristic equations. These pole locations are shown in Figure 33 for pitch and yaw-roll.

The NASA-supplied baseline vehicle configuration, with the center of gravity at 71.5% L_B, has rather conventional stable short period and phugoid poles. Aft movement of the center-of-gravity location causes the short period poles to split into two real, stable poles. At the same time, the phugoid pair moves to the right of the j-axis, which results in slow divergent oscillations.

The poles of the yaw-roll motion showed interesting characteristics. Instead of the conventional complex pair representing dutch roll and two real roots that characterize the roll and spiral motion, they were replaced by two complex pairs. These are the so-called lateral "short-period" and "phugoid" cases. With lateral phugoid poles to the right of the j-axis, the vehicle's movement results in a slow divergent oscillation.

The pitch and yaw-roll autopilots are shown in Appendix B, Figure 105. The set of gains for the baseline configuration with a center-of-gravity location at 71.5% L_B is also shown. Root-locus and frequency-response techniques were used iteratively with simulations in order to arrive at this set of gains. Examples of the root-locus plotting and frequency-response (Nichol's) plots are shown in Figures 34 to 36.

Normal acceleration and roll responses for various center-of-gravity locations at a subsonic flight condition are shown in Figure 37. There is very little difference between the responses of the baseline configuration with the center of gravity at 71.5% L_B and 72.5% L_B. Further aft movement of the C. G. location to 73.5% L_B results in degradation of vehicle performance, especially in roll. At this aft C. G. location (73.5% L_B), the vehicle cannot hold a 30° roll angle for more then one second, since the rudder actuator saturates three seconds into the maneuver and the elevons are locked up at the end of the simulation. (See Figure 38.)

Transonic - Forms similar to the subsonic (M = 0.3) pitch and yaw-roll autopilots were used in transonic flight regime, with the major loop in the pitch autopilot closed around angle of attack. (See Block Diagrams in Figure 106.) Root-locus and frequency-response analyses were made in order to select a set of gains that gave good gain and phase margins and produced acceptable time responses.

The autopilots gains selected are:

Pitch:

$K_e = 1.0$, $K_q = 1.25$, $K_I = 1.0$

and

Yaw-Roll:

$K_r = 16$, $K_{y_r} = -2$, $K_{r_r} = 1$, $K_A = 1$, $K_{P_A} = -1$

The vehicle's response to a combined pitch and roll maneuver of $\Delta\alpha = 2^O$ and $\Delta\Phi = 30^O$ is shown in Figure 39. All variables seem to be well behaved. The major concern in this flight regime was the control surface deflections. (See Figure 40.) The vehicle trimmed with an up elevon deflection of -19°. After performing the required maneuver, the elevons trimmed at -26° (upward deflection). However, with an elevon actuator limit at -30°, the elevon control authority is marginal. Fortunately, the problem can be easily solved by moving the center-of-gravity location aft of .715 L_B.

Supersonic - The Space Shuttle autopilots with some modifications were employed in this flight regime. (See Figure 108 and 109.) The root locus, frequency analyses, and simulations produced a set of gains for the autopilots which had good gain and phase margins and acceptable time histories.

The final set of gains is:

Pitch:
$K_I = 6$, $K_e = 1$, $K_q = 12$

Yaw:
$K_R = 7$, $K_{pr_R} = -5$, $K_{y_R} = -3$, $K_R = 4$

Roll:
$k_A = 1$, $K_{pr_A} = -1$

Time response for a combined maneuver of $\Delta\alpha = 2^O$ and $\Delta\phi = 30^O$ is shown in Figure 41. The vehicle's performance is good, and all variables seem to be well behaved.

15

Hypersonic - The simulation configuration for this flight regime was taken from Reference 1, NASA Contract Report 2723, and the block diagram is given in Figure 107.

The supersonic pitch autopilot with a new set of gains was employed in the hypersonic case. The gains are:

$$K_I = 1, \ K_E = 1, \ K_q = 6$$

A root locus and frequency response analysis indicates good phase and gain margins.

The aileron command block has been taken intact from Reference 1.

The RCS command block was adapted from the same reference with one minor change. The so-called "dead zone" (Figure 111) in the saturation block of the roll error has been changed from $\pm \ 3^O$ to $\pm \ 5^O$. The increase in the width of the dead zone is due, primarily, to smaller inertias. The RCS and aileron command blocks are shown in Figures 112 and 113.

Time responses of the vehicle to $\Delta\alpha = 2^O$ and $\Delta\phi = 30^O$ manuevers are shown in Figure 42. All variables seem to be well behaved.

CCV/Shuttle Comparions.-The responses of the baseline configuration, with a center of gravity at 71.5% L_B, to pitch-axis commands are shown at various design points in Figure 43. Shuttle response requirement envelopes are shown for comparison. The baseline configuration moment of inertia in pitch is five (5) times that of the Shuttle. The responses obtained compare reasonably well with the Shuttle requirements, showing that adequately fast and well damped dynamic responses can be maintained at all flight conditions.

The responses of the baseline configuration (c.g. at 71.5% L_B) to roll commands are shown in Figure 44. Considering that the baseline configuration moment of inertia in roll is over nine (9) times that of the Shuttle and this vehicle is more unstable, the responses come close to meeting the Shuttle requirements.

The baseline configuration is a statically unstable vehicle. Therefore, control surfaces are used for trim as well as maneuvering the vehicle which places an additional burden on the flight control actuation system, and high actuator rates become necessary to perform the required maneuvers. Unfortunately, high actuator rates mean higher weight penalties.

A trade-off analysis was done to determine the vehicle performance as a function of the rate of actuator movement. From this analysis, it was determined that the minimum acceptable actuator rate which would not degrade vehicle maneuver capability is 20 deg./sec. (See Figure 45.) When gust response is taken into account, the actuator rates increase to approximately 40 deg./sec. Thus, all work described in this document was performed with actuator rates of 40°/sec.

"Drooped-Nose" Configuration.-An alternate aerodynamic configuration was investigated to extend the aft center-of-gravity limit in the hypersonic flight regime. The vehicle's nose was drooped, as explained in "Aerodynamics and Performance", and it was analyzed at a hypersonic design point of M = 8 with a center-of-gravity location of 75% L_B.

The time response of the vehicle to $\Delta\alpha = 2^{\circ}$ command is shown in Figure 46. It is somewhat less damped than the baseline configuration response with the center of gravity at 71.5% L_B, but overall it compares well.

Roll responses are almost identical for both configurations.

Tip-Fin Configuration.-An alternate control effector configuration was investigated. The vertical tail was replaced by two small fins at the tips of the wing. The tip-fin simulation block diagram is shown in Figure 114.

Three design points were analyzed with tip-fins:

- Subsonic, M = 0.6
- Transonic, M = 1.2
- Supersonic, M = 3.5

Subsonic - The pitch autopilot and fin command block diagrams are shown in Figure 115 to 117. Enough root locus and time response analyses were performed to get an acceptable set of gains.

Roll responses of the vehicle for baseline and tip-fin configurations are shown in Figure 47. As expected, the tip-fin response is slower than the baseline vehicle. This is due, primarily, to lower rudder power. The vehicle's response to an "unroll from 30°" command is shown in Figure 48. All variables seem to be well behaved.

17

<u>Transonic (Baseline and Tip-Fin Configurations)</u> - Pitch and roll responses
for the transonic flight regime are shown in Figure 49. There is very little
difference in the pitch responses for the two configurations. This is due to
small values of $\Delta C_{m\alpha}$ from the tip fins.

The roll response for the tip-fin configuration is somewhat slower than for
the baseline. Again, as for the subsonic case, this was to be expected, since the
yaw-control effectiveness of the tip fins is much lower than for the vertical tail.

Both configurations are compared with Shuttle response criterion. Considering
the larger inertias of the CCV vehicle, the responses compare quite well with the
Shuttle requirements.

Initially, the transonic tip-fin configuration was analyzed with a center-of-
gravity location at 71.5% L_B. At this C. G. location, the vehicle trimmed with
28° of upward elevon deflection. That left only 2^O of upward elevon movement to
perform the $\Delta \alpha = 2^O$ maneuver. However, the vehicle could only perform
$\Delta \alpha = 0.5^O$, since there was not enough control authority left for pitch control.

As suggested before, by moving the center-of-gravity location to 72.5% L_B,
the pitch control problem was solved. The vehicle trimmed with the elevon at
$\delta_e = -23^O$ (upward), and there was enough control authority left to perform a
combined maneuver.

<u>Supersonic</u> - Pitch and roll autopilots were taken intact from the baseline
supersonic configuration. (See Figures 107 to 109.) The tip-fin command block is
shown in Figure 116 with: KFIN = 20 for the left tip fin and KFIN = -20 for the
right tip fin.

The time response to a combined maneuver of $\Delta \alpha = 2^O$ and $\Delta \phi = 30^O$ is shown
in Figure 50. The vehicle has no problems in pitch, but roll response is
obviously unacceptable. The vehicle becomes dynamically unstable after
rolling more then 20°, and control surfaces saturate by the time the vehicle rolls
over 25°.

To improve vehicle performance, the tip-fins were doubled in size and effec-
tiveness. Time responses of the vehicle to a combined maneuver of $\Delta \alpha = 2^O$ and
$\Delta \phi = 30^O$ are shown in Figure 51. All variables seem to be well behaved with
control surfaces activities well within the limits.

18

A 27.9 m^2 rudderless vertical tail was put on a vehicle in addition to double-size tip-fins. The time response of this new configuration to a combined maneuver is shown in Figure 52. As expected, the control surface activity was smaller than the double-size tip-fins alone, but the overall performance of the vehicle is almost identical to the double-size tip fin configuration performance.

The effect of tip-fin size on roll capability is illustrated in Figure 53. These results indicate the need for the double-size tip fins to be used on the vehicle of this size.

Payload Study.-The baseline vehicle configuration was scaled-up from 17 metric tons to accommodate 80 and 160 metric-ton payloads.

The effect of vehicle size on vehicle dynamics can be shown by the location of poles of the characteristic equations. Figure 54 shows the pole location of all three vehicles with a center of gravity located at 72.5% L_B.

As the vehicle increases in size, a phugoid pair moves to the left of the $J\omega$-axis, and the vehicle becomes statically stable in pitch.

In the yaw-roll motion, the "Lateral Phugoid" pair moves closer to the $j\omega$-axis, making the vehicle less unstable; and the "Lateral Short Period" roots move towards the real axis, giving more damping to the vehicle's yaw-roll motion.

Time responses to a 0.25g pitch-up and 30° roll commands for a subsonic flight regime for vehicles with 80 and 160 metric ton payloads are shown in Figures 55 and 56, respectively.

All variables are well behaved. In both cases, the angle of attack increases after the initial transient, because the vehicle is slowing markedly and the control system is calling for a constant acceleration. A command of this size would not be held for so long under real conditions.

Approach and Landing.-The landing phase of the study was explored in greater depth to assess the feasibility of the control configured design concepts to handle crosswind and gust landing conditions. Because of the limited scope of the study, only lateral gust and crosswind conditions were examined. Design Point 1, subsonic at M = 0.3, was used as a point of departure.

Before proceeding with the analysis of the landing phase, an automated literature search was conducted by the Boeing Technical Library using the key words "crosswind", "gust", and "automatic landing". A list of well over 100 titles were obtained from NASA, DOD, and Boeing sources. Since many of the papers scanned are repetitive, only a fraction of the titles available have been included. It is believed that they are representative. Very brief descriptions of the concepts in most of the papers in the bibliography are given when the title is not adequately descriptive.

Most papers dealt with conventional autoland systems, though some (11 and 12) described modern techniques for addressing the landing problems.

Crosswind Landing Literature Survey

Item 1.-"Study of Automatic and Manual Terminal Guidance and Control Systems for Horizontal Landing, Space Shuttle Vehicles" (Boeing D2-126222-1, October 1969).

Item 2.-"Directional Control Study of ACLS Aircraft in Sidewind Landings" (Boeing D180-18541-1, Aug. 1975).

Air cushion landing systems examined. Not applicable to our study, except for a few ideas on sidewind forces.

Item 3.-"Study of Automatic Flare and Decrab Guidance and Control System for the Space Shuttle" (NASA CR-114436).

Final Report, W. Cockayne et al. (Bell Aerospace Co.), July 1971

Very useful in selecting lateral guidance design approach. Concludes that decrab alignment maneuver is sufficient for the Shuttle-type vehicles.

Item 4.-"Flight Performance of a Navigation, Guidance and Control System Concept for Automatic Approach and Landing of Space Shuttle Orbiter". F. G. Edwards et al. (NASA TN D-7899), Feb. 1975.

Item 5.-"Shuttle Autoland Support Program" (NASA-CR-147589) Sperry Flight Systems, Phoenix, Ariz., April 1976.

Item 6.-"Direct Side Force Control (DSFC) for STOL Crosswind Landings"
Edward M. Boothe and K. J. Ledder, Journal of Aircraft Vol. 11, No. 10
Page 631-638; October 1974 - Calspan Corp.; Feb. 1973.

Several interesting concepts on crosswind landing investigated, though
none directly applicable to our study.

Item 7.-"On the Effect of Gusts and Crosswind on the Dynamic Response of
Aircraft in the Landing Approach", Report No. RAE-LIB-TRANS-1524 - Royal Aircraft
Establishment (English Translation of German Paper) P. Kamel, 1969.

Item 8.-"Some Flight Measurements of Crosswind Landings on a Small Delta
Aircraft"(AVRO 707A) K. Staples, Report No. ARC-R&M 3476, Aeronautical Research
Council (Gr. Brit.) April 1965.

Item 9.-"Wind Modeling and Lateral Control for Automatic Landing", W. E.
Kolley and A. E. Bryson, Jr., Journal of Spacecraft and Rockets; Feb. 1977.

Lateral Control system for the automatic landing of a DC-8 aircraft discussed.

Item 10.-"Background Data for Automatic Landing System Design Requirements,
Criteria, and Objectives." (Boeing D6-44635, Oct. 1977).

A compendium of information and background data useful to automatic landing
system designers and analysts.

Item 11.-"Multi-Input, Multi-Output Regulator Design for Constant Disturbances
and Non-Zero Set Points with Application to Automatic Landing in a Crosswind"
(NASA CR-136618); W. E. Holley et al. (Stanford Univ.); Aug 1973.

Optimal control theory techniques applied to the problem of crosswind landing.

Item 12.-"Development of a Digital Guidance and Control Law for Steep
Approach Automatic Landings Using Modern Control Techniques" (NASA CR-3074)
N. Halyo; Feb. 1979.

Gust Analysis

Only the baseline vehicle configuration performance was investigated under
gust conditions.

A gust in the form of 1-cos ωt was used in the analysis. This gust form is
shown in Figure 57. Only the worst gust response was analyzed. The worst perform-
ance would be a response to a gust with ω being a critical frequency.

To determine that critical frequency, a recording was made of the maximum control surface deflections in response to a 1-cos ωt lateral gust for a range of $0 < \omega \leq 16$ rad/sec and a maximum gust velocity of V_{max} =0.305 m/sec. The results are shown in Figure 58. From these data, the critical frequency was determined to be 2.5 rad/sec.

Vehicle response to a lateral gust at the critical frequency with a maximum gust velocity = 12.2 m/sec is shown in Figure 59. Sideslip angle and rudder deflection responses are seen. Sideslip variation is over 8 degrees, and rudder travel is from one limit to the other. However, at the end of the simulation, both sideslip and rudder return to zero, and the vehicle recovers.

Crosswind Approach and Landing

A horizontal-plane-only autoland system that is compatible with the yaw-roll autopilot was investigated.

Lateral Guidance Design Approach.-The laws required for the lateral guidance may be classified into two distinct phases. These are the laws for (a) initial approach and (b) final approach and landing.

At far ranges (the initial approach), it is sufficient to direct and maintain the vehicle's velocity vector aligned with the runway centerline.

To achieve that objective, a hold-to-ground-track mode (HGTM) was designed. (See Figure 119.)

The ability of a HGTM system to align the vector velocity of the vehicle with the runway centerline with a crosswind is shown in Figure 60 for two initial offsets. The effect of tip-fin size on lateral offset capability is presented in Figure 61.

The vehicle's performance on approach under a constant crosswind was examined for three configurations: (a) baseline, (b) baseline tip fin and (c) double-size tip fin. Maximum drift on approach is shown in Figure 62. As expected, the baseline configuration with the vertical tail had the best performance of the three, with the baseline tip fins having the worst. Double-size tip fins performed quite well in keeping the vehicle on track.

The final runway alignment maneuver is the transition from the far range lateral guidance to that required for touchdown. At touchdown, ideally, the vehicle's heading and velocity vector should be aligned with the runway centerline, and the wings should be level. (It should be noted that crosswind landing gear was not examined.) In practice, compromises must be accepted. The alignment maneuver options are shown in Figure 121.

A pure decrab maneuver has been chosen for this study. The decision to use the decrab maneuver was based on the conclusions of Item 3 in the literature survey. The maximum crab-angle that may remain at touchdown was assumed to be $\pm 4^o$. This is an established Boeing policy, proven successful on subsonic jets. The yaw autopilot with the crab-angle command is given in Figure 122.

Prior to the final alignment maneuver, the vehicle was crabbed into the wind. The magnitude of crab angle depends on the crosswind. If the vehicle requires more than 4° of crab to withstand crosswind, it would drift substantially off of the runway centerline when the decrab maneuver is performed. Figure 63 shows maximum crab angle variations of the three configurations because of crosswinds. When the crab angle limit of 4° (maximum allowable at touchdown) is superimposed on the same graph, maximum crosswinds for all three configurations can be determined.

Without drifting substantially off of the runway centerline, the baseline tip-fin configuration can withstand about 3.4 m/sec crosswind, the double size tip fins can withstand crosswinds of up to 5.2 m/sec., and the baseline vertical tail can withstand a 7.0 m/sec crosswind. Those results are further substantiated by the data presented in Figure 64. Maximum lateral drift during crosswind landing for all three configurations is recorded.

The results of the crosswind-landing study indicate that although the baseline tip fin performance is not as good as for the baseline vertical tail in crosswind approach and landing, by doubling the tip-fin size, the vehicle's crosswind performance becomes quite adequate. This, in turn, supports the results of the Supersonic Tip-Fin Configuration Analysis.

Flight Control System Design

Flight Control System Arrangement - The general arrangement of the major components is shown in Figure 65. The auxiliary power units (APU) are located

further forward than would be desired from a system standpoint to aid in balancing the vehicle. The hydraulic system line weight is impacted by this location.

Control System Ground Rules - The previous CCV study, Ref. 1, developed a vehicle and subsystem configuration based on certain parameters, bounds, and constraints. Those ground rules which bear on the control and power subsystems are restated in Figure 66 for information and to clarify some of the subsequent impacts on system weights.

Rules 1 and 2, Figure 66, are derived from current practice and guidelines for computer-flown, stability-augmented, or power-servoed aircraft. The impacts are more severe for Earth-to-orbit vehicles during entry and landing than for aircraft in that there are no degraded performance levels acceptable during ascent or entry, whereas aircraft may, by reducing altitude and/or speed, accept a system performance capability of as little as 20% of the normal. This requires redundancy levels which do impact weight. This is further impacted by vehicles which have negative stability margins.

Rule 3 illustrates an aspect of these impacts. Aircraft with positive stability margins may, through busses and switching, accommodate malfunctions or failures in these elements without significant disturbance or serious consequence. The time interval associated with fault detection, fault isolation and correction, and phased element work load application can result in unacceptable vehicle attitudes.

Rule 4 is a reasonable limitations to the implications of Rules 1 and 2.

Rule 5 is the statement described under Rule 3.

Rule 6 is a weight-saving statement which has become an accepted aircraft practice.

Control System Definition.-The significant features of the control system are identified in Figure 67. The elevon and rudder duty cycles are summarized and presented as equivalent hours under displacement rates. This data supports development of horsepower hours. Thrust Vector Control (TVC) was ratioed from the Shuttle. The body-flap horsepower and weight were also extrapolated from Shuttle data. The parametric weight factors are consistent with those used in past system studies.

<u>Control Surface Displacement Rate Evaluation</u>.-The control system power
requirements were evaluated at various surface rates from 10 degrees per second
to 100 degrees per second. The vehicle control minimum was found to be 20 degrees
per second. Several conditions at 10 and 15 degrees per second resulted in
unsatisfactory vehicle attitudes. As the rate capability increased, the peak
horsepower required increased as shown in Figure 68. The individual elements
were weighed as a function of surface rate, and the resulting system weight
and C. G. values are summarized on Figure 69. As can be seen, high surface
displacement rates result in significant vehicle weight impact. As noted, the
horsepower hours remain relatively constant, but the peak horsepower requirements
increase by a factor of over 4:1 from 20 degrees per second to 100 degrees per
second. The implication of this is that the peak power may be partially supplied
by accumulators rather than the basic system, resulting in a weight reduction in
the basic system. This benefit has been incorporated in the weights shown.
Figure 70 graphically presents the summary data of Figure 69. The discontinuity
between 15 degrees per second and 20 degrees per second is the result of the
inability of the vehicle to perform required maneuvers at 15 degrees per second.
Therefore, although data for both rates are shown, weight comparisons and or
conclusions should not be made for those rates below 20 degrees per second. For
this vehicle, a rate of 40 degrees per second was selected based on the total
mission flight control requirements including gust encounters with appropriate
margins.

<u>Operational Requirements</u>.-The operational requirements established by the
flight control analysis is presented in Figure 71. Data are presented for both
a center body-mounted fin and wing-tip-mounted fins. The selected control
surfaces displacement rates are 40 degrees per second.

The basic CCV configuration was modified by removing the vertical fin and
rudder and installing tip-fin effectors to perform the function. Two sizes
of tip fins were assessed. One had 4.2 square meter deflectors, the other 8.2
square meter deflectors. The 4.2 square meter deflectors formed the baseline
configuration. Figure 71 compares the significant requirements of the tip-fin
deflectors with the vertical fin and rudder for an equivalent surface rate of 40
degrees per second. The vertical fin and rudder requirements are shown in
brackets. The use of tip fins resulted in the elevon hinge moments increasing by
approximately 17%.

Weight - Aerodynamic Control System - Control system element weights for both the two wing-tip-fin installations and the central-body fin are presented in Figure 72. The vertical-fin configuration has a summary weight of 13340 kg. The second set of numbers with a summary weight of 14440 kg is for a 4.2 square meter tip-fin deflector. The third set is for a 8.4 square meter tip-fin deflector.

The configuration weighed has the tip-fin actuators in the tip fin and routed hydraulic lines and signal lines through environmentally shielded conduits to an environmentally controlled bay for the actuators. The additional line lengths, insulation, and active cooling had an obvious impact. In an effort to reduce system weight, an alternate system was configured as shown in Figure 73. The configuration consists of a dual motor, dual torque tube drive in which the motors, control elements, and electronics were colocated with the elevon actuators in the environmentally controlled elevon bay. The angle drives, power hinges, bearings, and attachments are high temperature dry lubricated elements capable of accepting the environmental conditions with minimal protection. Much of this hardware has been developed in previous high-temperature programs, including the Space Shuttle. The benefit of this approach is that the penalty for providing adequate environmental control for the sensitive control elements is minimized.

Figure 74 shows the weights for the hardware deleted associated with the removal of the central body vertical fin and rudder, the hardware addition associated with the installation of the tip fin with the surface actuators in the tip fin, and the tip-fin installation with the motor and torque tube drive described on Figure 73. The tip-fin installation with the 4.2 square meter deflector results in a 11.7% weight savings with a 3.94 meter forward C. G. shift. The motor/torque tube configuration results in a 16.1% weight savings with an identical forward C. G. shift. This weight reduction represents a 3% weight reduction in the control system.

A weight for the 8.4 square meter fin deflector was developed for both the tip-fin actuator installation and the motor/torque tube installation and is summarized in Figure 75. These configurations resulted in a weight growth of 64.6% relative to the central body fin configuration. It should be noted that the tip-fin structure in this configuration weighs more than the entire system in the

4.2 square meter deflector configuration. This indicates that simply growing the area of fins may not be weight effective. The motor/torque tube configuration is still the lowest weight by approximately 5% because of the lighter actuation elements.

The evolution of the tip-fin configuration revealed some significant problem areas. While these represent concerns, none of the problems were considered to be so serious and without an evident solution as to conclude that tip-fin effectors were without merit. The following table presents some of these tip-fin problems and some of these suggested solutions:

ACTUATION

- High Heating Environment Poses Weight Penalties for Insulation and Active Cooling for Units Located in Fin.

- Relocate Sensitive Elements Inboard, i.e., Combine Units in Elevon Actuation Bay which Incorporates Active Cooling.

- Hinge Bearings Exposed to High Heat Environment.

- Utilize Concealed Insulated Hinges with Dry Film Lubrication.

- Remote Actuation Systems Increase Flutter Control Problems.

- Utilize Active Load Bias in Actuation Elements to Increase Stiffness and to Reduce Null Clearances.

Configuration Design

Vehicle Configuration.-The modification 1 baseline vehicle configuration developed in Ref. 1 was used to support the initial activities of this study. The inboard profile of this configuration is shown in Figure 1. Significant features of this configuration are the wing reference area of 557.4 square meters, the elevon chord of 4.33 meters, and the relative location of the liquid oxygen tank aft of the hydrogen tank. The technology used to arrive at this configuration is discussed in detail in Ref. 1. The gross lift-off weight of the configuration is 1,470,000 kilograms, the entry weight including payload is 188,000 kilograms, and the landing weight including payload is 185,300 kilograms.

Structural Design and Analysis.-Structural concept definition and analyses were accomplished for the wing, elevon, and tip fins for the configuration of Figure 1. These designs and analyses were used to update the configuration weight statement to reflect control-surface loads resulting from the flight control analysis.

Wing.-The critical design loads occur during ascent. The integrated shear, moment, and torsion for the wing at the intersection of the load reference axis with the side of the body are given in Figure 76. The ultimate loads, bending moment of 9,650,000 Nm, torsion of 4,190,000 Nm (nose down), and vertical shear of 214,094 kg were assumed to be carried by the structure located between the mid spar (M. S.) and rear spar (R. S.) located as shown on Figure 76. The shear center for this structure was assumed to be midway between the mid spar and the rear spar.

Figure 77 illustrates the structural system and summarizes the structural sizing and weight of the aft wing box structure. Wing torsion is modified through the shift of the vertical shear aft from the wing load reference axis. The wing spars are stiffened; intermediate shear webs are made from titanium 6AL-4V. The surface panels are aluminum brazed titanium (6AL-4V) honeycomb. The surface panels are bolted to the spar and rib tee caps. The honeycomb is densified at the bolted joints. The ribs running between spars are spaced at 0.51 meters. The rib webs are trusses constructed of boron fiber - aluminum matrix composite tubes for web members and titanium 6L-4V extruded chords. The weight difference between the upper surface (26.82 kg/m^2) and the lower surface (20.97 kg/m^2) is due to the upper surface design load being in compression. The structural weight of this wing section (excludes front spar) is 1920 kg/wing.

The structural system used on the forward wing is shown in Figure 78. The aluminum brazed titanium (6AL-4V) honeycomb panels are supported on truss ribs spaced at 0.51 meters. The ribs pick up surface pressures from the surface panels and send the loads to the front and mid spars. The weight of this wing area (excluding the wheel well area) is 820 kg/wing.

Wing weight (total for configuration) of 9739 kg is summarized in Figure 79. The forward wing unit weights were used for the trailing edge area. The leading edge and leading-edge spar unit weights were the same as those used in establishing structural weights for the Ref. 3 configurations. The wing thermal protection

system plus the insulated heat shield system weight is based on a unit weight of 11.23 kg/m^2, Ref. 1, page 62, Figure 36. The thermal protection is used over the lower wing surface and over the first 1.22 meters aft of the leading edge shell on the upper surface.

Elevon.-The elevon overall geometry and structural centerlines are shown in Figure 80. The maximum limit hinge moment, per elevon segment, of 0.44 (10)^6 Nm occurs at M = 1.2 during a reentry maneuver. At this condition, the structure temperature is approximately 589K. There are two surface actuators per elevon segment. Each actuator has two cylinders. Therefore, using the criteria that no single failure will reduce vehicle controllability below operational requirements (vehicle is control configured), each actuator requires a capability of 8.9 (10)^6 N based on an actuator arm of 0.36 m. Due to potential surges in the hydraulic system and frequency of load application, an ultimate factor of 2.5 is used in designing local actuator and hinge attach structure. The actuator support fitting is designed for an ultimate factor of 1.5 X 1.2 = 1.8. The actuator load distribution rib is designed for an ultimate factor of 1.5 times the actuator load. It is assumed that structural deformations will absorb the effects of maximum actuator load generated by surges and pressure relief valve tolerance after the actuator loads have been distributed into the basic elevon surface panels. Therefore, the remainder of the elevon is designed for an ultimate factor of 1.5 applied to the maximum operating (flight) loads.

Thermal protection is used on the lower surface and over the outboard and inboard ribs.

Aluminum brazed titanium (6AL-4V) honeycomb panels are used for the elevon surfaces. (See Figure 81.) Maximum surface shear flows are 1260 N/cm. The surface panels are bolted to the rib and spar caps. Unit weight, including panel joints, of the surface panels is 7.32 kg/m^2.

The sizing and weights for the elevon actuator rib and from spar structural system are summarized in Figure 82. Both the actuator rib and front spar are constructed by welding a sine wave corrugated web to flat-plate chords. All material is titanium 6AL-4V.

Typical elevon rib construction, sizing, and weights are shown in Figure 83. The ribs use truss construction for a portion of their length then switch to sine wave corrugated webs that are welded to flat-plate chords. Titanium 6AL-4V is used for all members. Figure 84 shows the elevon hinge fittings and the actuator/hinge support fitting. The actuator/hinge support fitting is mounted in the wing trailing edge. Each elevon segment has one outboard hinge fitting and two actuator/hinge fittings. The fittings are machined from titanium 6AL-4V forgings.

The elevon weight is summarized on Figure 85. The thermal protection system (TPS) unit weight of 26.84 kg/m^2 is based on the weight of a coated molybdenum heat shield TPS system as shown in Ref. 1, Figure 36. This system has limited life at an operating temperature of 1756 K. The elevon down displacement during entry was limited so as to not exceed 1756 K. The weight of the elevon structure including the thermal protection systems is 7080 kg for the total vehicle. No weight has been included for elevon-to-wing seals.

The very high operating temperatures will require development of new and unique materials and concepts to provide elevon-to-wing and elevon-gap seals. The elevon structure and thermal protection system (TPS) weight variations with elevon hinge moment are presented in Figure 86. The elevon surface area and chord are held constant for the presented weight trends.

Fin Installation - Wing Tip.-The installation of a vertical fin on the wing tip required modification of the outboard wing and outboard elevon. The modifications are required to provide a structural load path to transmit fin loads into the primary wing structure, Figure 3. The gaps formed by the sloped elevon leading edge and the elevon-to-fin base structure present major structural problems because of high local heating and the potential for boundary-layer ingestion. The sealing of these areas was not addressed in this study.

Tip fin design loads developed during the X-20 program were selected for use in preliminary structural sizing. Since the control configured vehicle had terminal entry flight trajectory characteristics similar to X-20, it was concluded that both systems would have to meet similar structural design load criteria. Both fin and rudder surface pressure are shown in Figure 87. As noted, it is anticipated that a detail external load analysis may show that the selected loads due to an arbitrary yaw in combination with a rudder kick (15°) may be exceeded when the vehicle is subjected to abrupt rolling maneuvers.

30

Temperature isotherms for the fin leading edge and inboard and outboard surfaces are shown in Figure 88 and 89. Ground rules and assumptions are given in the following Table.

Laminar Heating	$\rho_r \mu_r$
Turbulent Heating	Spalding - Chi
Laminar Factors	1.1
Turbulent Factor	1.25
Onset Transition	$R_{\theta_T}/M = 220$
Fully Turbulent Transition	$R_{TURB}/R_{ONSET} = 1.5$
Turbulent B. L. Virtual Origin	Onset of Transition
Emissivity	0.8

The tip fin structural system is shown in Figure 90. The leading edges are integral stiffened coated molybdenum shells, 0.15 m in length. The fin surface temperature of up to 1467 K requires the use of a thermal protection system (TPS). The selected TPS is a coated columbium heat shield stiffened by coated columbium corrugation, Figure 90. A Q-felt insulation is used to drop the temperature to approximately 1050 K. The load carrying structure consists of Rene'41 brazed honeycomb panels supported by a matrix of Rene'41 spars and ribs. The Rene'41 spars and ribs are constructed by welding sine wave corrugation webs to flat chords. Temperatures on the rudder are such that brazed Rene'41 honeycomb surface panels may be used without additional thermal protection. The lower portion of the fin has the same type of construction as the fin leading edge.

The tip-fin weight (per side) of 908 kg is itemized in Figure 91. This weight does not include wing weights that may be required due to increased loads to be transferred into the body or due to wing flutter.

The initially sized tip fin could not meet the vehicle stability and controllability requirements. As a result, the tip fin was increased in size as shown in Figure 4. This increase in size coupled with the corresponding significant increase in loads required further modification to the outboard wing. The recommended changes included increasing the wing tip chord and reducing wing sweep (holding the wing exposed area constant). The larger tip fin would use the same structural concepts as outlined for the smaller fin. Structural unit weights for the growth tip fin were assumed to be similar to those of the initially sized fin.

Weight Statement.-The control configured design weight statement is shown in Figure 92. This weight statement incorporates the wing and elevon structural sizing and the flight control system requirements developed during this study. The remainder of the weight statement elements are based on data developed during the Ref. 1 study. The gross lift-off weight is 1,471,000 kg. At this gross weight and a dry weight of 164,800 kg, the cargo capability is 10,100 kg for an easterly launch. The entry vehicle center of gravity (cargo in) is at 77.5% body length. For the entry condition, moving the vehicle center of gravity forward to 74.5% body length using ballast at station 6.86 requires 8,850 kg of ballast. Holding gross lift-off weight and entry dry weight constant, the use of ballast to move the entry center of gravity forward would result in a cargo capability of 10,100 - 8,850 = 1350 kg for configuration with tip fins.

TECHNOLOGY ASSESSMENT

Discussion

Based upon the study results, Task IV was to identify improvements needed to enable the operation of SSTO vehicles (VTO) at far-aft center-of-gravity locations. This survey includes description of critical technology areas and a brief outline of the types of programs required to develop these technologies.

Overall the technology assessment remains essentially the same as that identified in the original CCV study, Reference 1. The present study puts in focus the most pressing technology needs as follows:

. Establishment of stability criteria (i.e., degree of aerodynamic instability) to optimize CCV design and orbital payload.

. Aerodynamic configuration development is an essential key to CCV design success.

. Application of optimal control techniques can enhance flight control analysis which could reduce control rate requirements for CCV designs.

. Advanced flight control subsystems with control rates up to 40 deg./sec. (actuators, APU, hydraulics, etc.) should be identified for advanced development.

- Application of failure prediction, detection, and correction scheme of a fly-by-wire (FBW) flight control system to provide enhancement of CCV designs.

- TPS capable of sustained 1800 K (2800°F) reuse should be systematically developed.

These and other related critical technologies are presented in more detail in the following discussions.

Stability Criteria.-Upon reviewing both CCV studies (i.e., the present and that of Reference 1), it became increasingly apparent that most of the flight control characteristics were very strongly influenced by the degree of inherent instability in the baseline configuration. If a static stability criteria had been initially established as a design guideline, the flight control study results could have been significantly altered. Most conventional aircraft have stable characteristics in both pitch and lateral/directional modes. However, the baseline CCV configuration was unstable in both modes and was a major contributor to the unusually high control and actuator rate requirements. Undoubtedly, a configuration not as statically unstable would have reduced these requirements. The question that remains to be answered is: What is the range of instability (unaugmented) that optimizes a CCV design? Perhaps, a neutrally stable configuration is close to that region. Thus, future studies should be undertaken to establish this stability criteria.

Aerodynamic Configuration Development.-Configuration alternatives have a major impact on stability, control, and trim characteristics of VTO CCV vehicles as revealed in the study results of Tasks I and II. These trade results are based on estimated aerodynamics from various computer programs and, as such, are subject to wind-tunnel test verification. Although, much wind-tunnel test data exist for a variety of unrelated configurations with limited variations (or detailed information on a specific configuration), it was not possible to find appropriate parametric test data to support the trade-offs of this study.

To overcome this deficiency, a comprehensive wind-tunnel test program and analysis should be developed with the following features:

- Initially, a broad spectrum of wing/body parametric aerodynamic configurations should be identified. Samples for the body could include: nose droop, fineness ratio, planform, and cross-section. Wing parameters should stress those variables which mostly affect control power and static trim (including hinge moments).

- The first phase would be to generate by computer theoretical aerodynamic characteristics over a broad spectrum of speeds. (subsonic to hypersonic Mach numbers).

- The next phase would be to develop and implement wind-tunnel test plans based upon the most promising candidates of the theoretical analyses.

- The final phase would be to document the test results. Finally, these results should be formatted to meet the needs of advanced preliminary design configuration parametrics.

Flight Control.-The baseline vehicle examined in this study has been designed with relaxed static stability. Relaxed static stability is a CCV feature wherein the vehicle is designed with reduced, and possibly negative, inherent static margins, and acceptable vehicle stability characteristics are provided by the flight control system. In addition to the full-time stability augmentation, the flight control system has to provide maneuver and gust load alleviation, flutter suppression, and fatigue damage reduction.

The complexity of the control task and the dynamic characteristics envisioned for a CCV design concept motivate the departure from classical single-loop control law synthesis, which is ill-equipped to deal with coupled multivariable systems, to new approaches based on modern control theory. Despite the mathematical rigor of the theory of modern control science, its application to the synthesis of practical controllers for aerodynamic vehicles is not well understood. Particular concerns are the relationship between design methods, the achievement of specific design goals, and the preservation of good closed-loop performance in the face of uncertainties and system parameter preservation.

One of the most promising design techniques for a multi-input multi-output flight control system is optimal control theory. It is believed, that the application of this theory to the CCV type vehicle would result in improved controllability and stability, reduced gust response, improved crosswind landing performance, and low control surface activity. Therefore, it is suggested that further studies be directed towards the development of the practical and operational optimal control system design techniques.

Recent advances in the fly-by-wire (FBW) control systems (See Ref. 1, Table 2, Items 2, 5, 8, and 15) indicate possible application of FBW to the CCV type vehicles. Since the control system is substituting for inherent stability, it must function continuously with reliability comparable with primary structure. Because of this, it is recommended that failure prediction, detection, and correction schemes for a fly-by-wire flight control system be investigated.

Structures.-The development of a thermal protection system capable of sustained operation at 1800 K will require significant technology advances. The TPS requirements will include lightweight, dimensionally stability throughout the operational temperature range, oxidation resistance, reasonable damage resistance and essentially all-weather operation (rain, etc.) capability. In addition, it will be highly desirable that the structural components of the TPS have some measure of ductility. The systems must have the capability for continued reuse if the goal of low cost space transportation is to be achieved.

Subsystems.-The extensive technology assessment conducted under NASA (Reference 3) Technology Requirements for Advanced Earth Orbital Transportation Systems, is directly applicable to the advances in flight control system technology required for advanced control configured space transportation systems. Specific technology advances that would result in reduced subsystem weight include:

- 40 MPa hydraulic systems - Results in reduced line and actuator sizes as well as reduced quantities of hydraulic fluid.

- Composite material application - Use of composite materials as titanium matrix composites in fabrication of actuator, high-pressure containers, pump housing, and for large hydraulic fluid delivery lines.

CONCLUDING REMARKS

A summary of the study results is contained in the following concluding remarks:

Task I

Baseline Vehicle.-Analyzed at five design points along entry flight profile including establishment of an operational center-of-gravity range from 0.715 to 0.725 of body length.

- Gust analysis showed vehicle survived a 12.2 m/sec (40 FPS) gust with control rates of 40 deg/sec.

- Ascent analysis with winds indicated engine gimbal angles of 6 deg can hold a nominal flight bearing course.

- Relative high actuator rates requirements of CCV configuration (20 to 40 deg/sec.) significantly increase flight control subsystem weights.

Task II

Aft C. G. Study.-Developed alternate configuration for stable flight control response and hypersonic trim for C. G. as far aft as 0.75 body length.

- Landing approach (course error and drift analysis):

  - Baseline vertical tail can accommodate crosswinds up to 9.2 m/sec (17.8 KT)

  - Small reference size tip fins are good only to 3.7 m/sec.

  - Twice-size tip fins increase crosswind to 7.6 m/sec.

Task III

Payload Size Study.-Increased payload size (from 17 to 160 metric tons) with large increase in vehicle GLOW and inertia did not impact flight control response. Hypersonic trim significantly improved due to the increase in size of the wing relative to the body planform area.

Task IV

Technology Assessment.-Overall remains essentially the same as that identified in the original CCV study. The present study puts into focus the most pressing technology needs as follows:

- Establishment of stability criteria (i.e., degree of aerodynamic instability) to optimize CCV design and orbital payload.

- Aerodynamic configuration development is a key to CCV design success.

- Application of optimal control techniques can enhance flight control analysis which could reduce control rate requirements for CCV designs.

- Advanced flight control subsystems with control rates up to 40 deg/sec. (actuators, APU, hydraulics, etc.) should be identified for development.

- Application of failure prediction, detection, and correction scheme of a fly-by-wire (FBW) flight control system to provide enhancement of CCV designs.

- TPS capable of sustained 1800 K (2800°F) reuse should be developed.

REFERENCES

(1) Hepler, A. K.; Zeck, H.; Walker, W. H.; Shafer, D. E.: Applicability of the Control Configured Design Approach to Advanced Earth Orbital Transportation Systems, NASA CR-2723, August 1978.

(2) Freeman, Delma C., Jr.; and Wilhite, Alan W.: Effects of Relaxed Static Longitudinal Stability on a Single-Stage-to-Orbit Vehicle Design. NASA TP-1594, 1979.

(3) Hepler, A. K. and Bangsund, E. L.: Technology Requirements for Advanced Earth Orbital Transportation Systems. Volume 2: Summary Report, NASA CR-2879, July 1978.

(4) Freeman, Delma C.; Powell, Richard W.: The Results of Studies to Determine the Impact of Far-Aft Center-of-Gravity Locations on the Design of A Single-Stage-to-Orbit Vehicle System. AIAA Conference Paper 79-0892; May 11, 1979.

APPENDIX A - AERODYNAMIC CHARACTERISTICS

For the baseline CCV configuration, aerodynamic data were obtained from current NASA/LRC wind tunnel-test results (unpublished). For those characteristics not available, estimates were made using scaled Shuttle Orbiter values or DATCOM methods. At each design point, control power, rotary derivatives, and hinge-moment coefficients were estimated as shown in the following tabulated data of Figure 93 to 97.

In order to trim at transonic speeds, additional control power was required. Aerodynamic characteristics were estimated as shown in Figure 98 for elevon deflections to -40 degrees (Up) and a body-flap deflection of -14 degrees.

Ascent analysis used linearized aerodynamic characteristics, since angle-of-attack seldom exceeded 5 degrees up to $M \simeq 4$. These estimated characteristics are presented in Figures 99 to 101.

For alternate configurations which replaced the vertical tail with small wing tip fins, representative control characteristics which were used for the flight control design point analysis are summarized on Figures 102 to 104. For cases where the tip fins were increased to twice the original size, the control effectiveness doubled, plus there were small adjustments to the rotary derivatives.

APPENDIX B - FLIGHT CONTROL

Flight control block diagrams for all five design point analyses are presented in this appendix. Also, included are definitions of schematics for the approach and landing analysis. (See Figures 105 to 122 for all this data.) The hold-to-ground-track-mode system is similar to the lateral-beam intercept and hold mode (VOR) with $\lambda \simeq d$, where λ is the lateral beam error. Both modes are designed to minimize the variable, λ or d.

To align the vehicle's velocity vector with the centerline, a bank command is developed which is a function of the vehicle's offset from the runway centerline, the vehicle's crosstrack rate, and heading angle. The block diagram for the HGTM system is shown in Figure 118.

The final alignment maneuver may be:

a) Decrab - With the velocity vector aligned with the runway and the sideslip angle held to zero, the vehicle is initially "crabbed" into the wind. (See Figure 120 for "Crab Angle" definition.) The vehicle is yawed (decrabbed) so that its heading is aligned with the runway to within acceptable limits at touchdown.

b) Deroll - With the velocity vector and heading aligned with the runway, the vehicle is initially rolled into the crosswind. The vehicle is derolled so that the roll angle is within acceptable limits at touch down.

c) Combined - this is a combination of the first two. By partially crabbing and partially rolling into crosswinds, both the heading and roll angle misalignments are reduced.

d) Predictive - Utilizing any of the above approaches, the velocity vector and lateral flight path are oriented such that an apparent lateral drift and offset from the runway centerline exists. The alignment maneuver is executed such that the predictive net drift and offset at touchdown are zero (0).

39

LH$_2$ TANK

APU MMH TANK

LO$_2$ TANK

14.48 m (570 in.)

37.08 m (1460 in.)

50°

4.33 m (170 in.)

HELIUM REPRESSURIZATION TANK

PAYLOAD BAY

4.6 m Dia X 18.3 m Lt. (15'D X 60' L)

MAIN ENGINES

ENTRY

TAIL SCRAPE

WING REF. AREA = 557.4 m^2 (6000 ft^2)
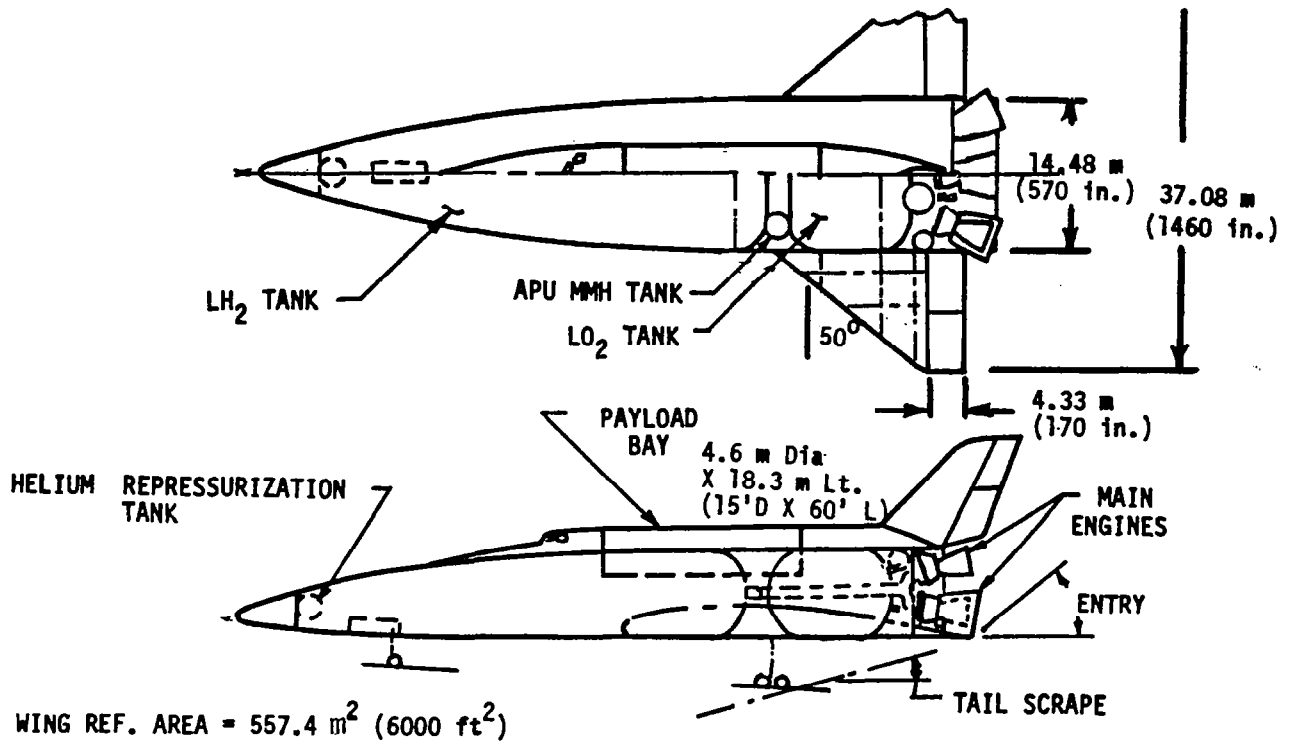
Figure 1: Baseline Control Configured Vehicle

TIP FIN DEFLECTIONS

TIP FIN

66.8 m (219.2 ft.)
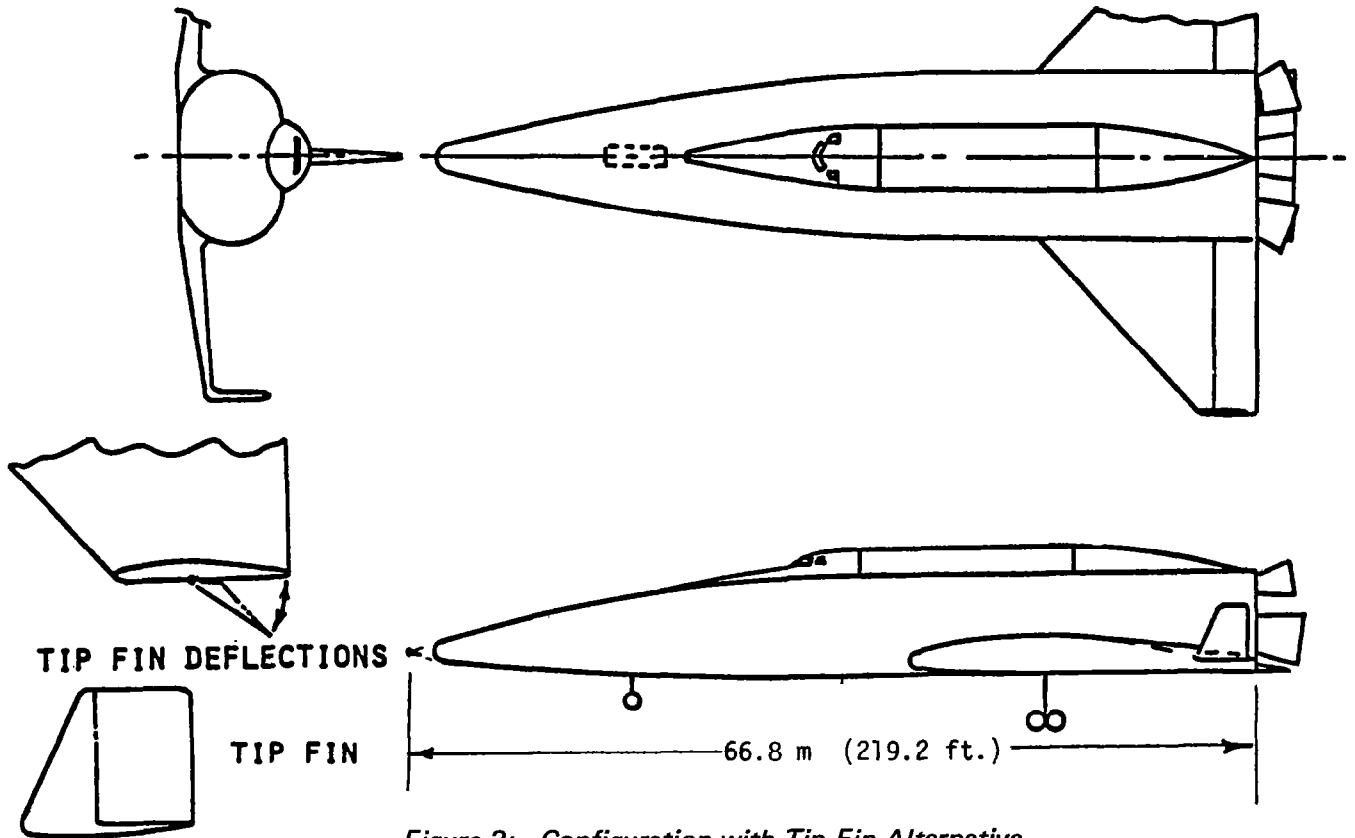
Figure 2: Configuration with Tip Fin Alternative

40
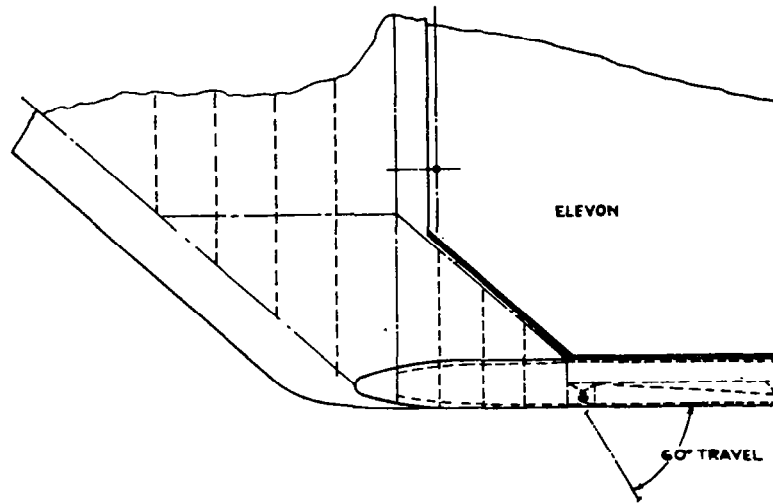
Figure 3: Reference Fin Installation — Wing Tip

WING PLANFORM REVISION

BASELINE LEADING EDGE
REVISED LEADING EDGE

5.99 m

3.02 m

3.22 m

4.32 m

5.38 m

251 m

15.59 m² 167.8 FT² FIN AREA
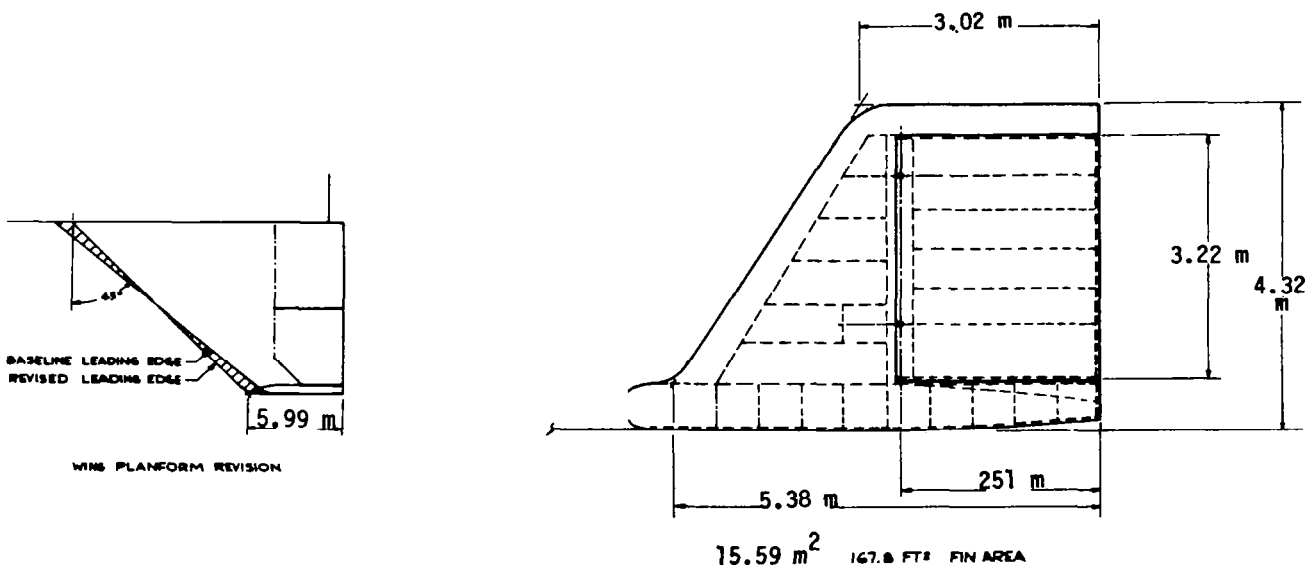
Figure 4: Growth Fin Installation — Wing Tip Control Configured Design
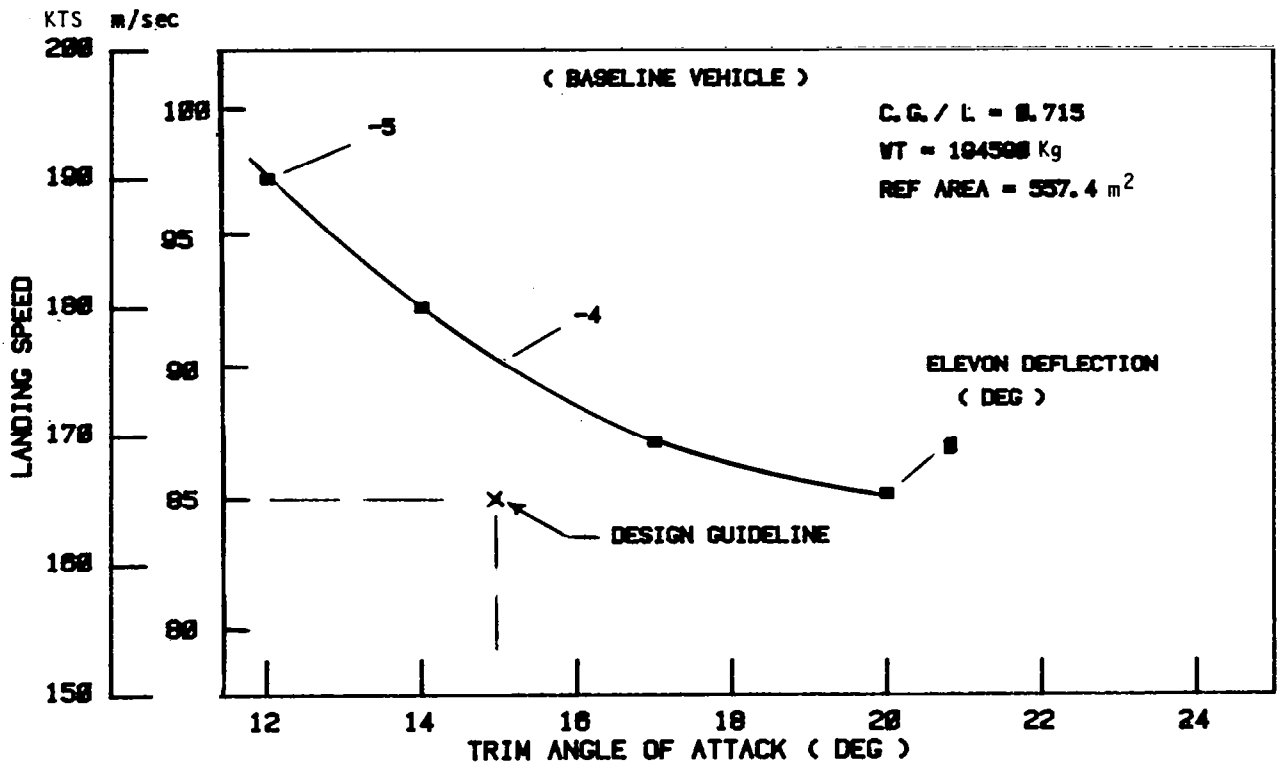
Figure 5: Landing Speed
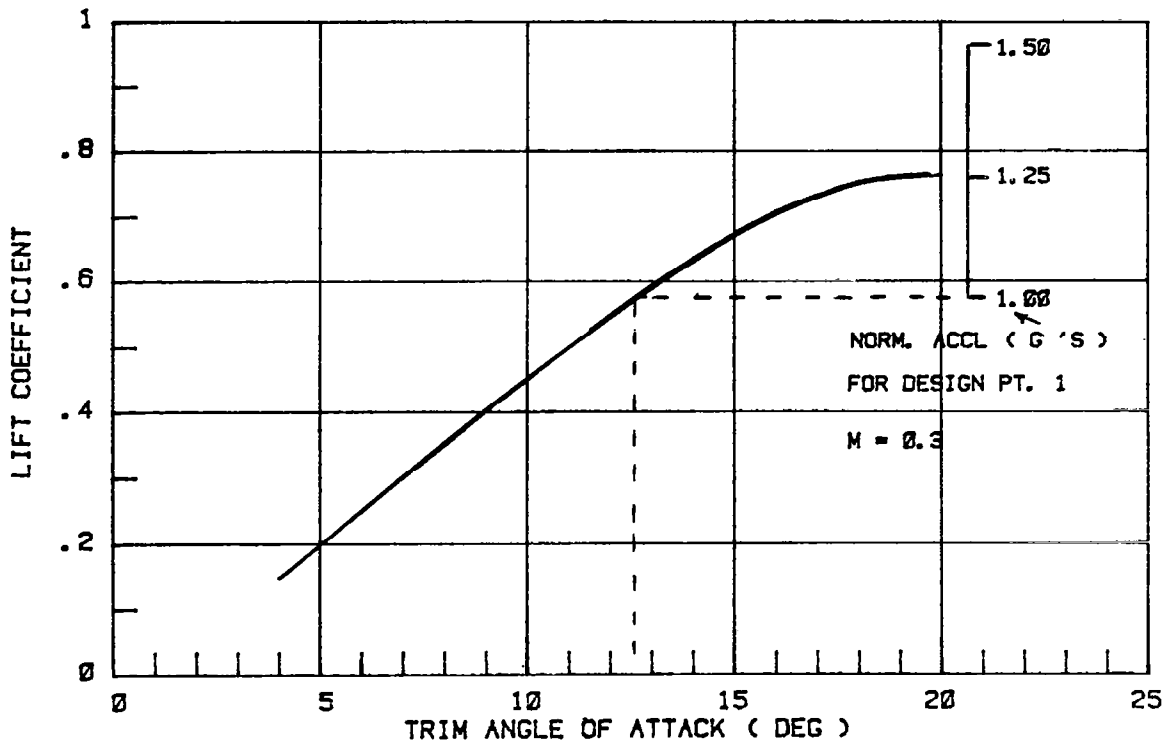
Figure 6: Subsonic Lift — Baseline Vehicle

42
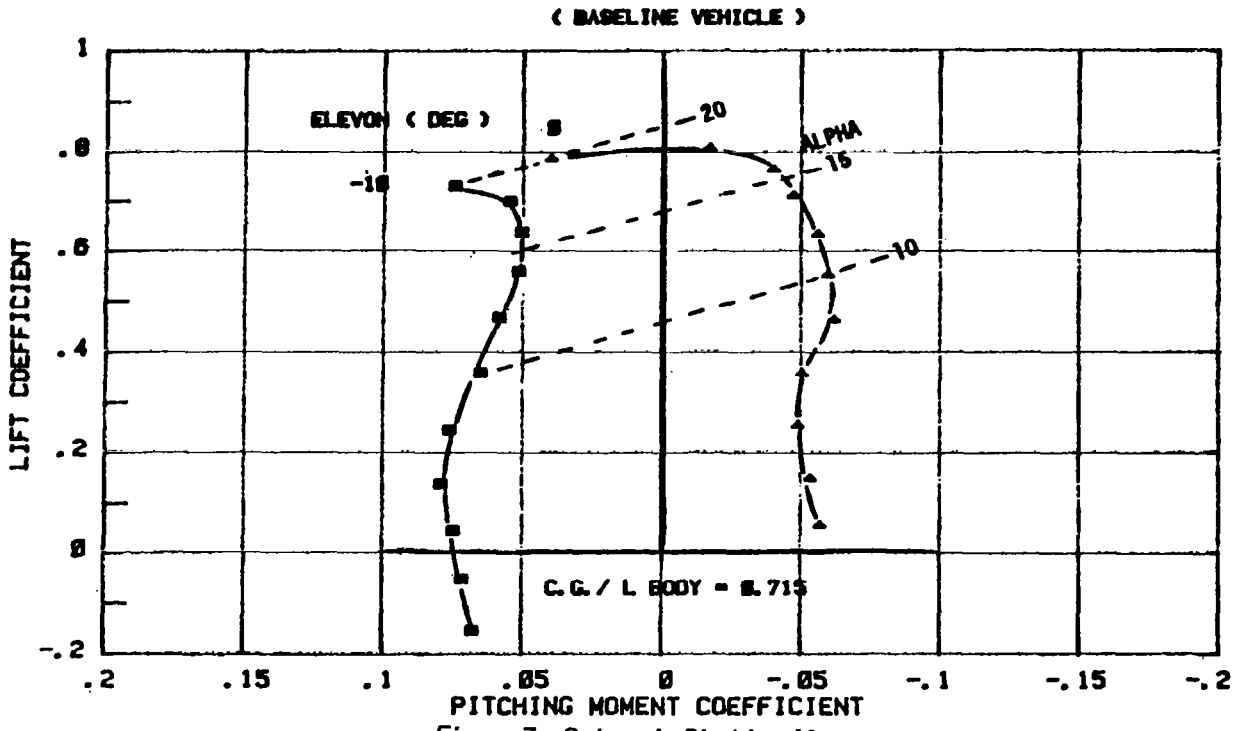
Figure 7: Subsonic Pitching Moment
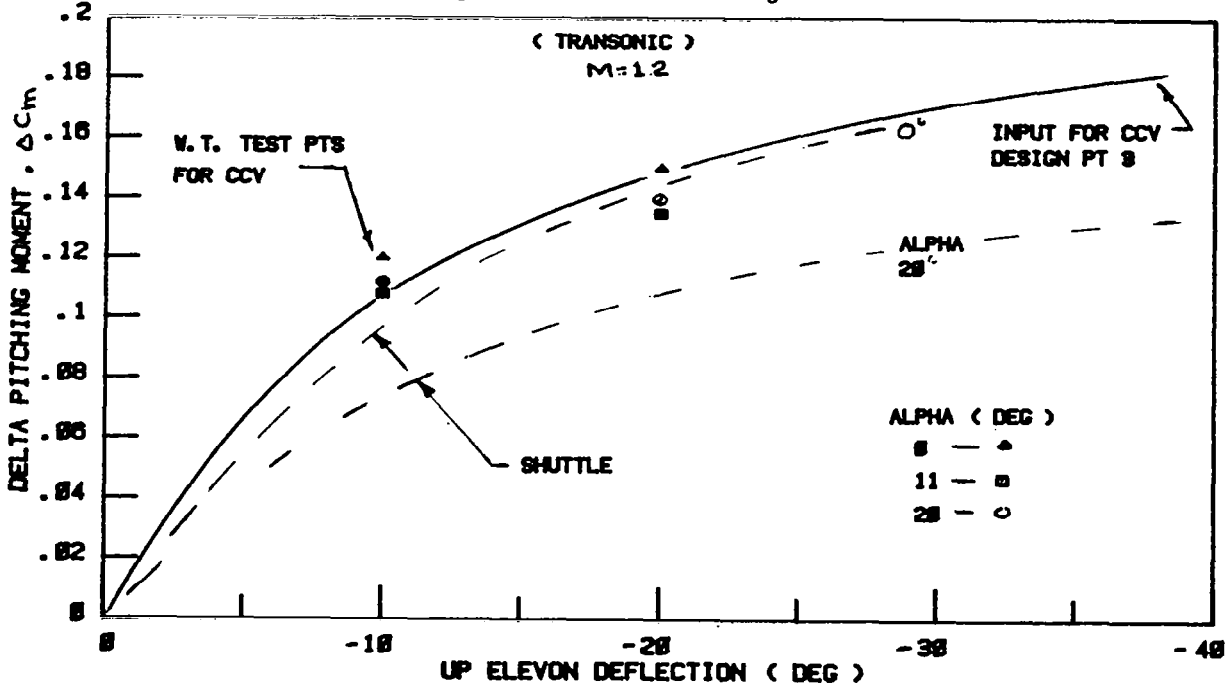
Figure 8: Elevon Effectiveness

Figure 9

(TRANSONIC M = 1.2)

ESTIMATE FOR CCV (SCALED BY $\bar{V}$ FROM SHUTTLE)

ALPHA = 18 (DEG)

DELTA PICHING MOMENT , ΔC_m

.04

.02

0

.02

-.04

SHUTTLE
W.T. PTS

CONFIG	$\bar{V}$
SHUTTLE	.048
CCV	.124

$$\bar{V} = \frac{L}{C} \frac{S_{BF}}{S_{REF}}$$

-20   -10   0   10   20

BODY FLAP DEFLECTION (DEG)
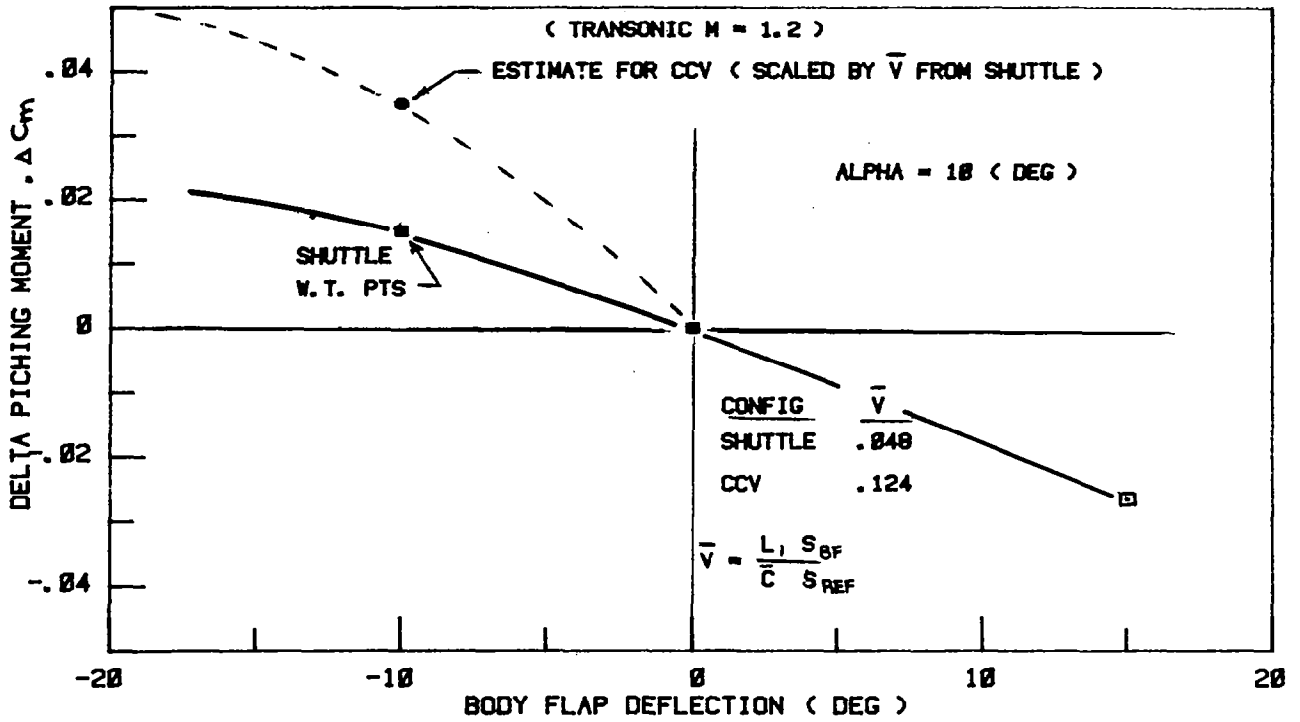
Figure 9: Body Flap Effectiveness

Figure 10

PITCHING MOMENT COEFFICIENT , CM

.3

.2

.1

0

-.1

-.2

-.3

W.T. TEST PTS HELIUM
M = 20.3

CONFIG : CCV-MOD 1

CONTROL SURFACE
DEFLECTION (DEG)
ELEVON / BODY FLAP

0/-4

0/10

10/-4

10/10

10/10

CURVES CALC BY COMPUTER
PROGRAM "HYPEREZ"

REF MOMENT CENTER = .715 L BODY

0   5   10   15   20   25   30   35   40   45   50   55   60

ANGLE OF ATTACK (DEG)
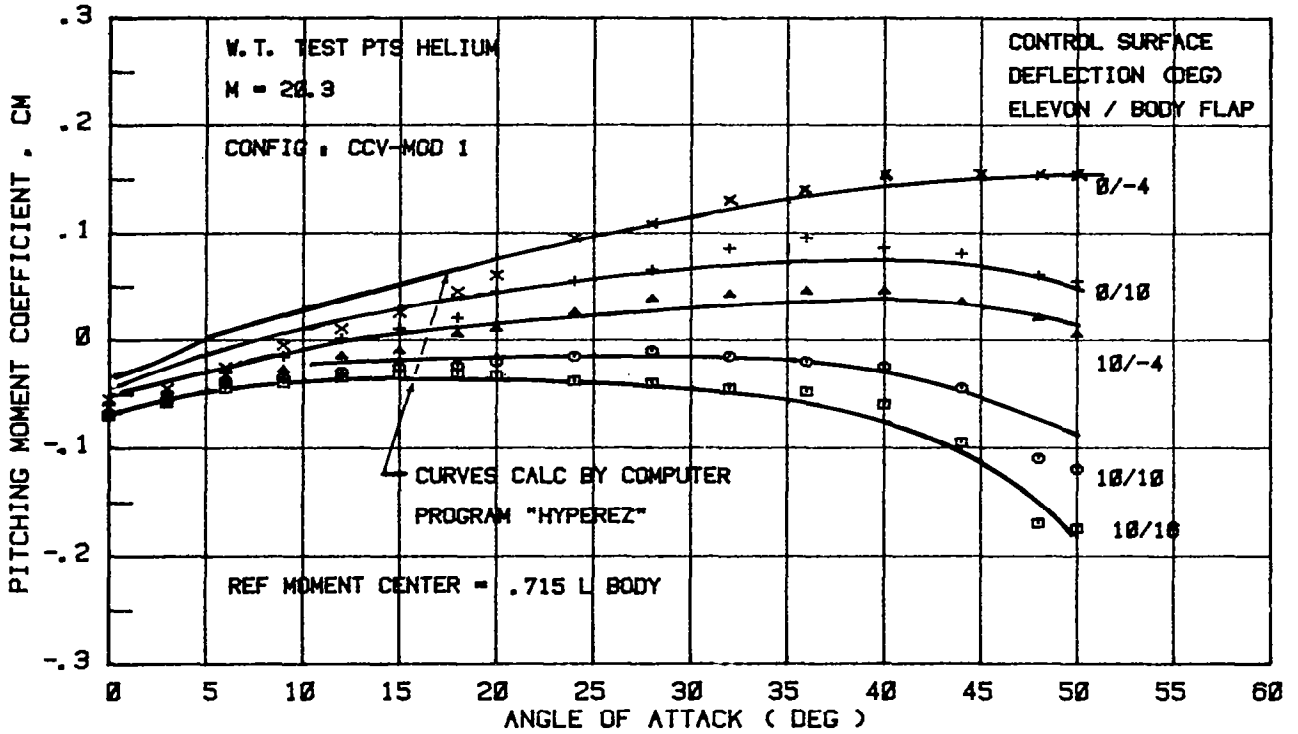
Figure 10: Hypersonic Aero Comparison
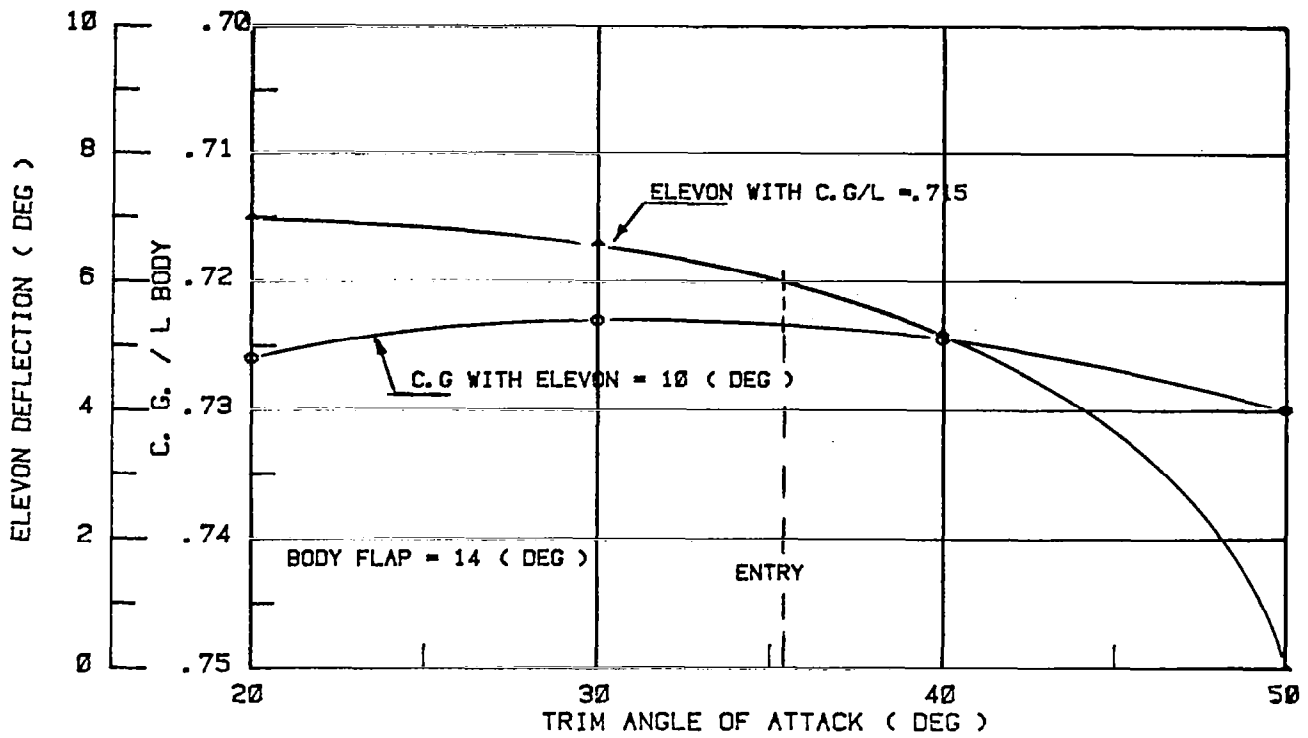
Figure 11: Hypersonic Trim — Baseline Vehicle
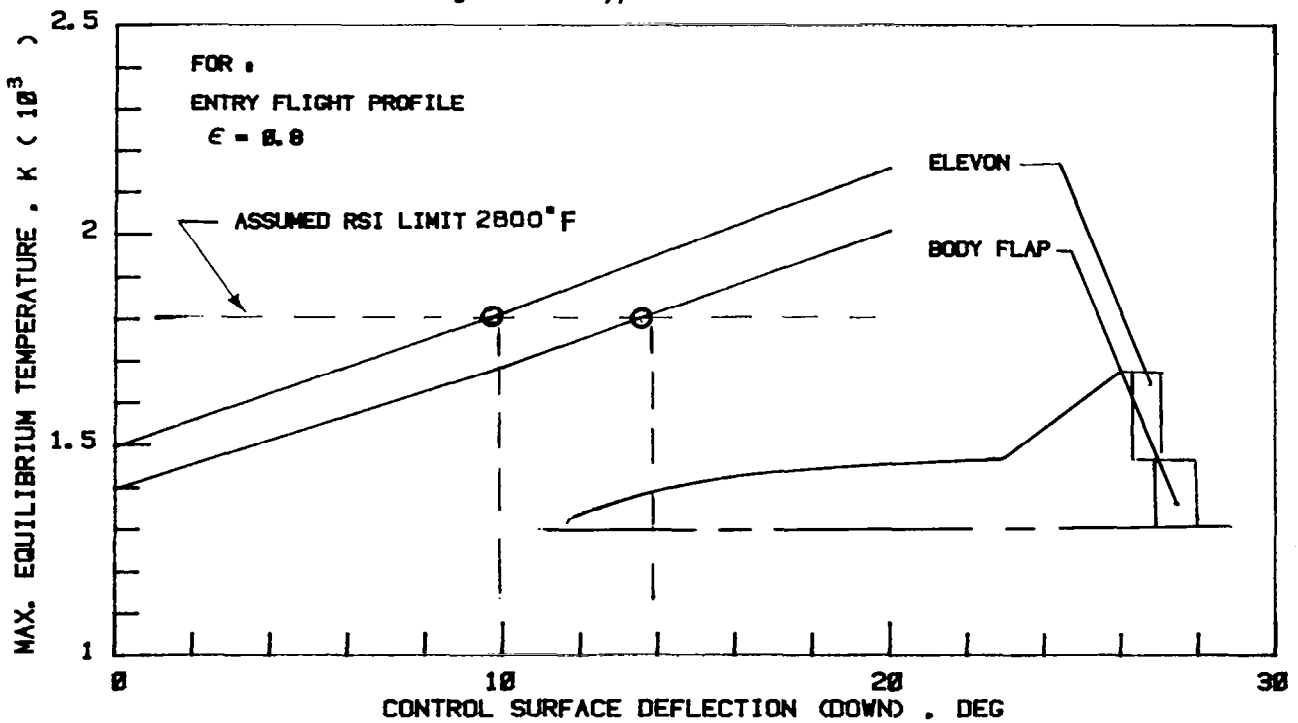
Figure 12: Control Surface Temperature
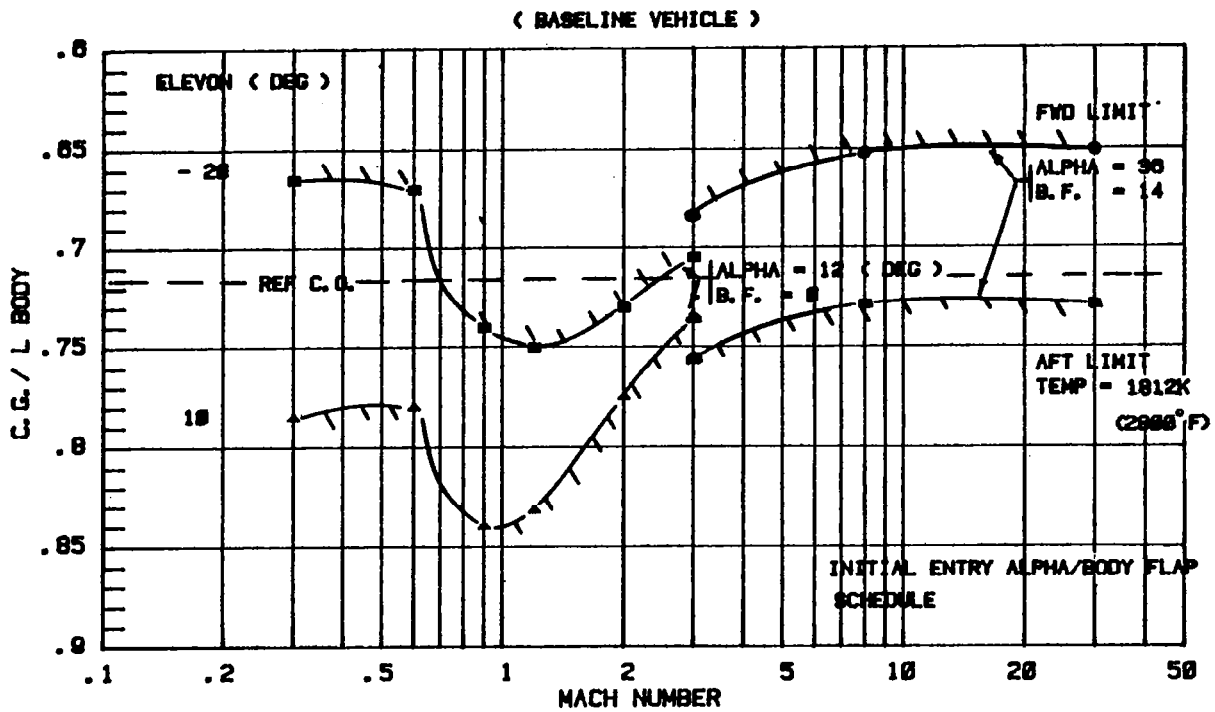
Figure 13: Initial Operational C.G. Limits
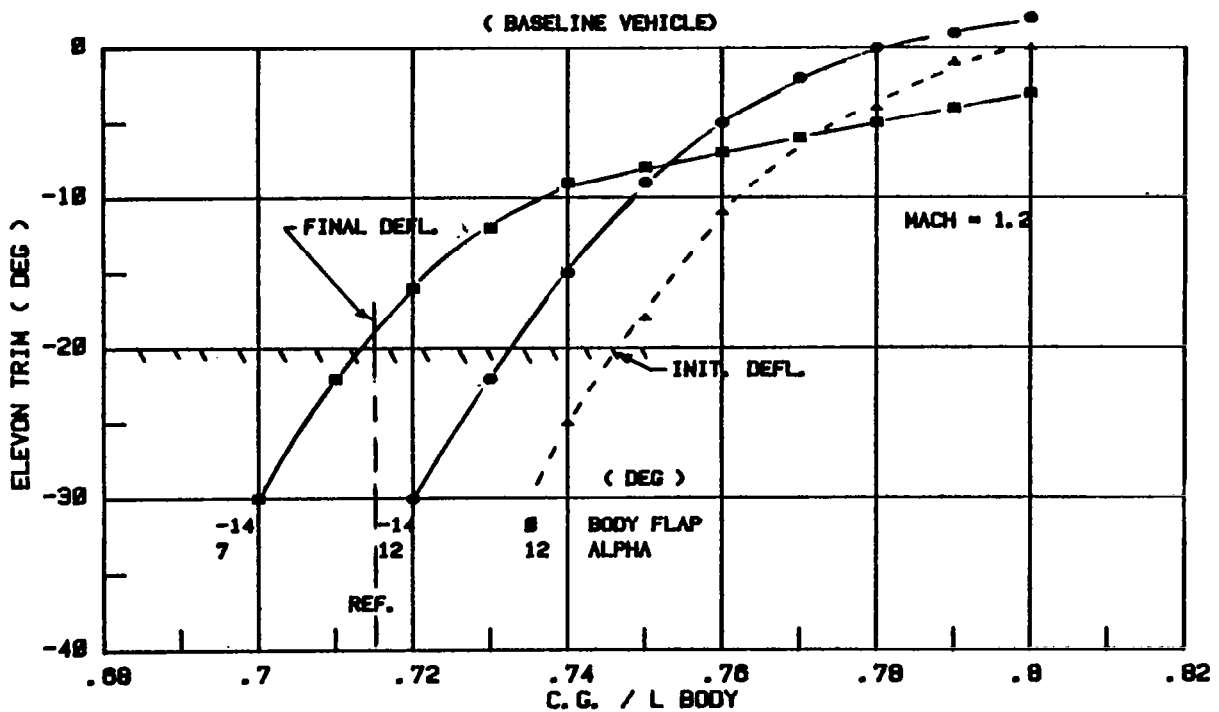
Figure 14: Transonic Trim Trade

(BASELINE VEHICLE)
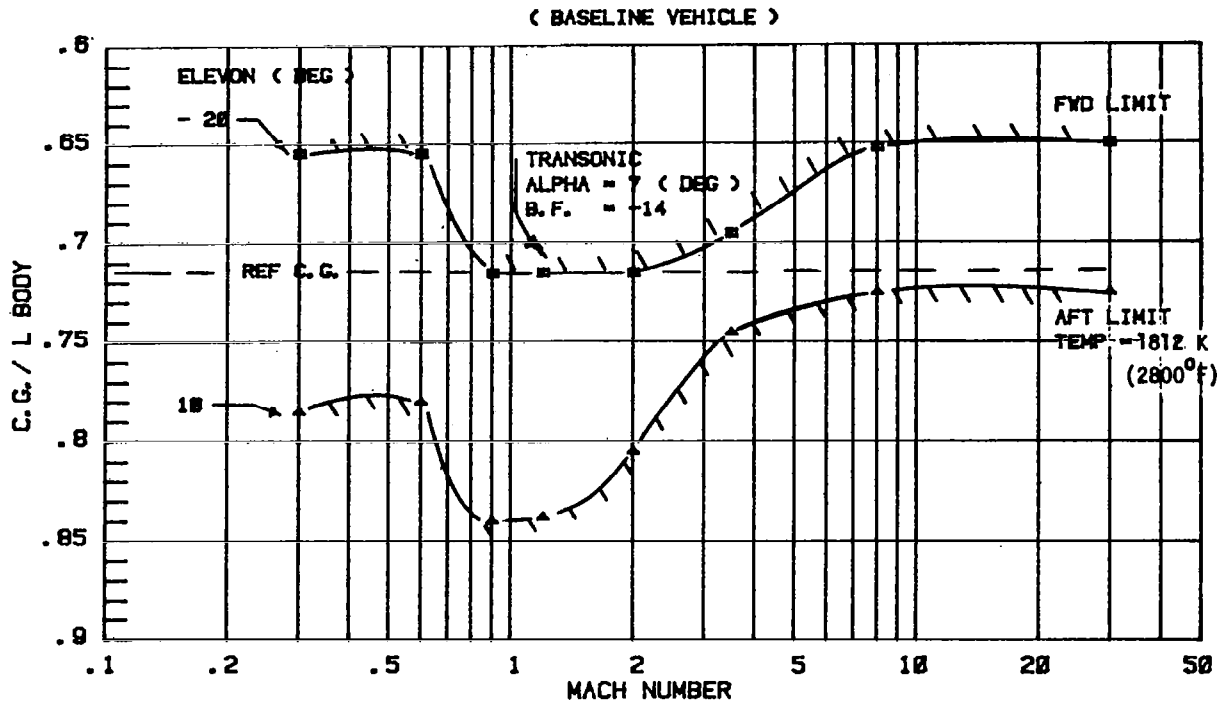
Figure 15:   Final Operational C.G. Limits
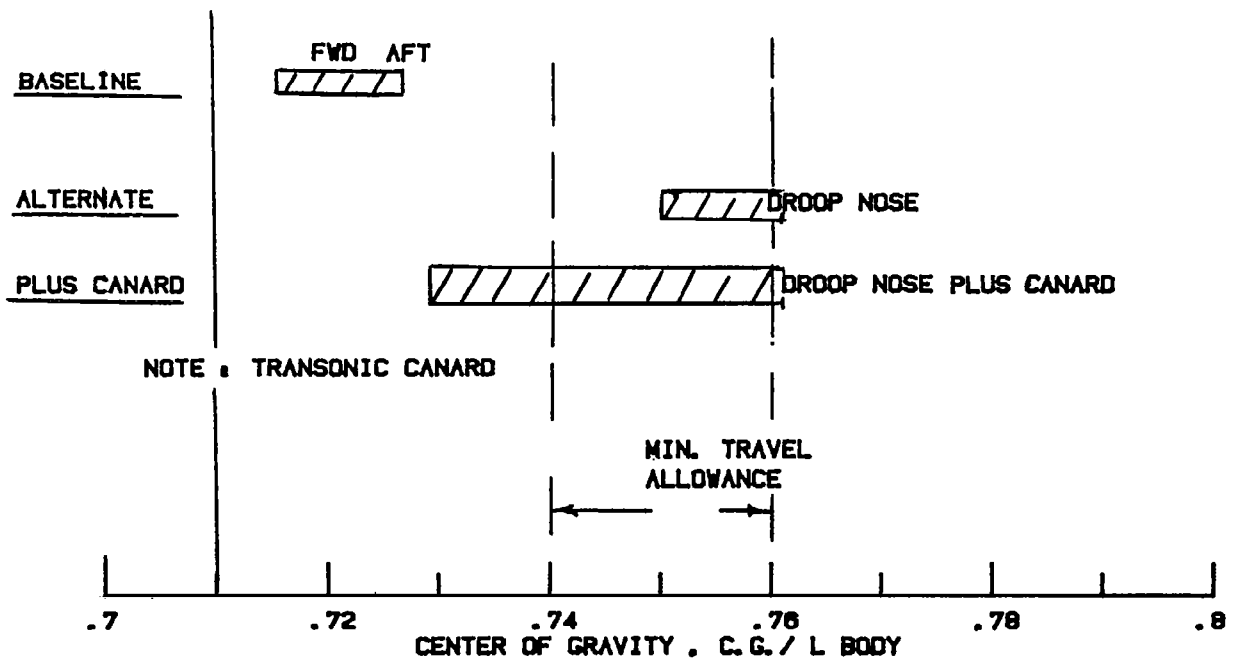
Figure 16: Summary C.G. Limits
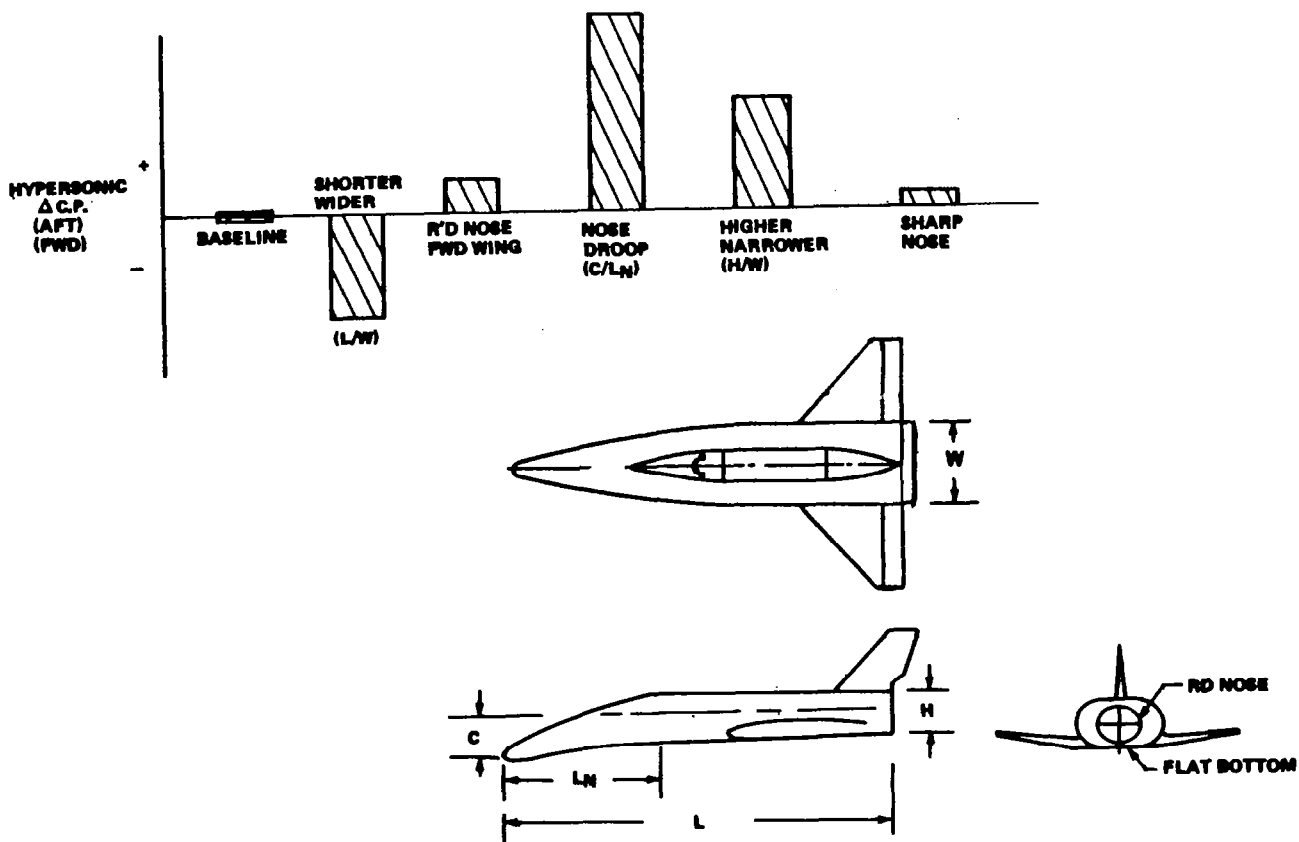
Figure 17:   Definition Body Configuration Trades
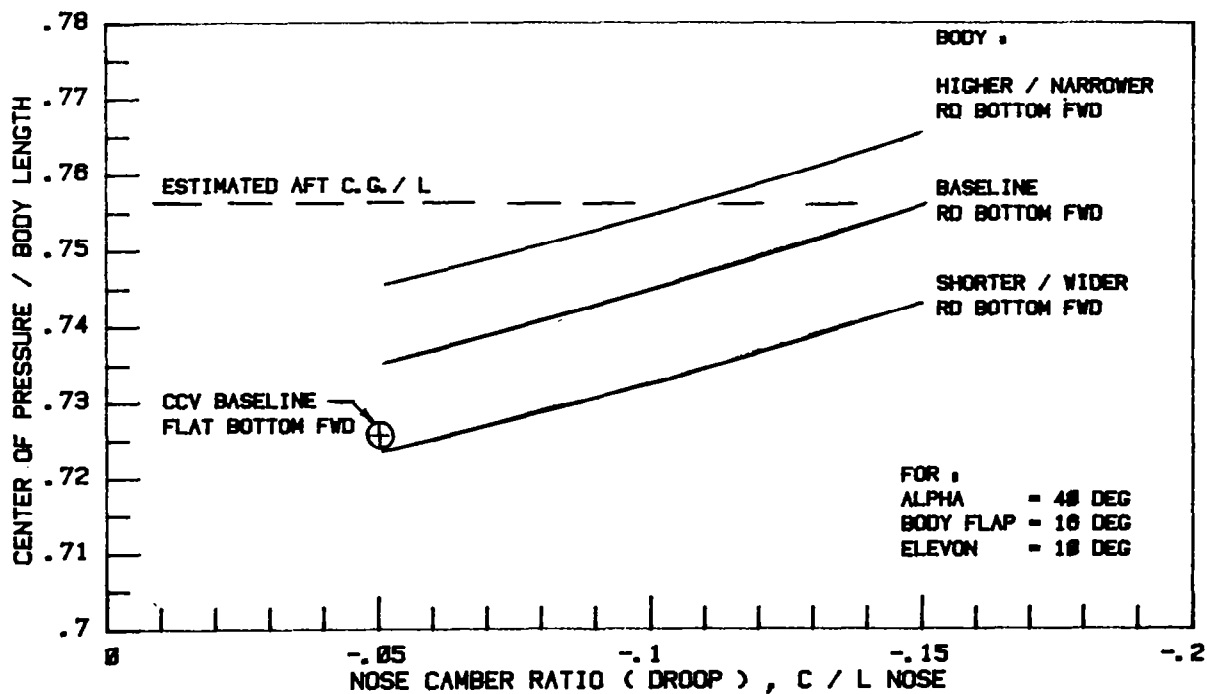
Figure 18:   Hypersonic C.P./Configuration Trade

48
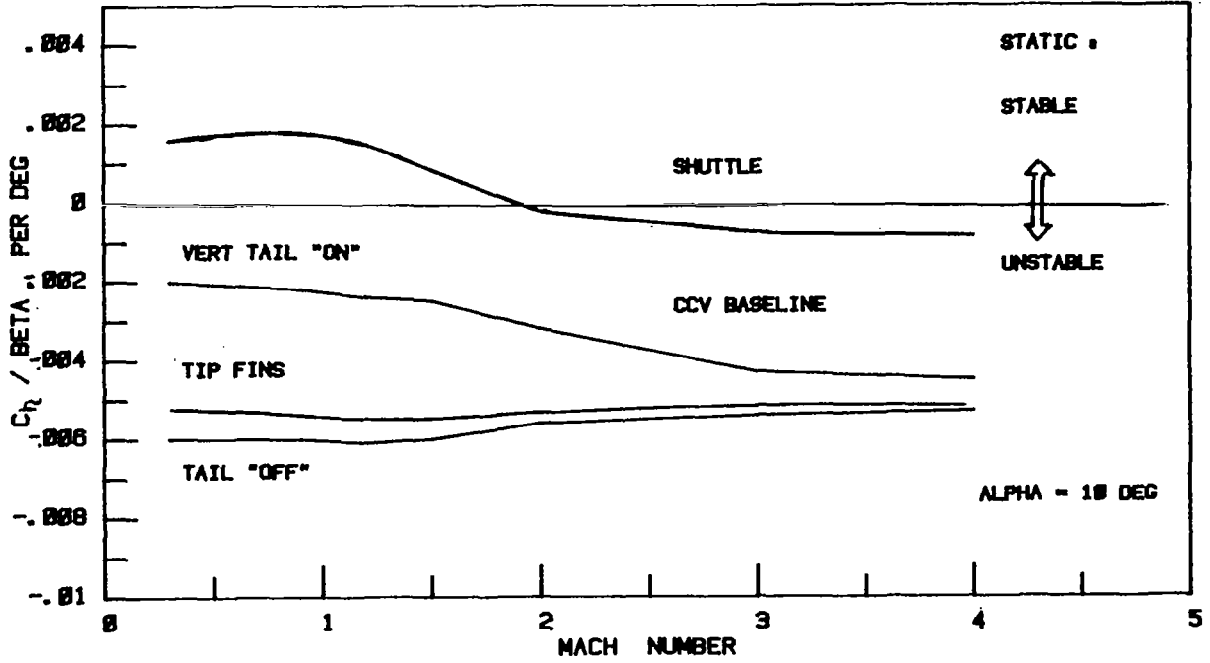
Figure 19: Directional Stability/Mach Trend
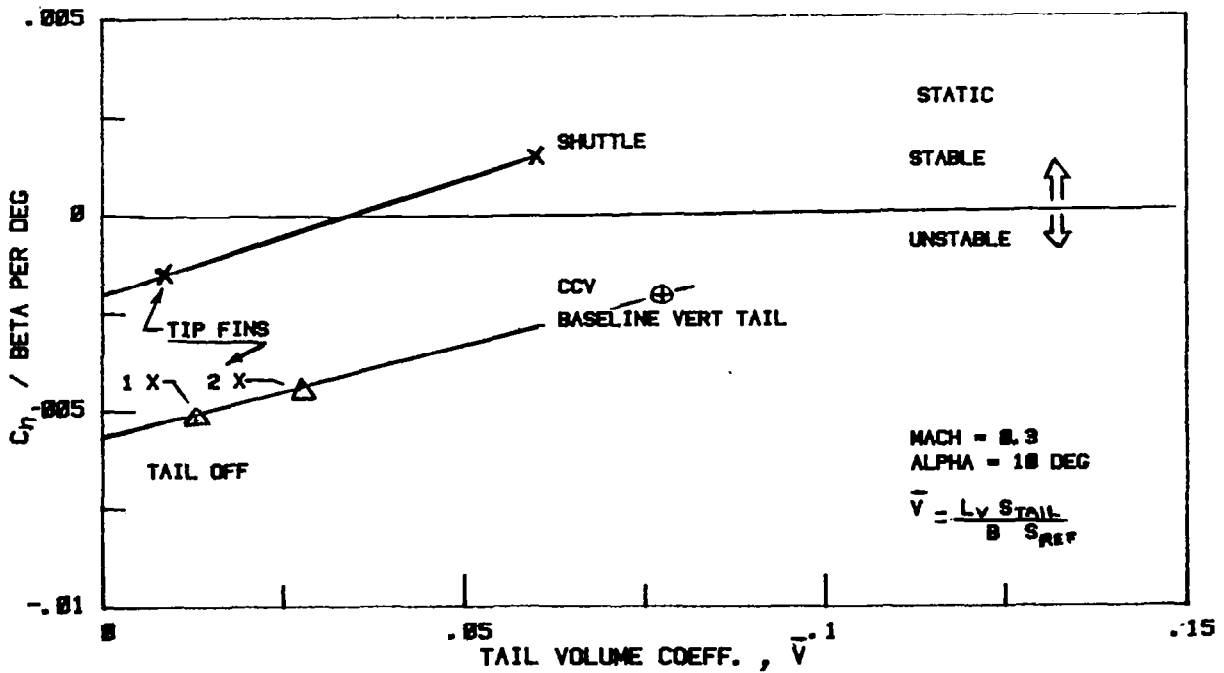
Figure 20: Subsonic Directional Stability
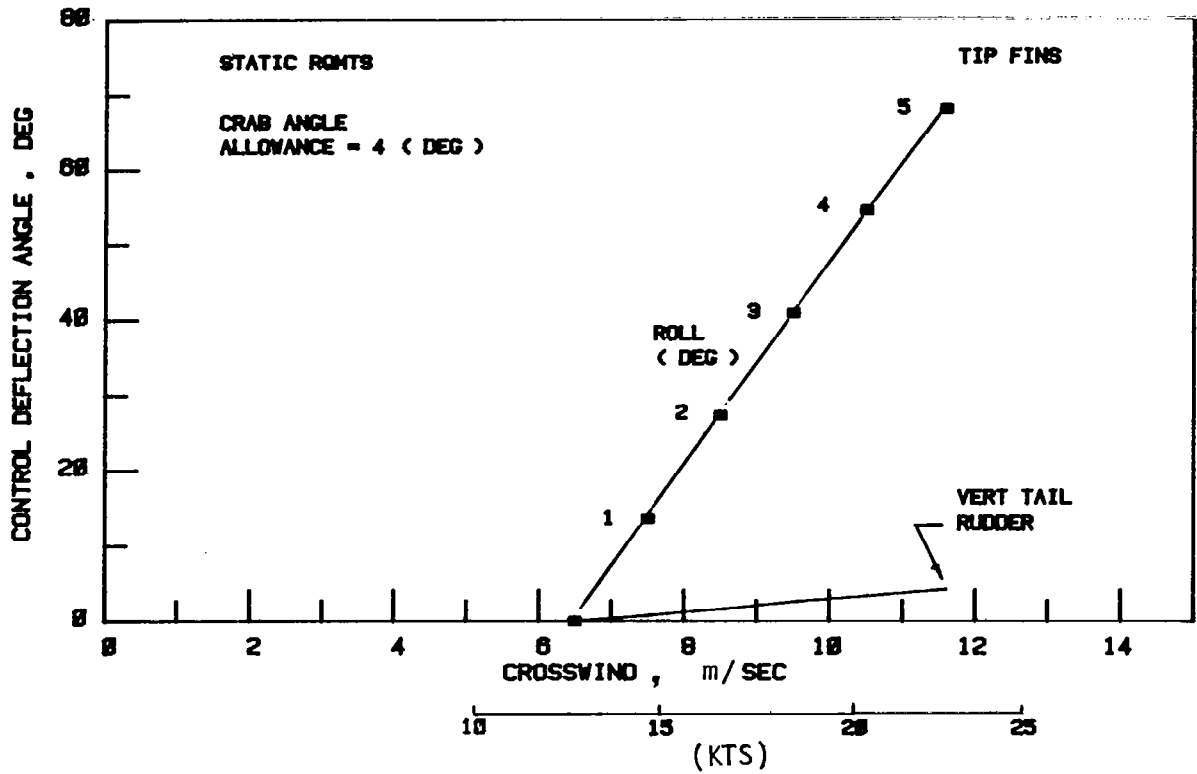
Figure 21:   Crosswind Approach Trim Control
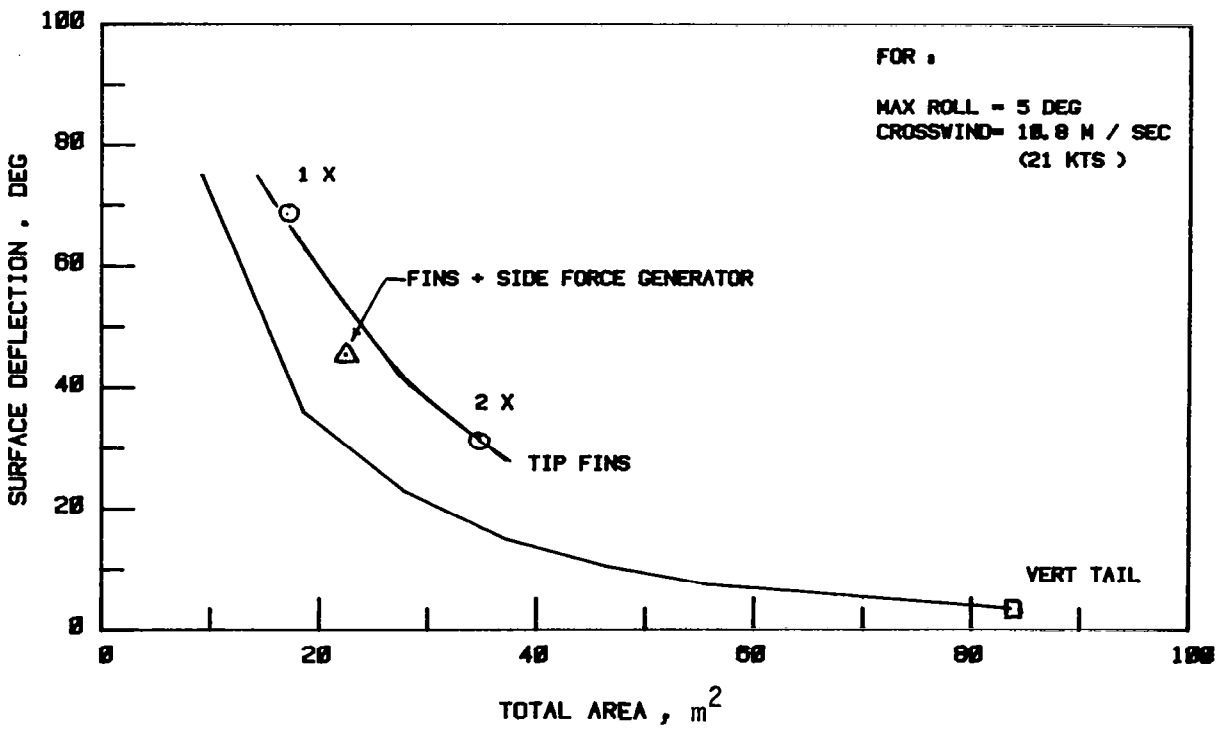
Figure 22:   Crosswind Approach/Control Trade

50
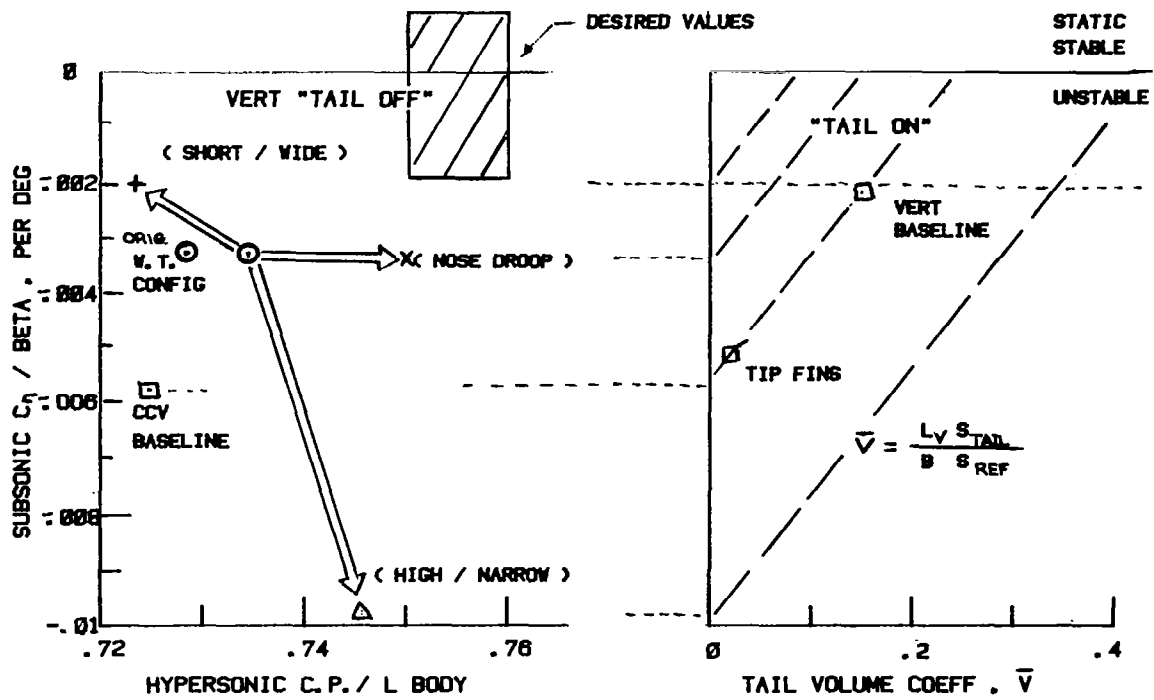
Figure 23: Summary Body Configuration Trades
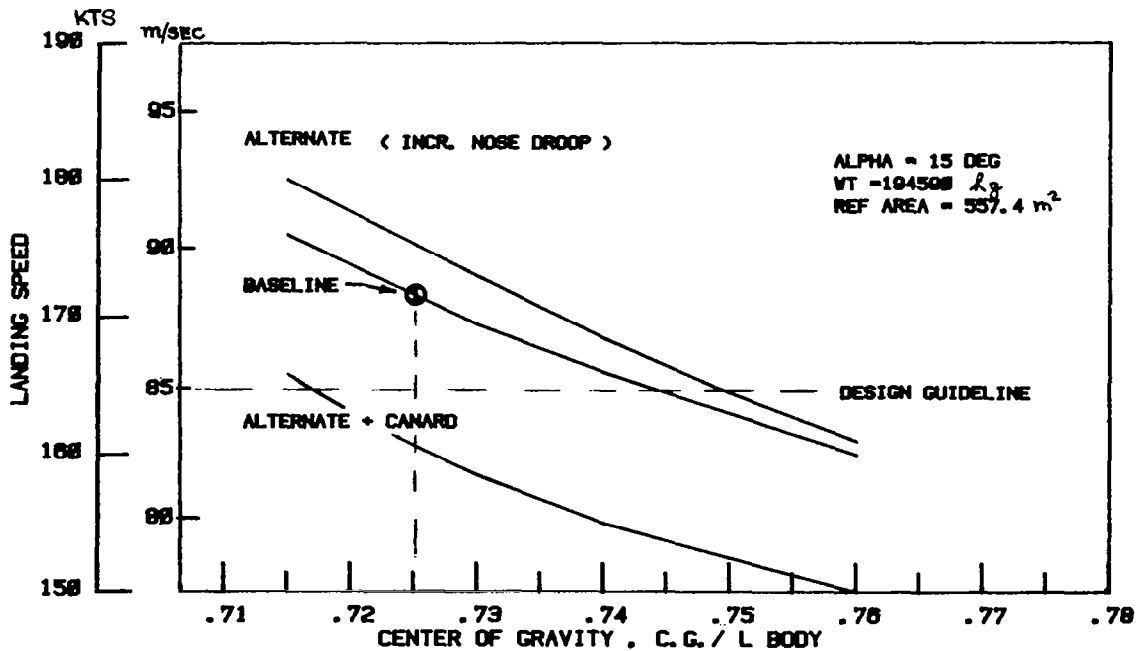
Figure 24: Summary Landing Speed
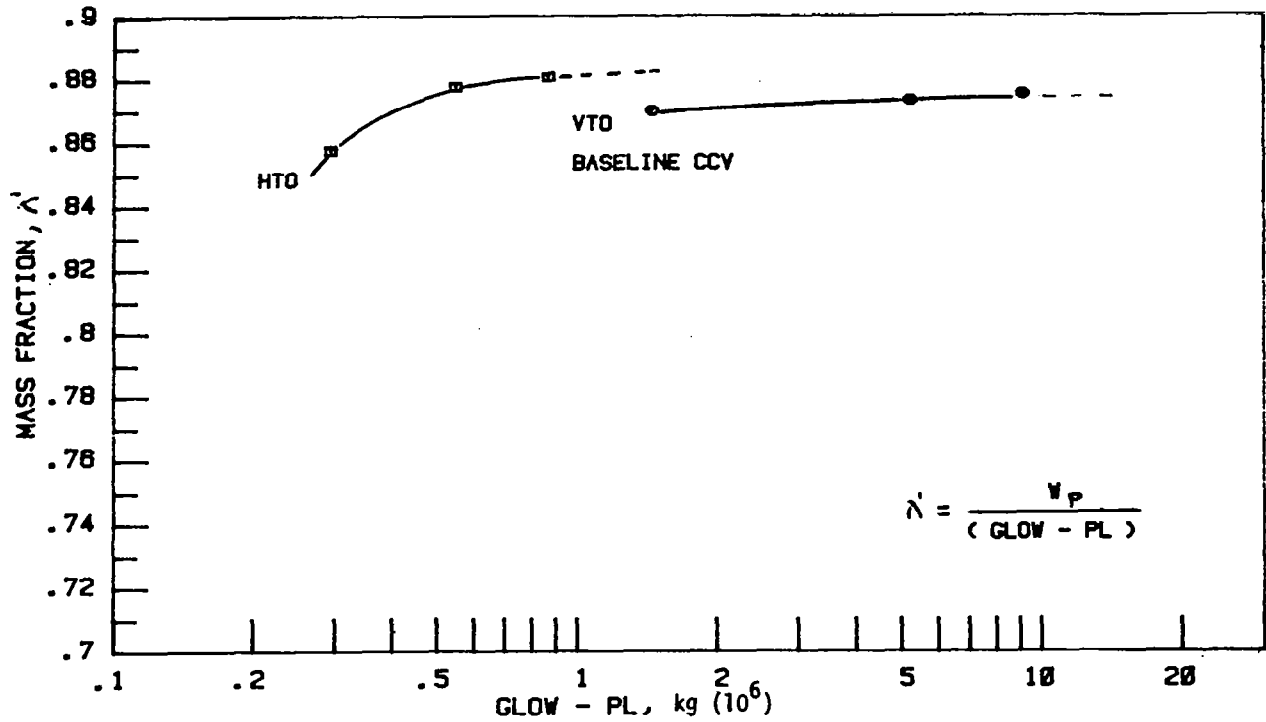
Figure 25: Mass Fraction/Glow Trend

$$\lambda' = \frac{W_P}{(\,GLOW - PL\,)}$$

CONFIG.	PAYLOAD t	GLOW kg (10^6)	INERT WT kg (10^3)	USEFUL PROPELLANT kg (10^6)	L_{BODY} m	WING SPAN m	REF. WING AREA m^2	MOMENT OF INERTIA kg m^2 (10^6)		
								PITCH	YAW	ROLL
Baseline CCV	17	1.45	188	1.26	66.8	37.2	557	39	50	11
Scaled Up Versions Of CCV	80	5.21	653	4.49	101.2	69.2	1934	315	437	122
	160	9.12	1,118	7.82	121.0	90.5	3312	770	1136	366

Figure 26: Scaled Vehicles for Large Payloads
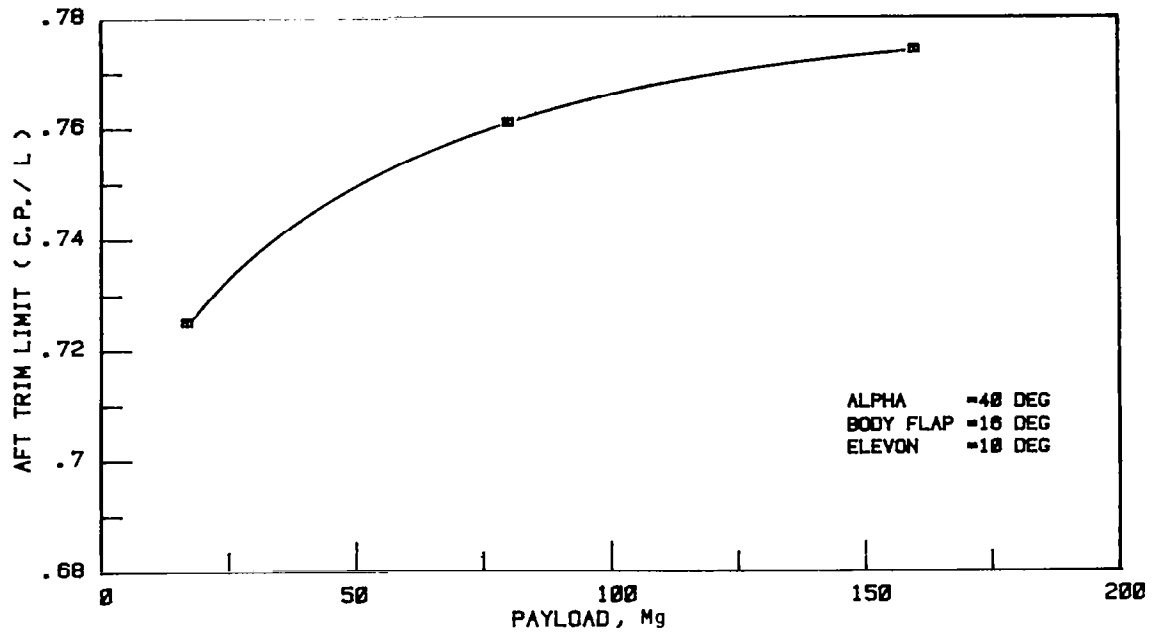
Figure 27: Hypersonic Aft Limit/PL Trade
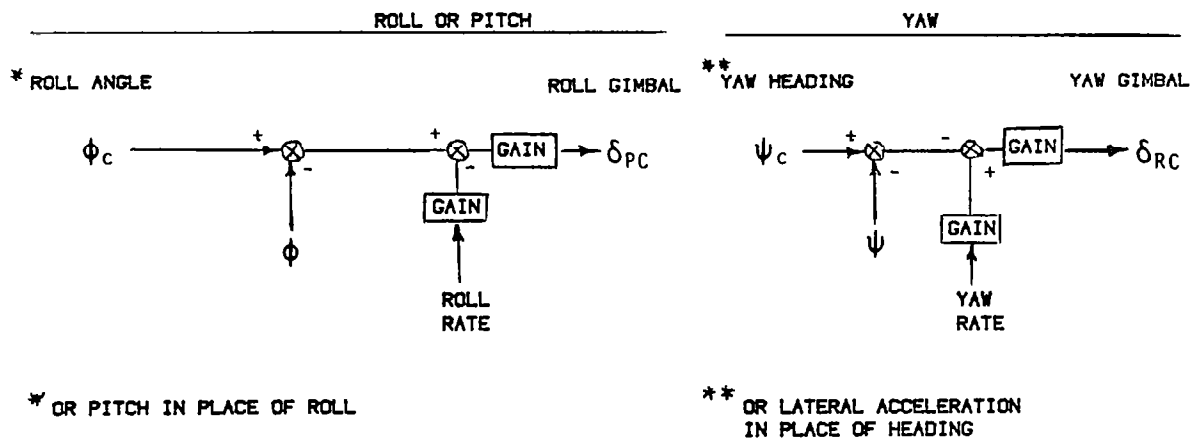
Figure 28: Ascent Control System
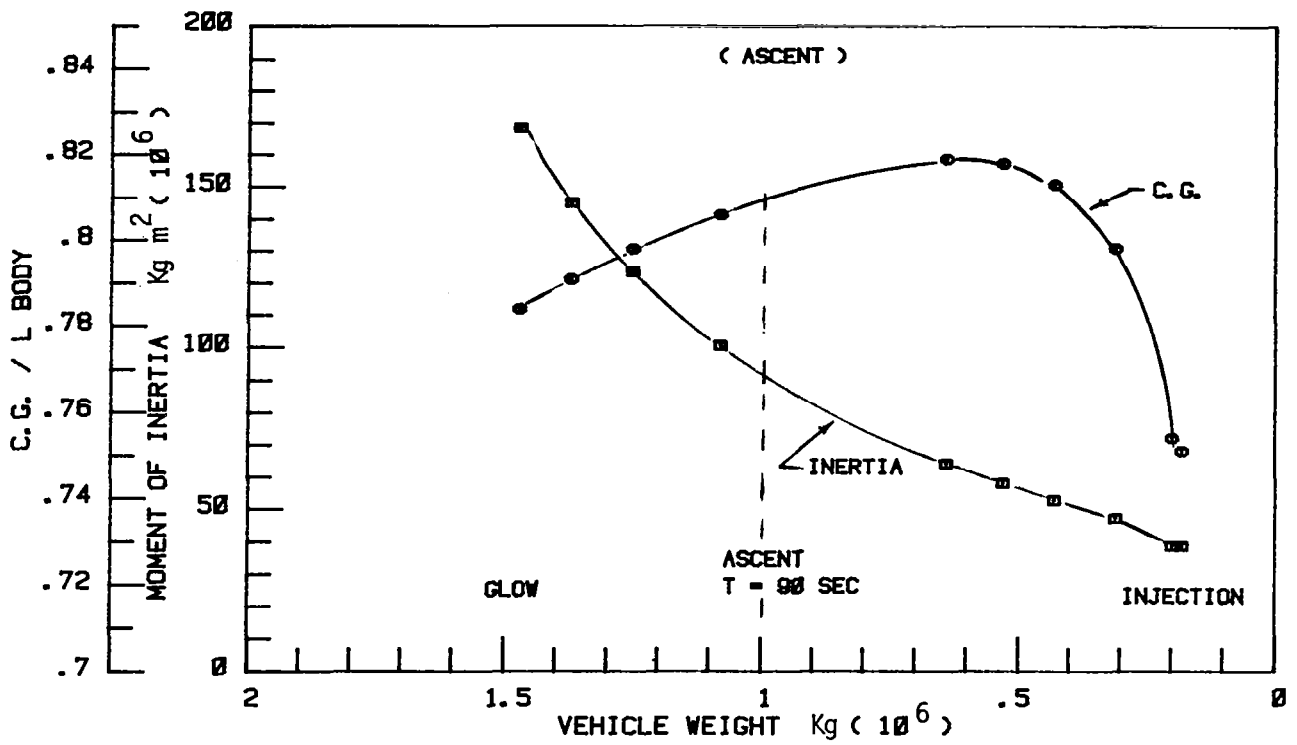
Figure 29: Inertia/C.G. Travel
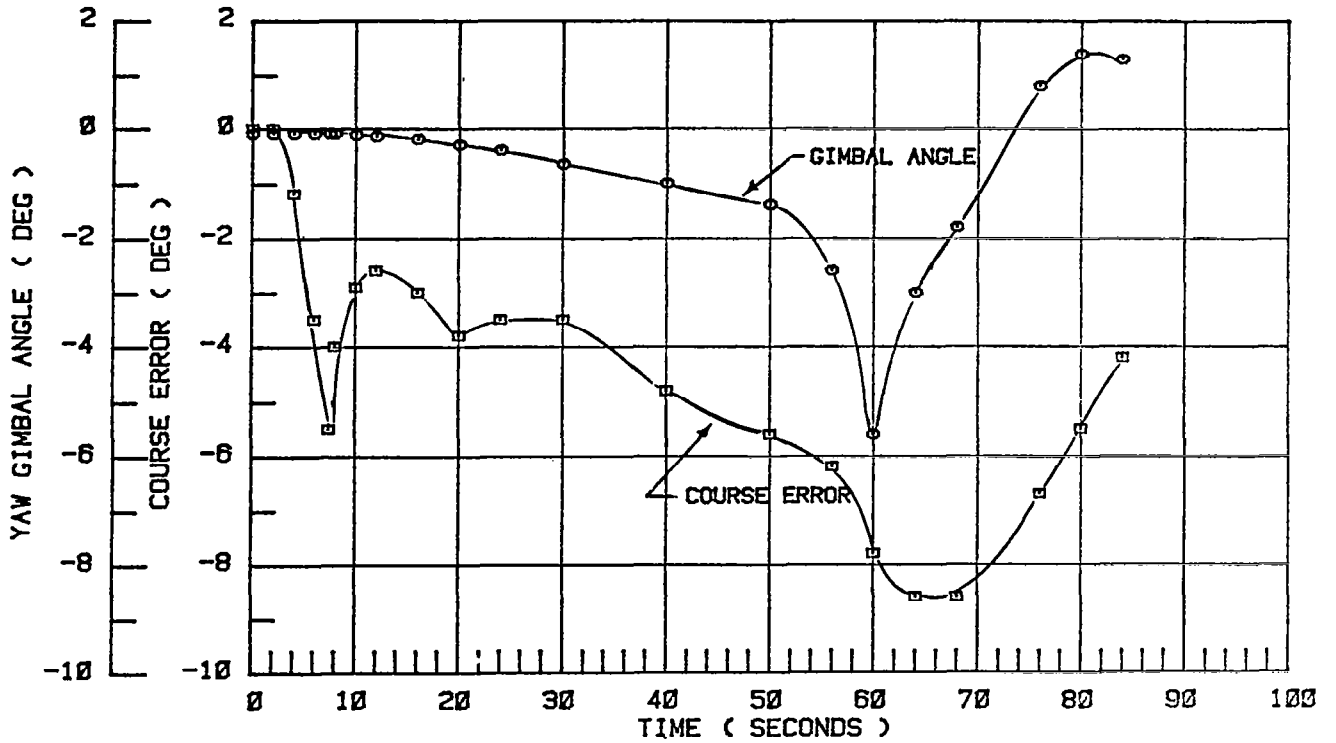
Figure 30: Ascent Quartering Headwind

54

WIND DIRECTION	q_a N/m^2 X DEG	q_β N/M^2 X DEG	ELEVON H. M. PER SIDE Nm (10^6)	RUDDER HM Nm (10^6)	FLIGHT PATH ERROR DEG	HEADING ERROR DEG
No Wind	-30.4	0	.048	0	1.62	0
Headwind	140.7	0	-.282	0	6.18	0
Crosswind	-30.2	183.6	.0469	.3036	1.63	-7.72
45° From Headwind	128.0	128.0	-.1978	.1200	4.61	-5.46

Wind Peak Altitude = 9 KM

Figure 31: Ascent Simulations Through Wind Shears
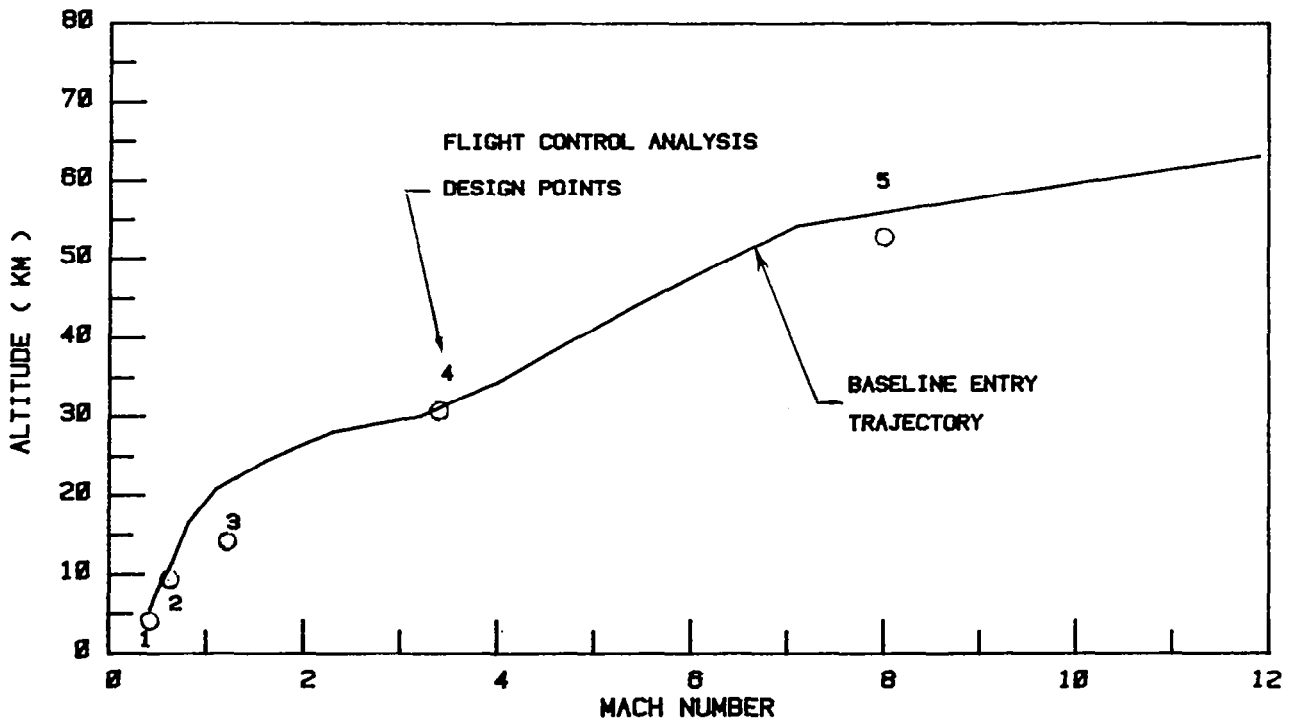
Figure 32: Selection of Design Points

PITCH AXIS ROOTS M = 0.3
BASELINE CCV-1 CONFIGURATION

C.G. LOCATION
    -0.715 L$_B$
    -0.725 L$_B$
    -0.735 L$_B$
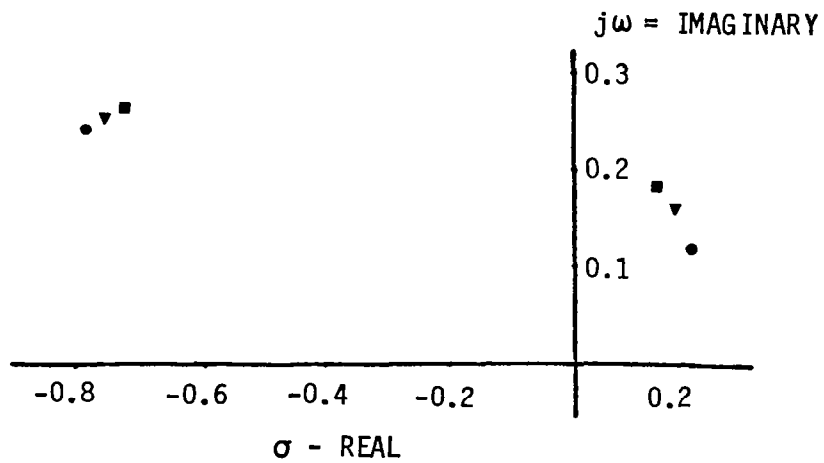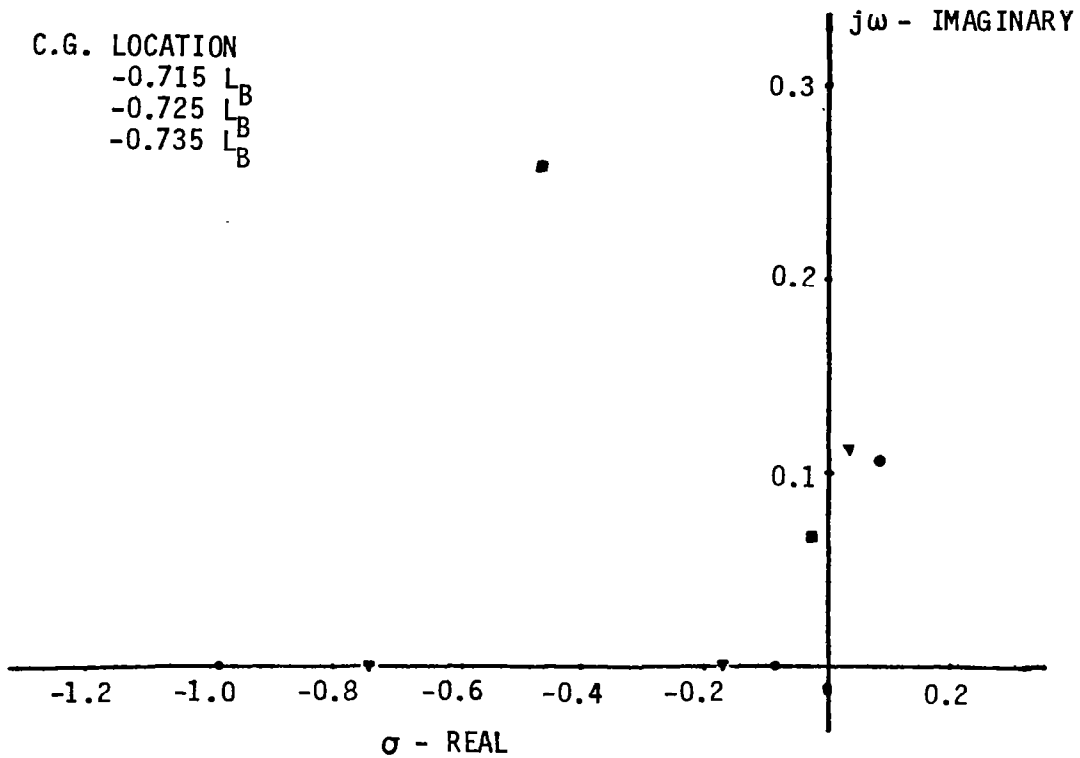
YAW-ROLL ROOTS - FREE AIRPLANE M = 0.3

Figure 33: Vehicle Dynamics Stick-Fixed C.G. Effect
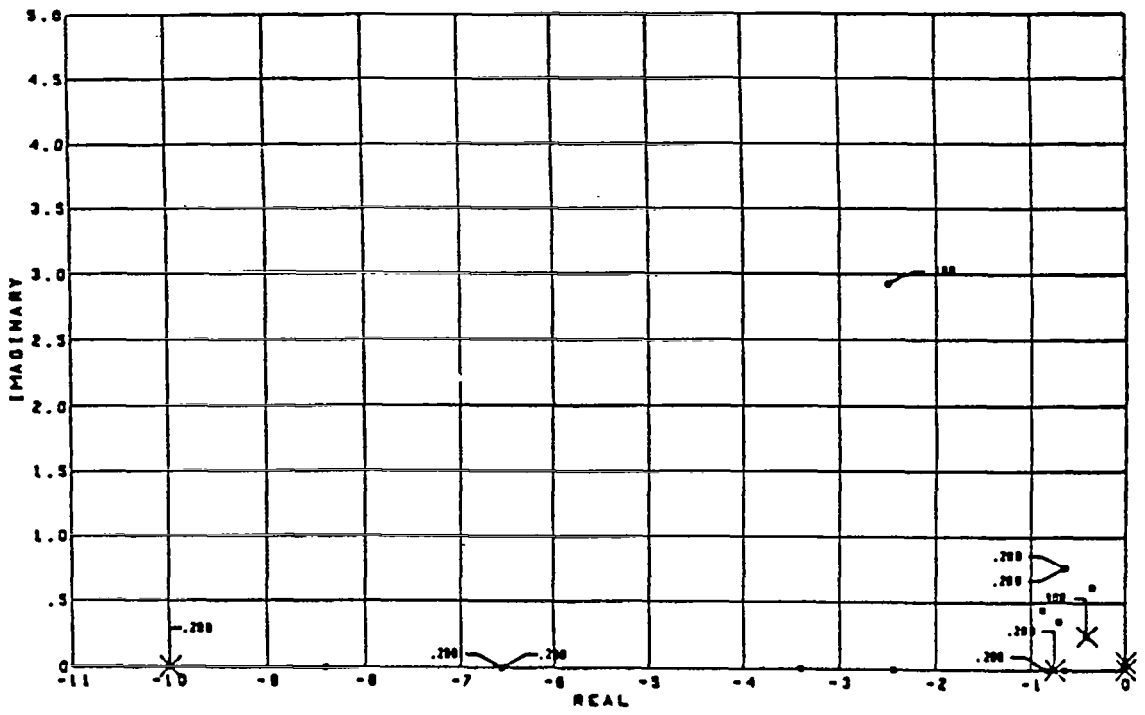
Figure 34:   Root Locus On - KE
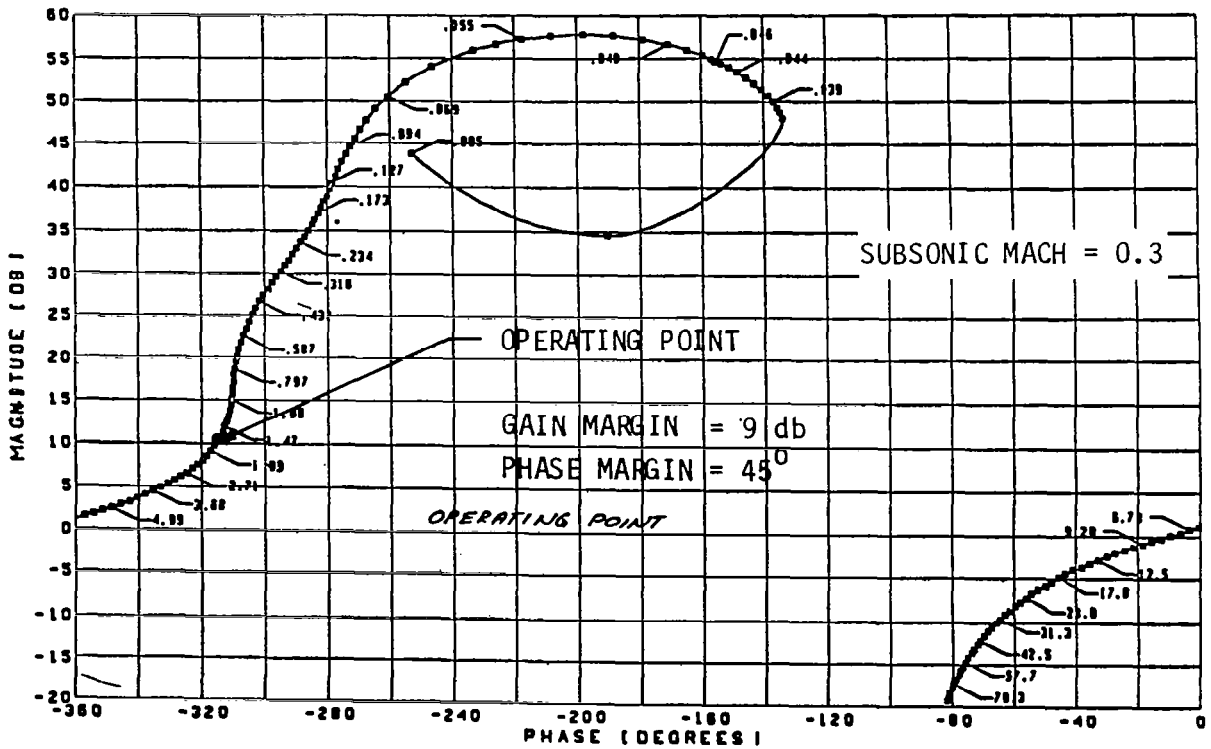
Figure 35:   Pitch Autopilot Frequency Response Design Point 1
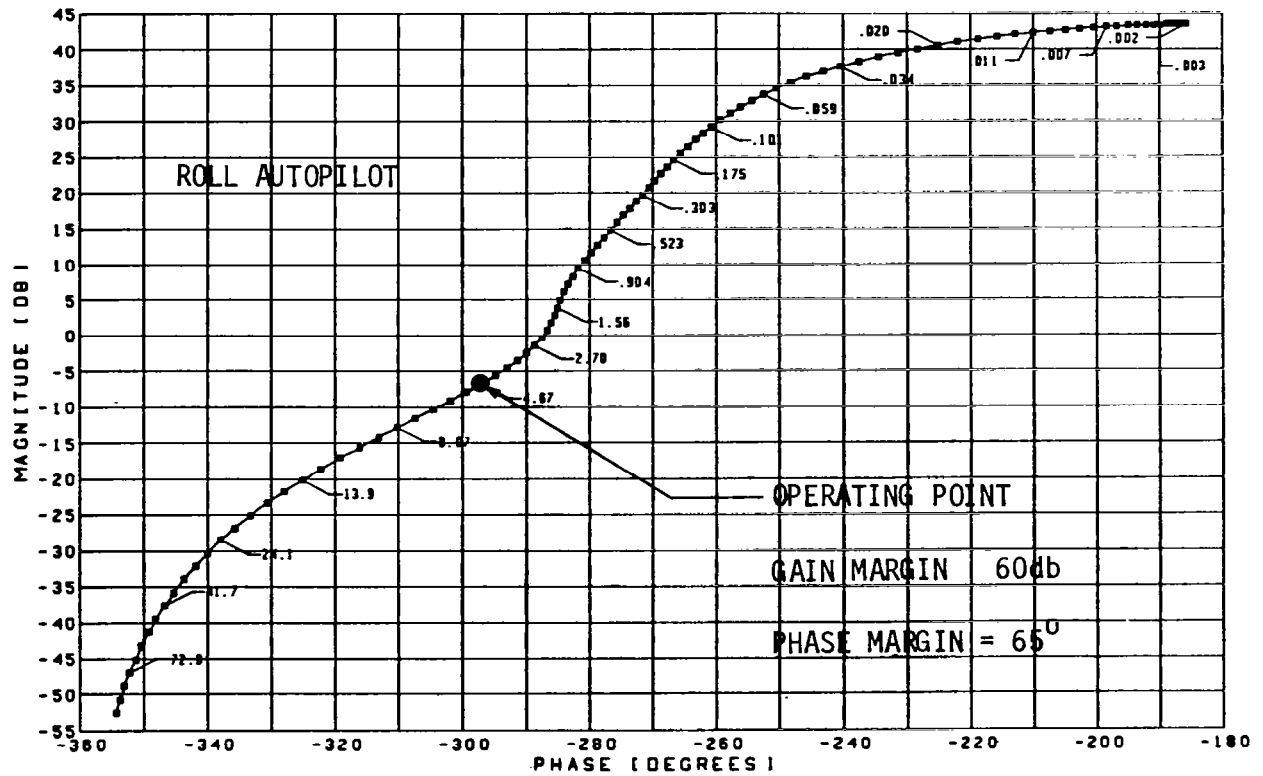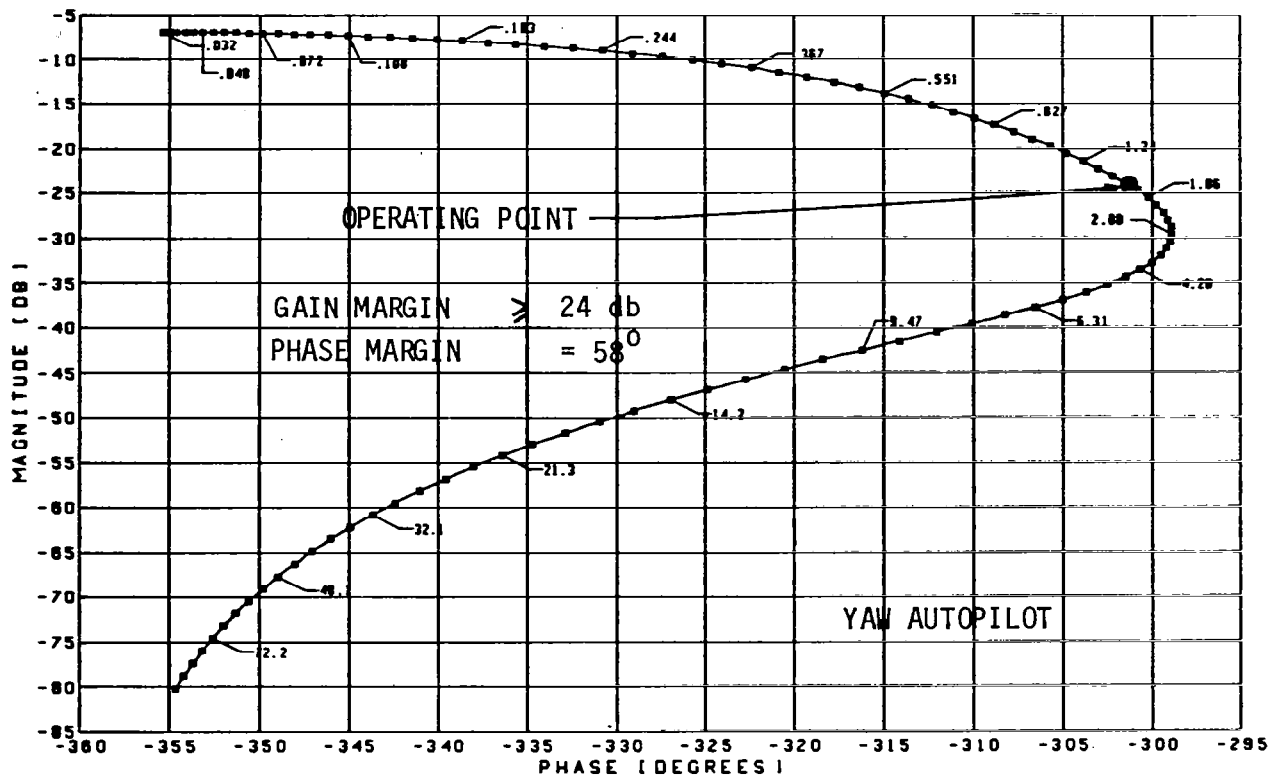
Figure 36: Frequency Responses Design Point 1 Subsonic Mach = 0.3

PITCH AND ROLL RESPONSES   FOR VARIOUS C. G. LOCATIONS

BASELINE CONFIGURATION   CCV 1

SUBSONIC MACH = 0.3
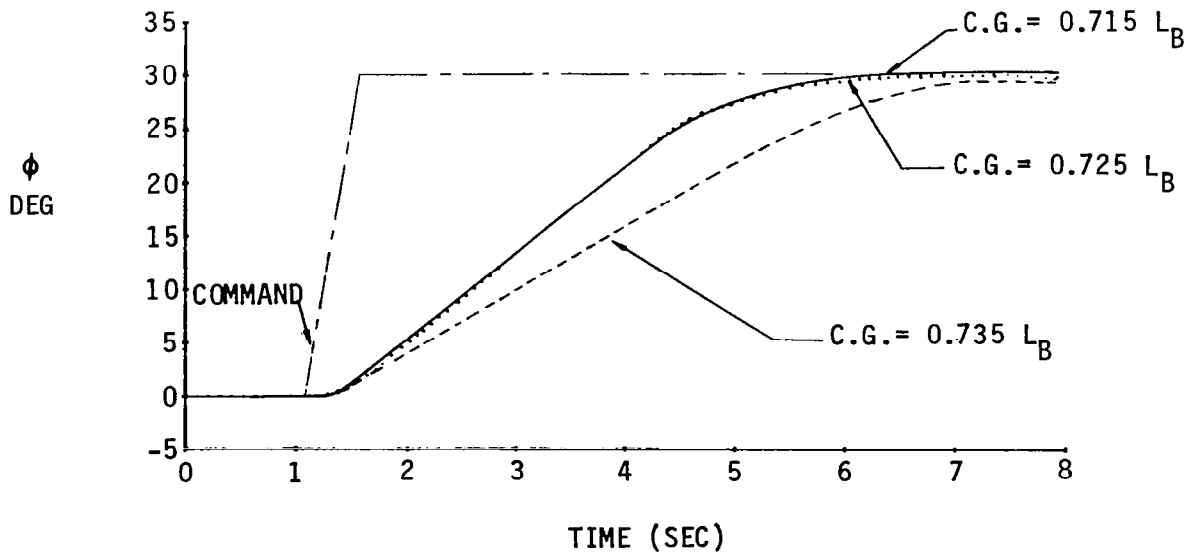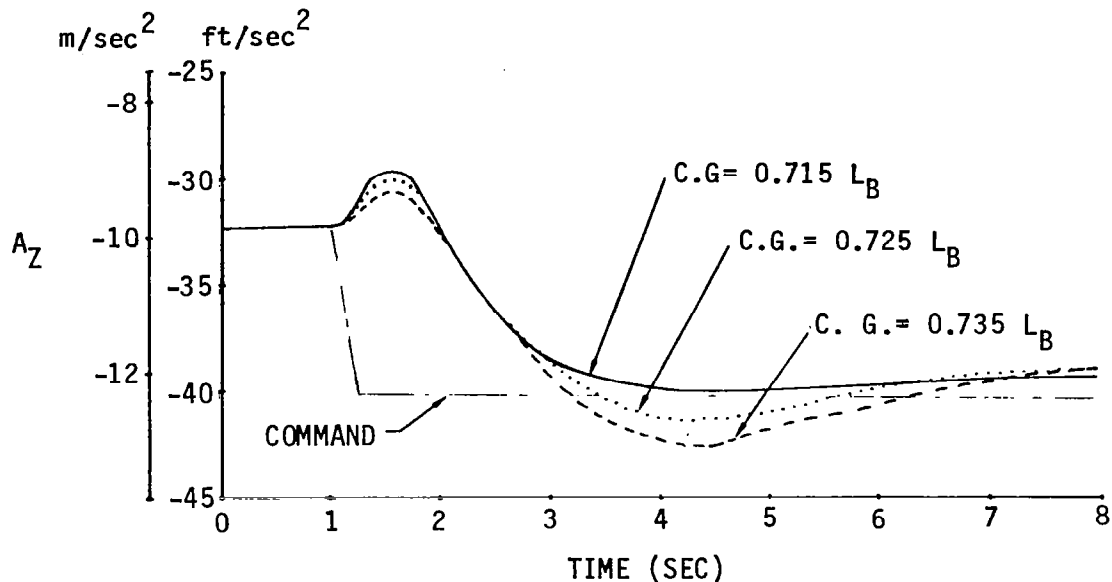
Figure 37: Pitch and Roll Responses for Various C.G. Locations

RUDDER   RT ELEVON   L ELEVON
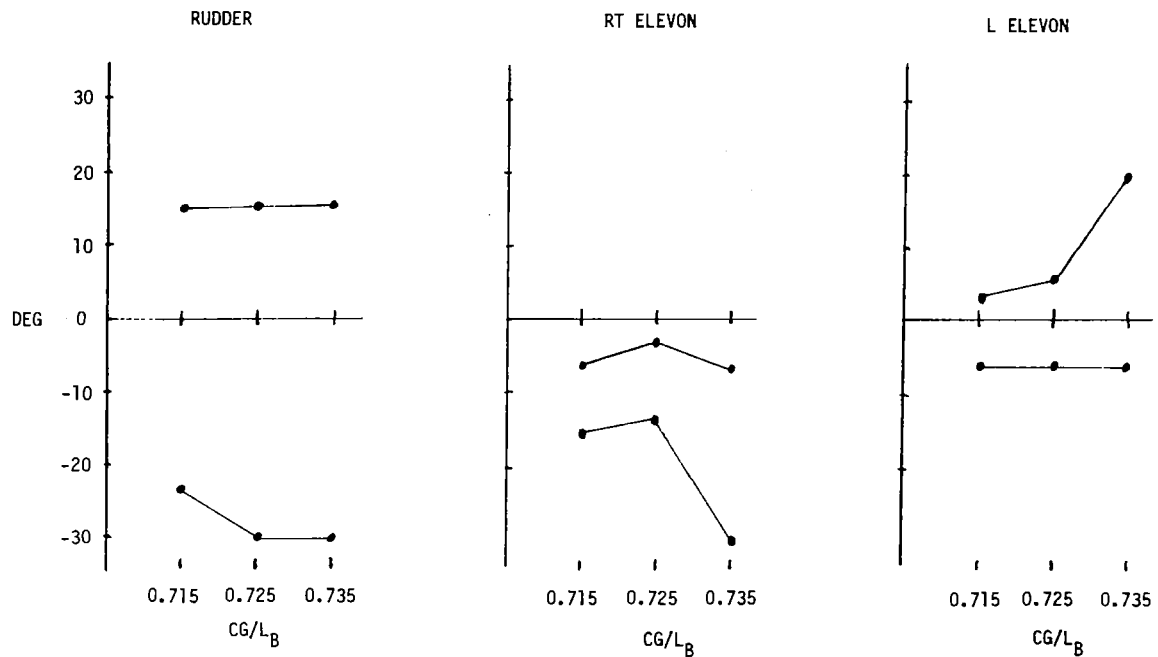
Figure 38:   Control Surface Requirements vs C.G. Subsonic

TRANSONIC MACH = 1.2 α = 7°
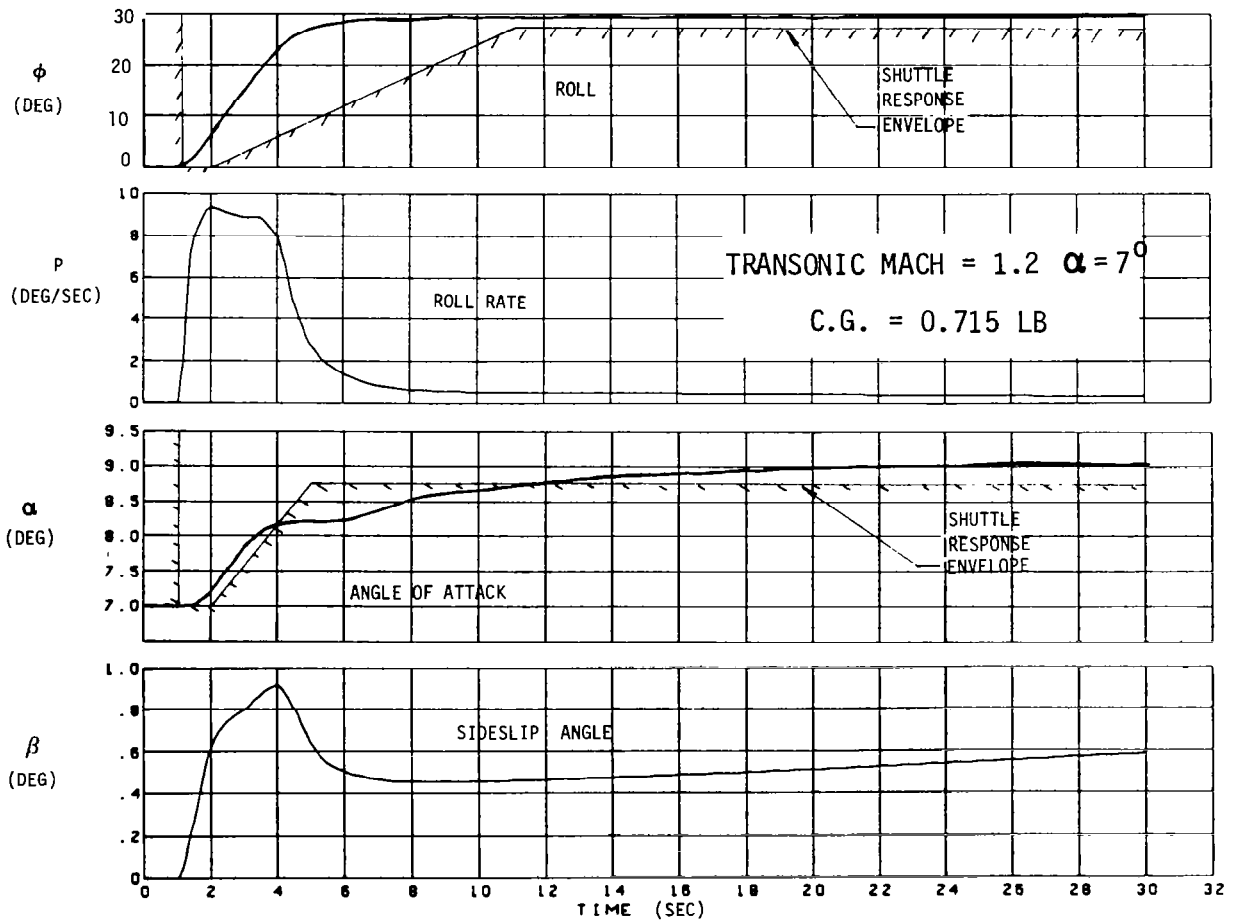
C.G. = 0.715 LB

Figure 39: Transient Responses — Design Points 3

60

TRANSONIC MACH = 1.2 $\alpha = 7^{O}$

C.G. = 0.715 LB

CONFIGURATION CCV 1

$\Delta \alpha = 2^{O}$ 30° ROLL

CONTROL SURFACES DEFLECTIONS
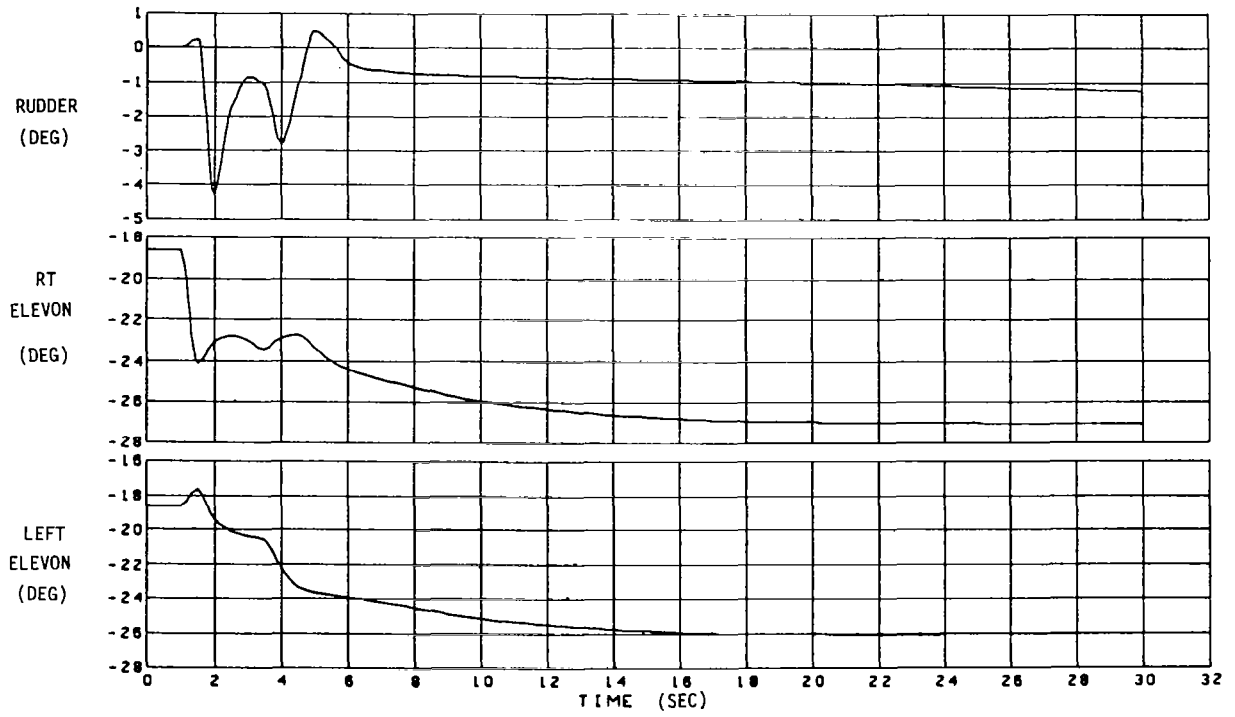
Figure 40:   Transient Responses - Design Point 3

C.G. = 0.715 LB

CONFIGURATION CCV 1

$\Delta\alpha = 2^0$ 30^0 ROLL COMMAND

COMMAND AFTER 1.2 SEC
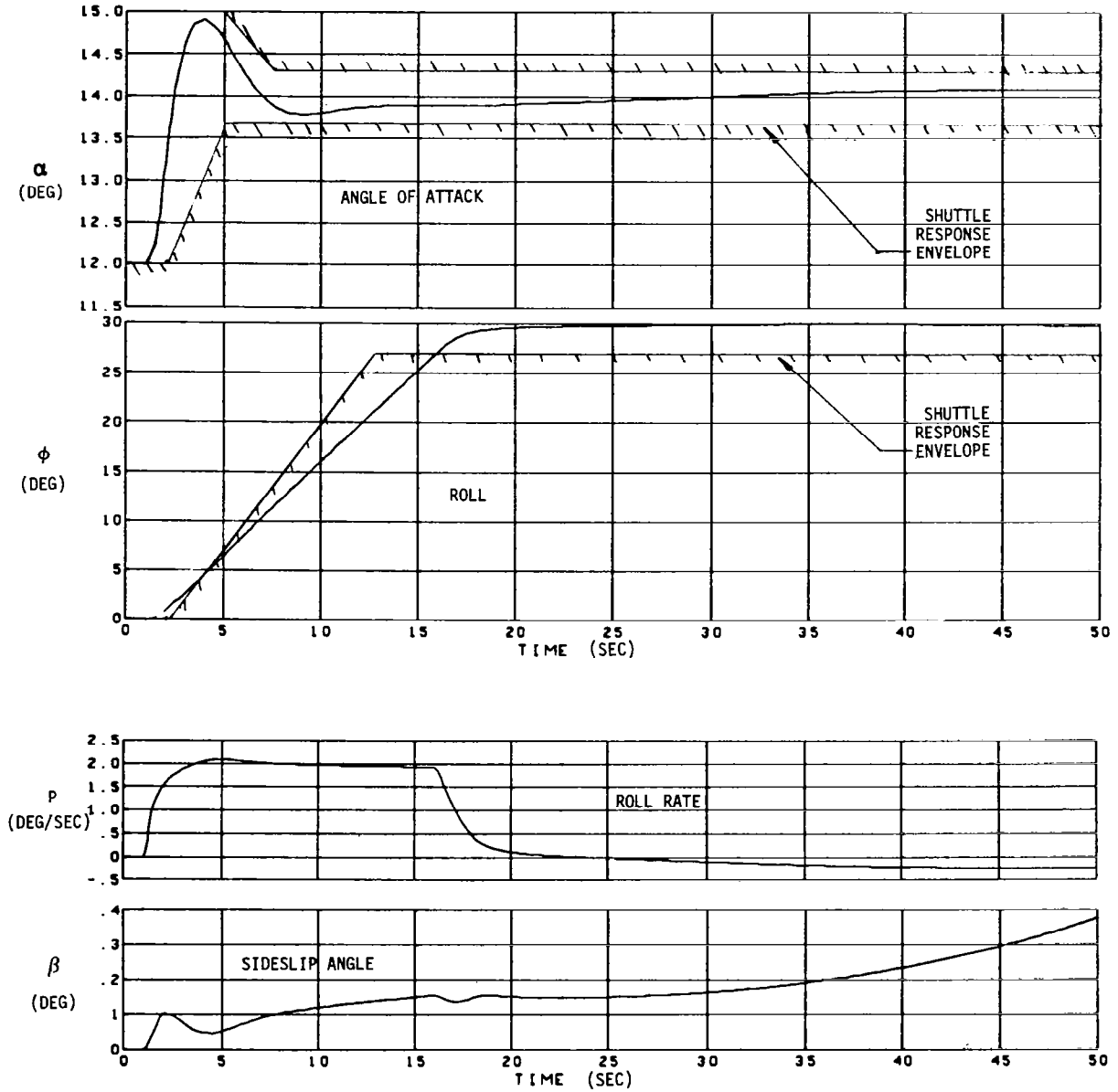
SUPERSONIC MACH = 3.5 $\alpha = 12^0$

Figure 41:   Transient Responses — Design Point 4
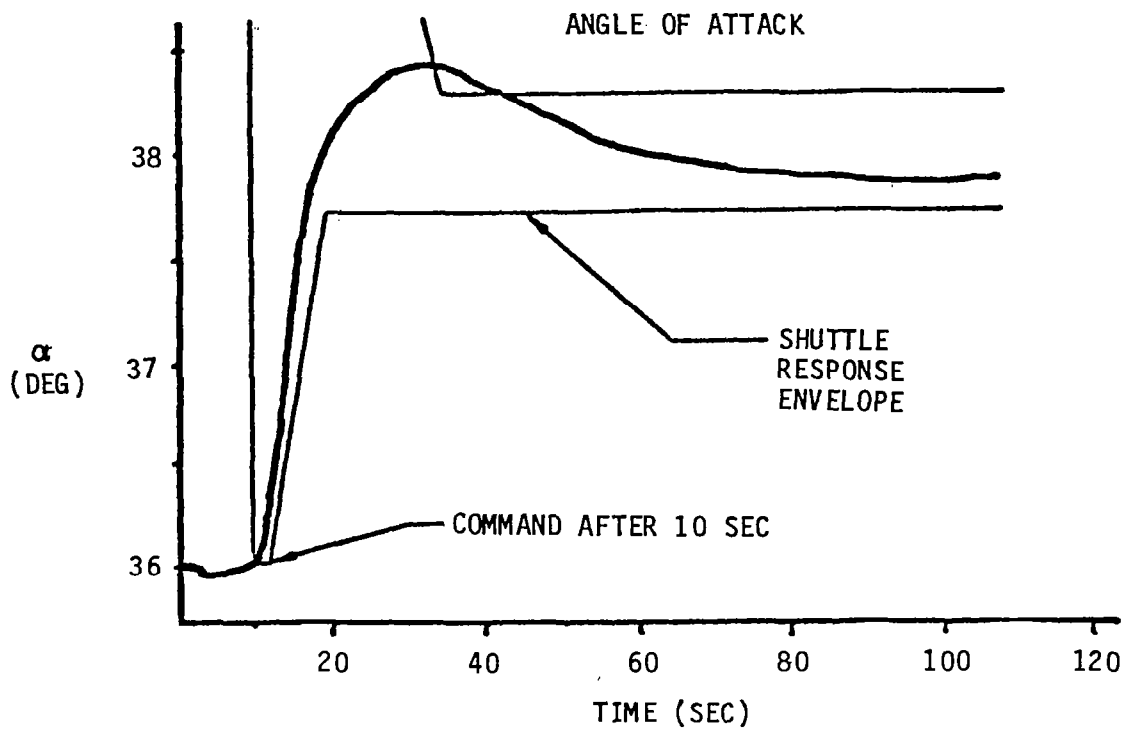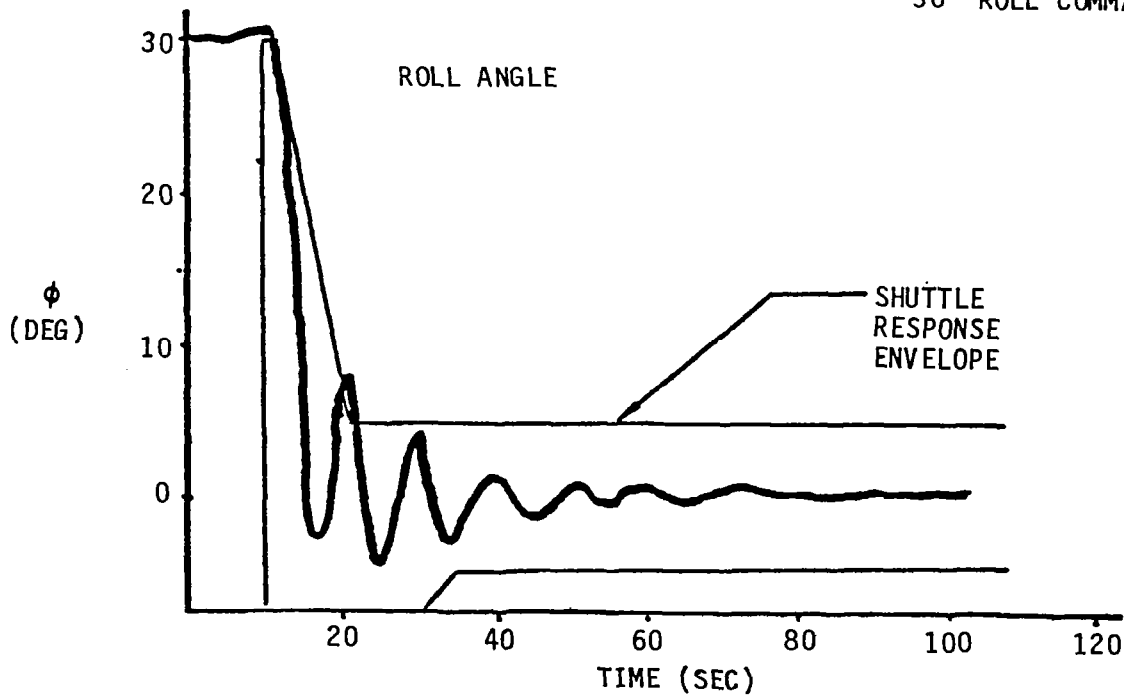
Figure 42: Transient Responses – Design Point 5

PITCH RESPONSE AT DESIGN POINTS

ANGLE OF ATTACK

α
(DEG)

SHUTTLE RESPONSE ENVELOPE

COMMAND AFTER 10 SEC MACH = 8.0

TIME (SEC)

α
(DEG)

ANGLE OF ATTACK

MACH = 3.5

SHUTTLE
RESPONSE
ENVELOPE

TIME (SEC)

α
(DEG)

ANGLE OF ATTACK MACH = 1.2

SHUTTLE
RESPONSE
ENVELOPE

TIME (SEC)

A_Z m/sec^2 ft/sec^2

SHUTTLE
RESPONSE
ENVELOPE

NORMAL ACCELERATION   MACH = 0.3

TIME (SEC)

BASELINE CCV-1 (C.G. = 0.715 L_B)
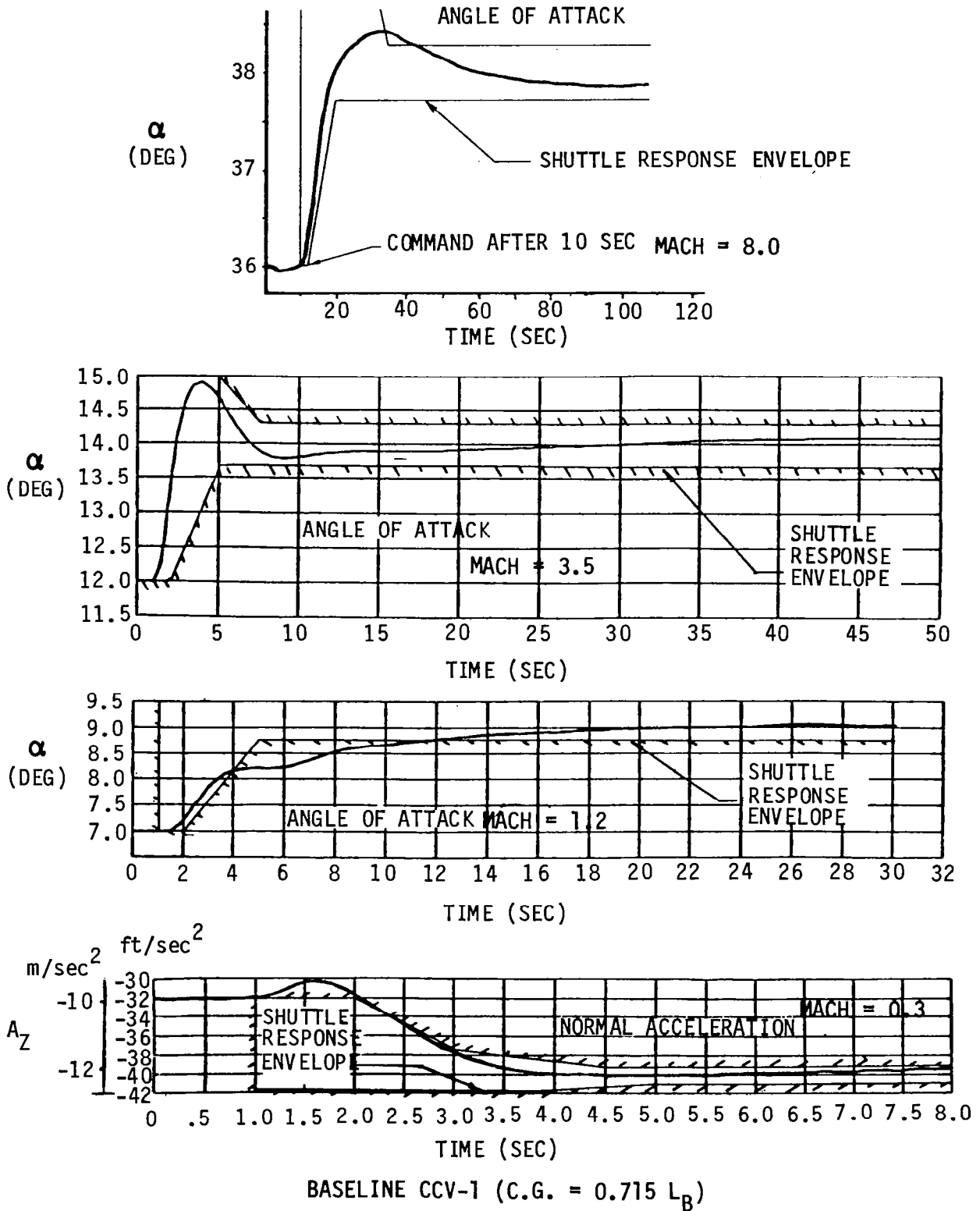
Figure 43:   Pitch Response at Design Points

64
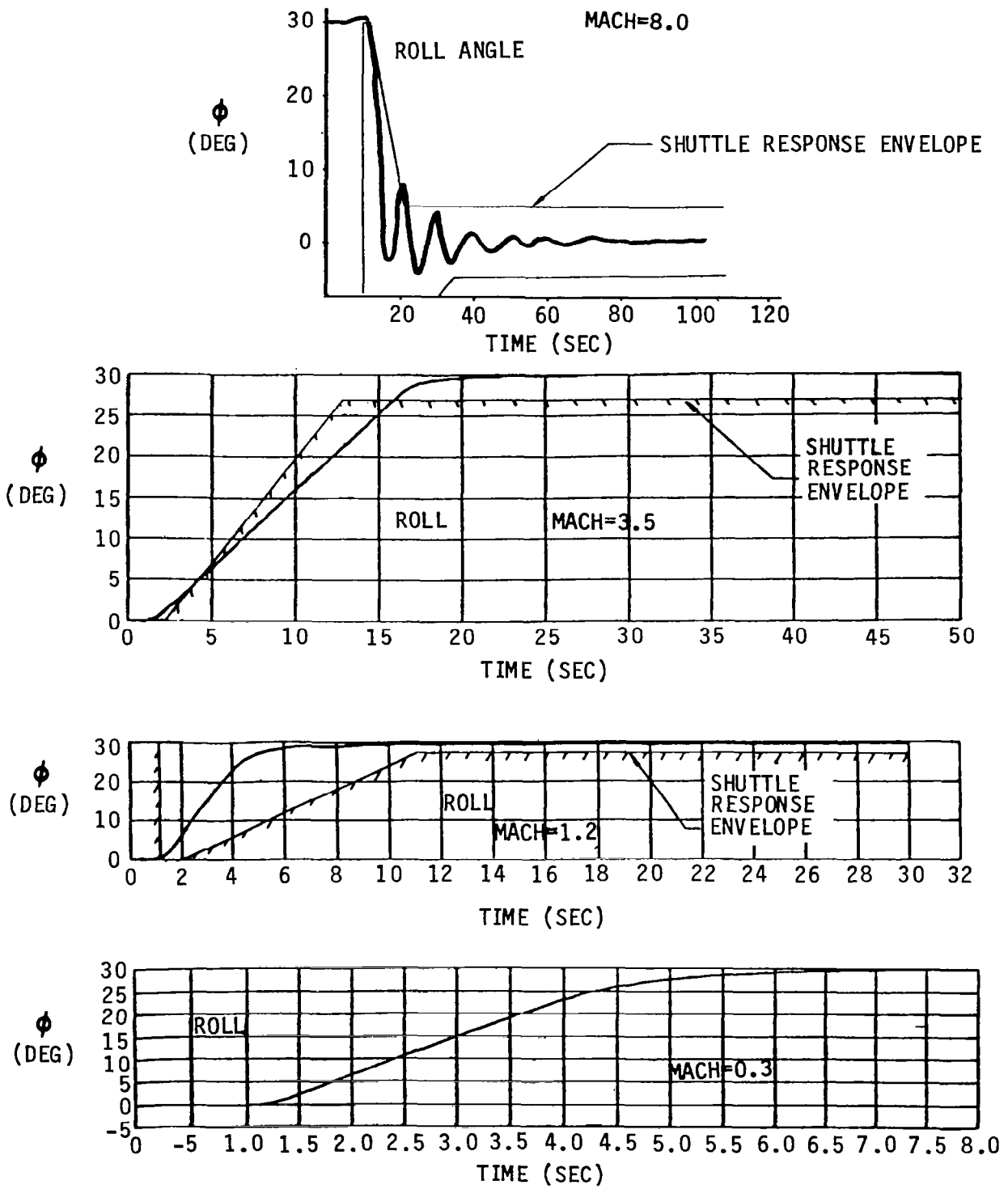
ROLL RESPONSE AT DESIGN POINTS
BASELINE CCV-1 (CG=0.715 L$_B$)

Figure 44: Roll Response at Design Points Baseline CCV-1 (CG=0.715 L$_B$)
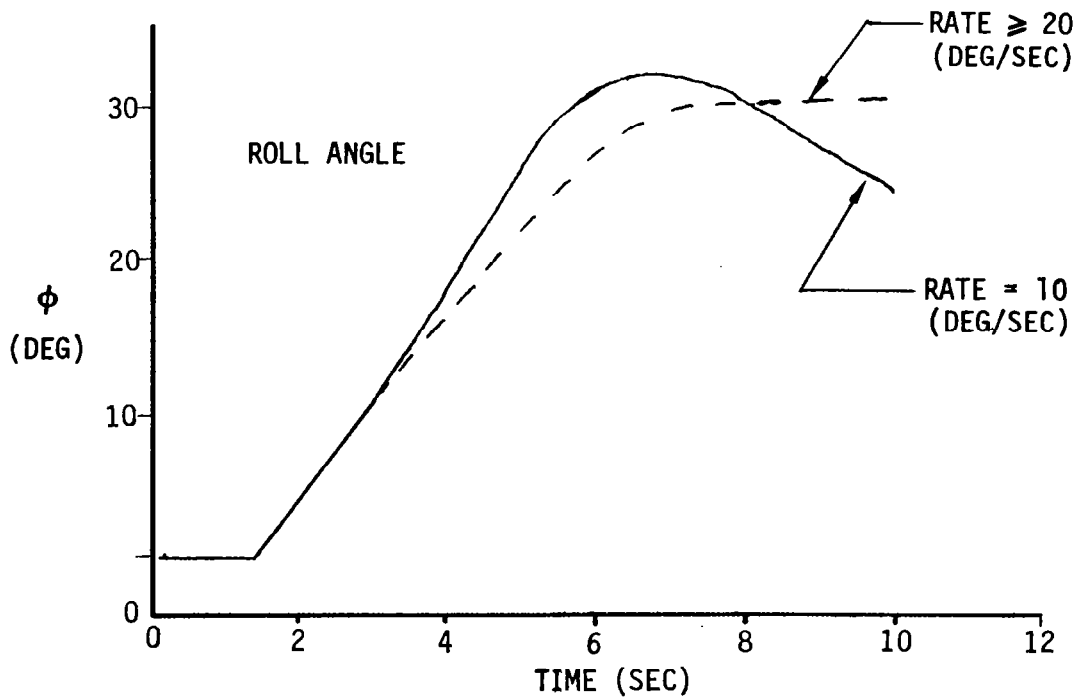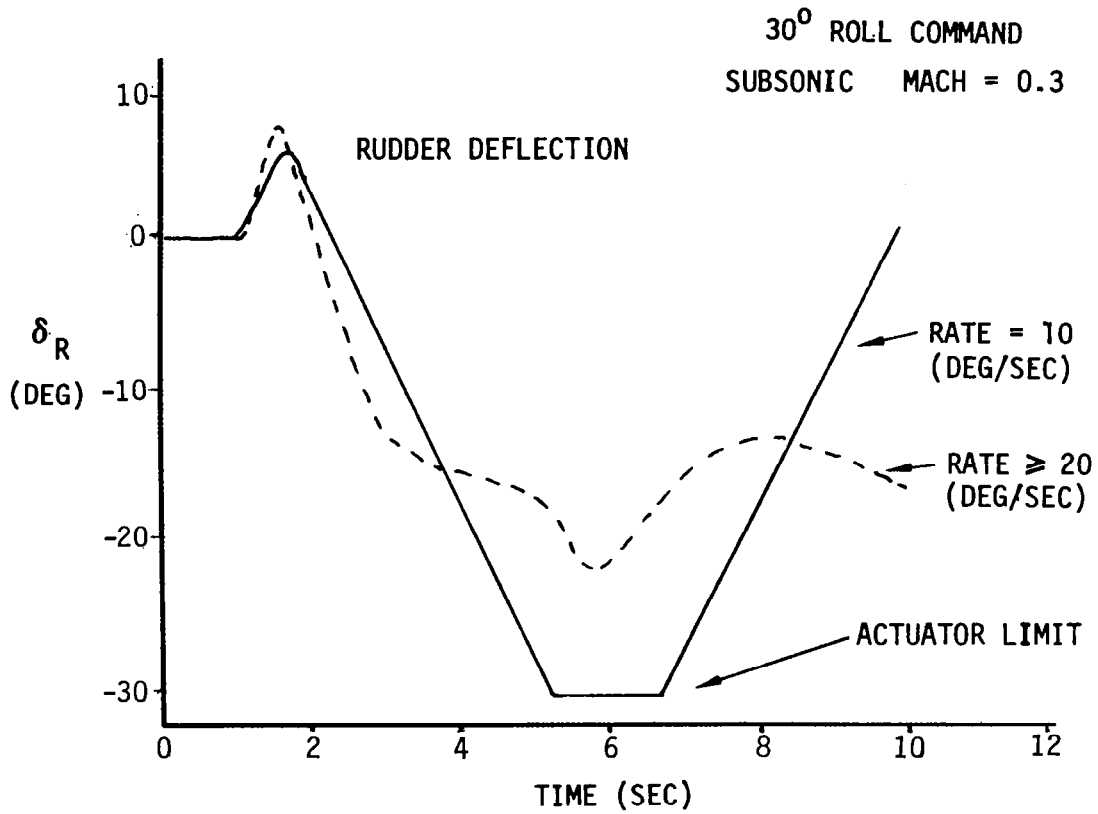
Figure 45: Actuator Rates Comparison

Figure 46: Pitch Maneuver Δα = 2° — Hypersonic Mach = 8.0
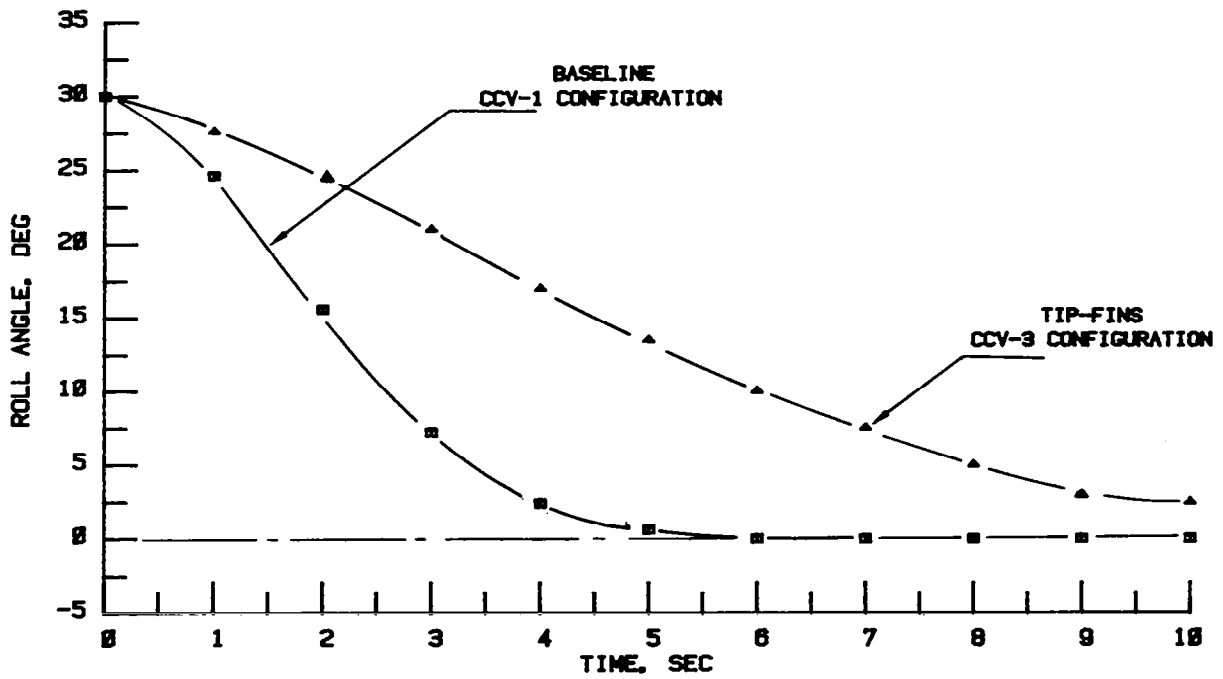
Figure 47: Subsonic Mach = 0.6

67
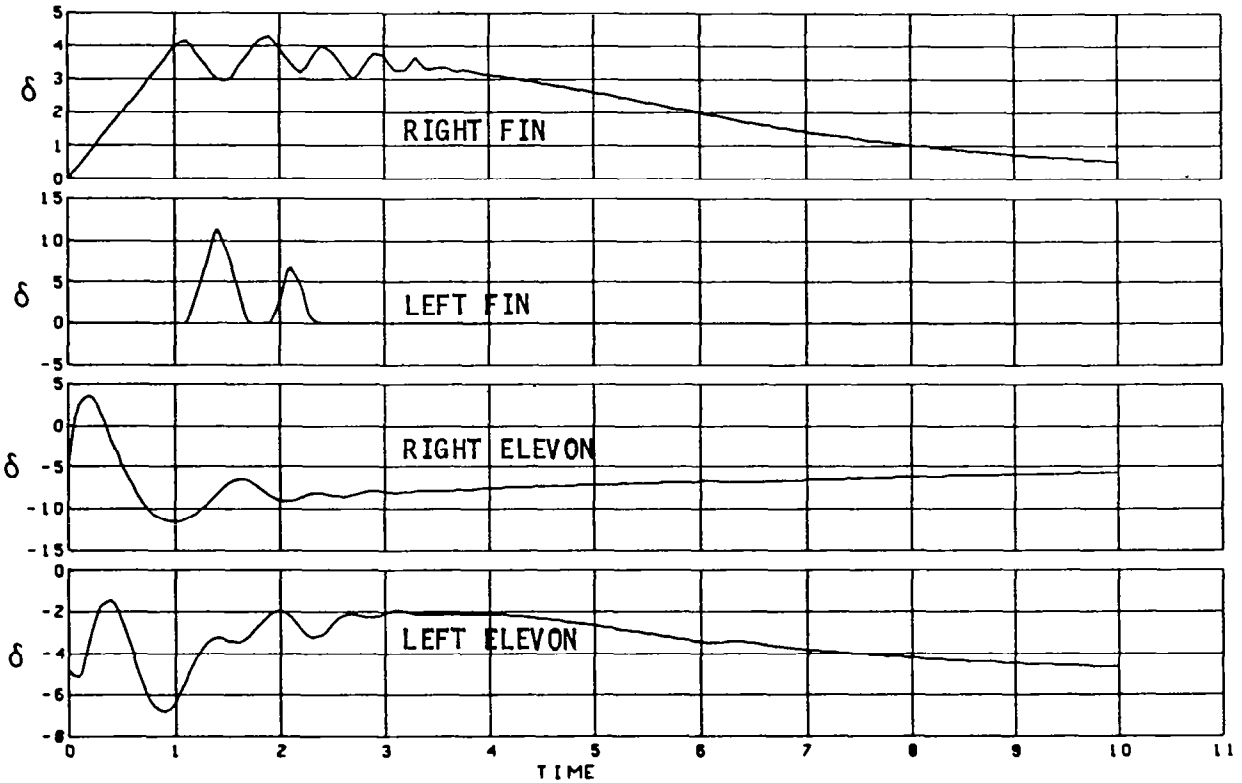
Figure 48: Tip-Fin Configuration CCV-3   Subsonic M = 0.6
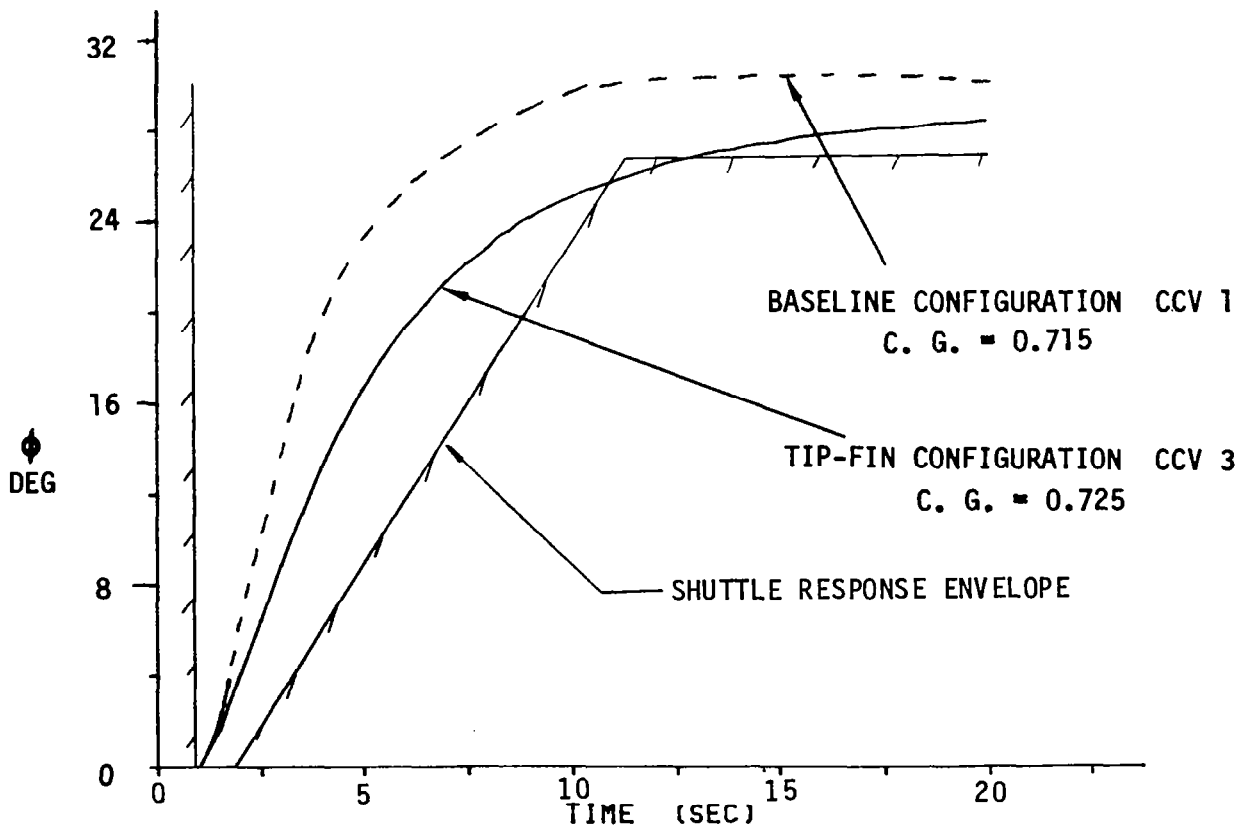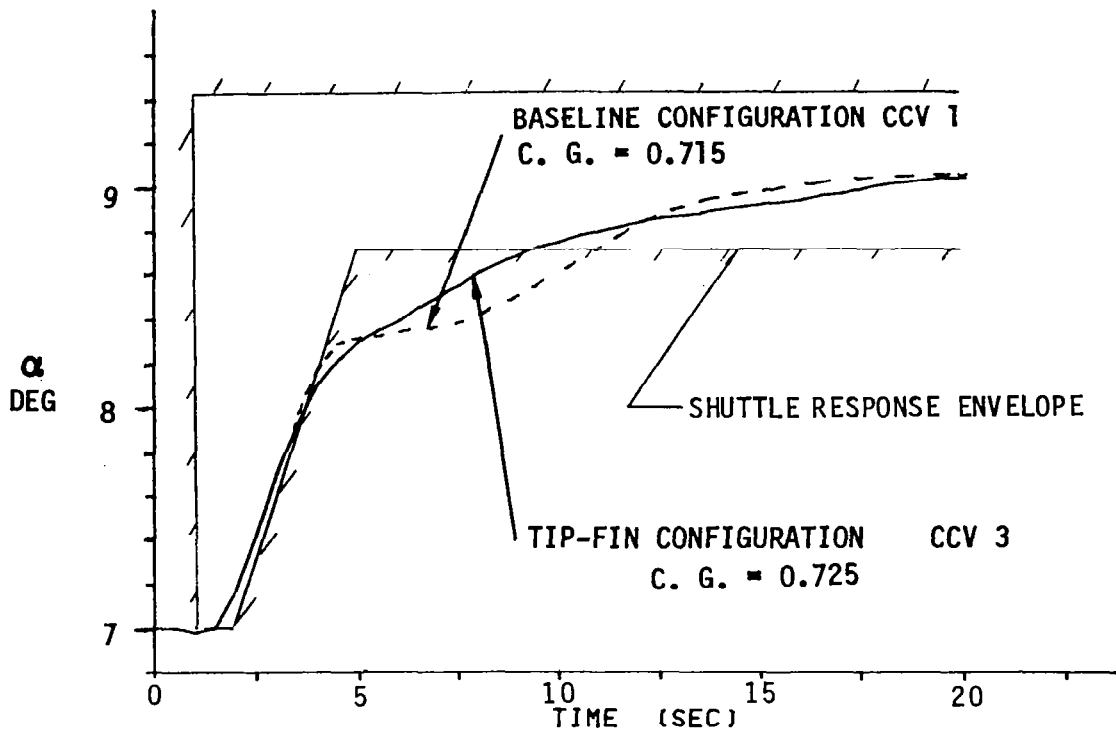
Figure 49: Pitch and Roll Response — Transonic Mach = 1.2
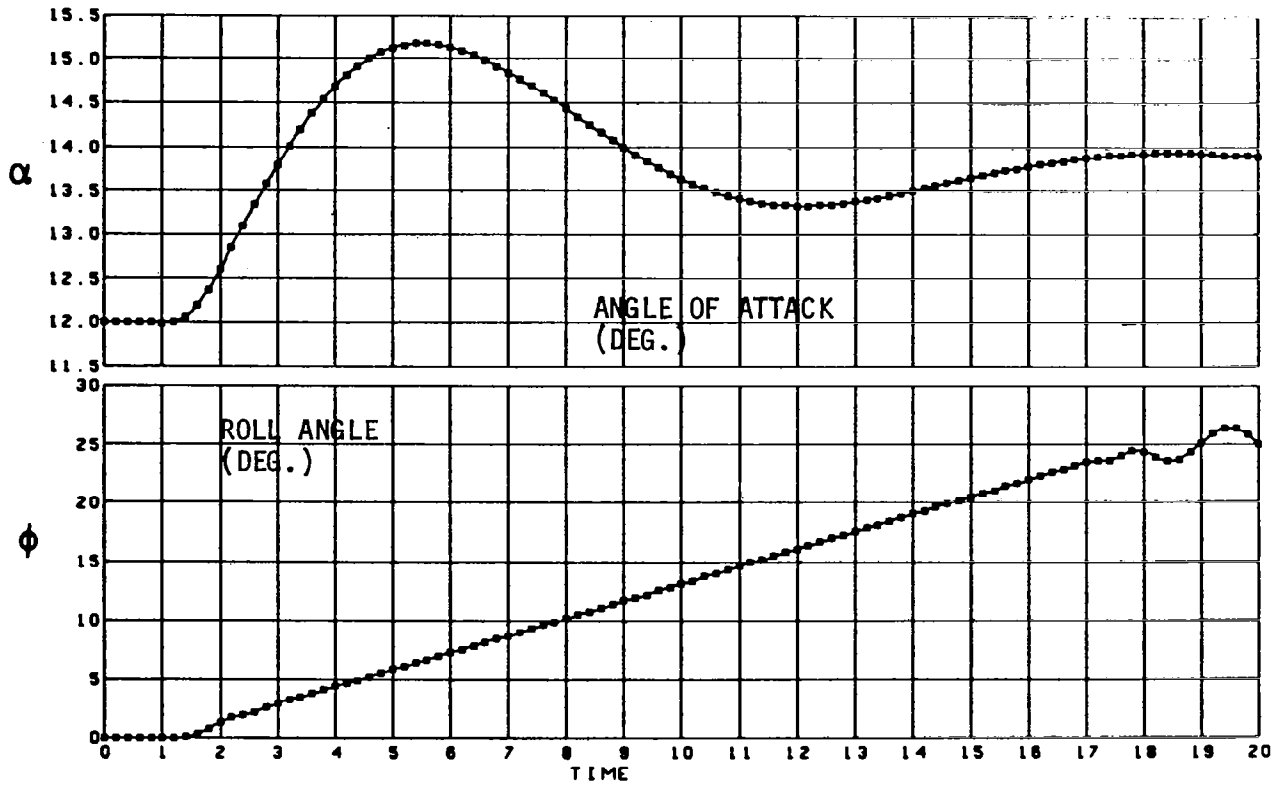
CONTROL SURFACE DEFLECTIONS (DEG.)
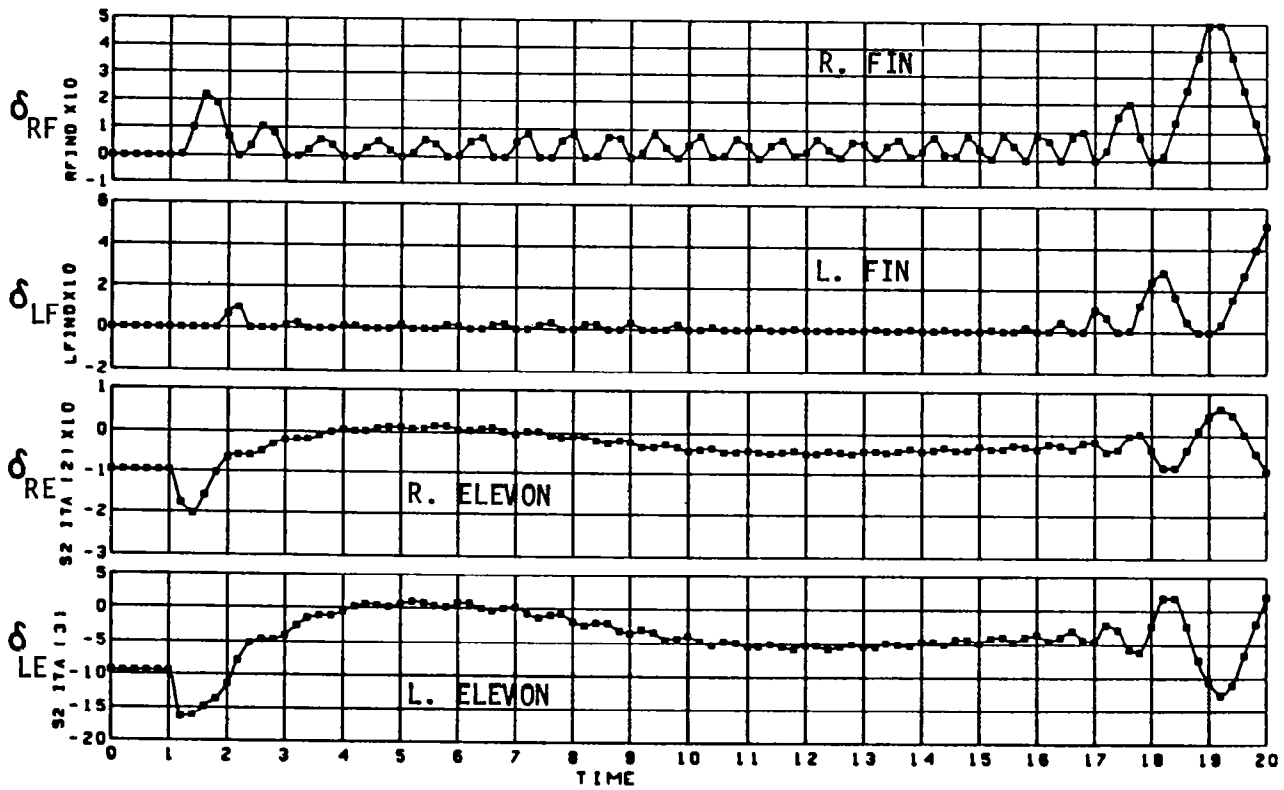
Figure 50:   Tip-Fin Configuration M = 3.5

70
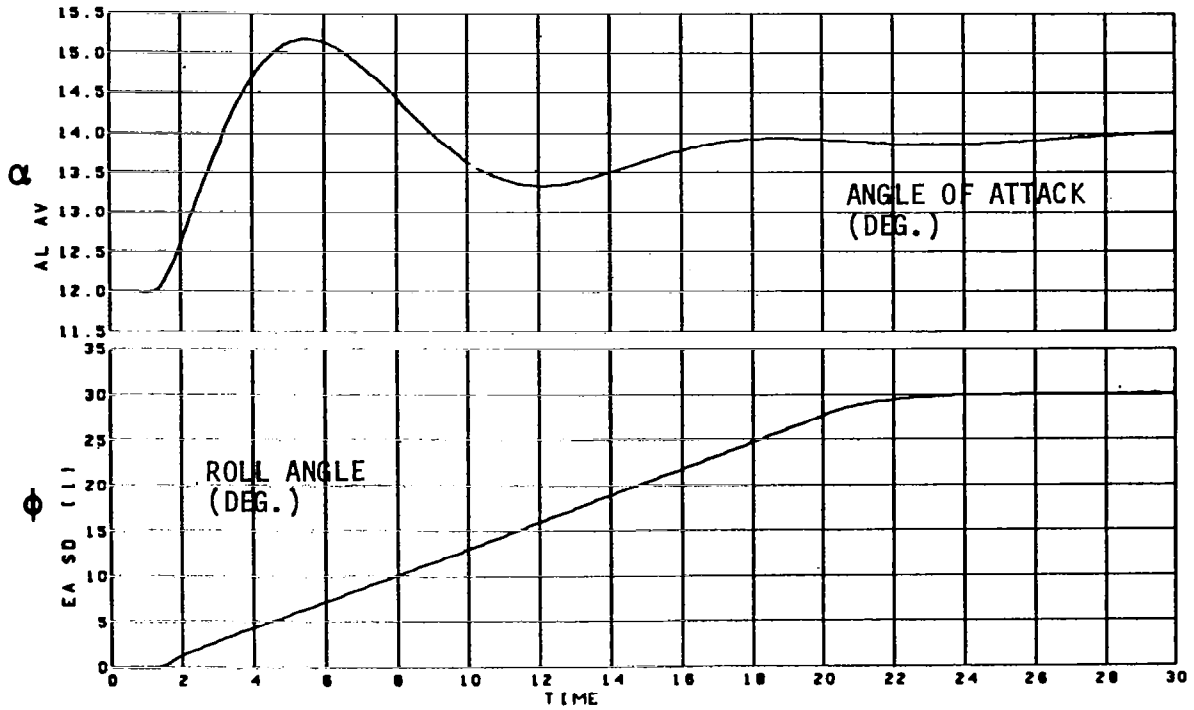
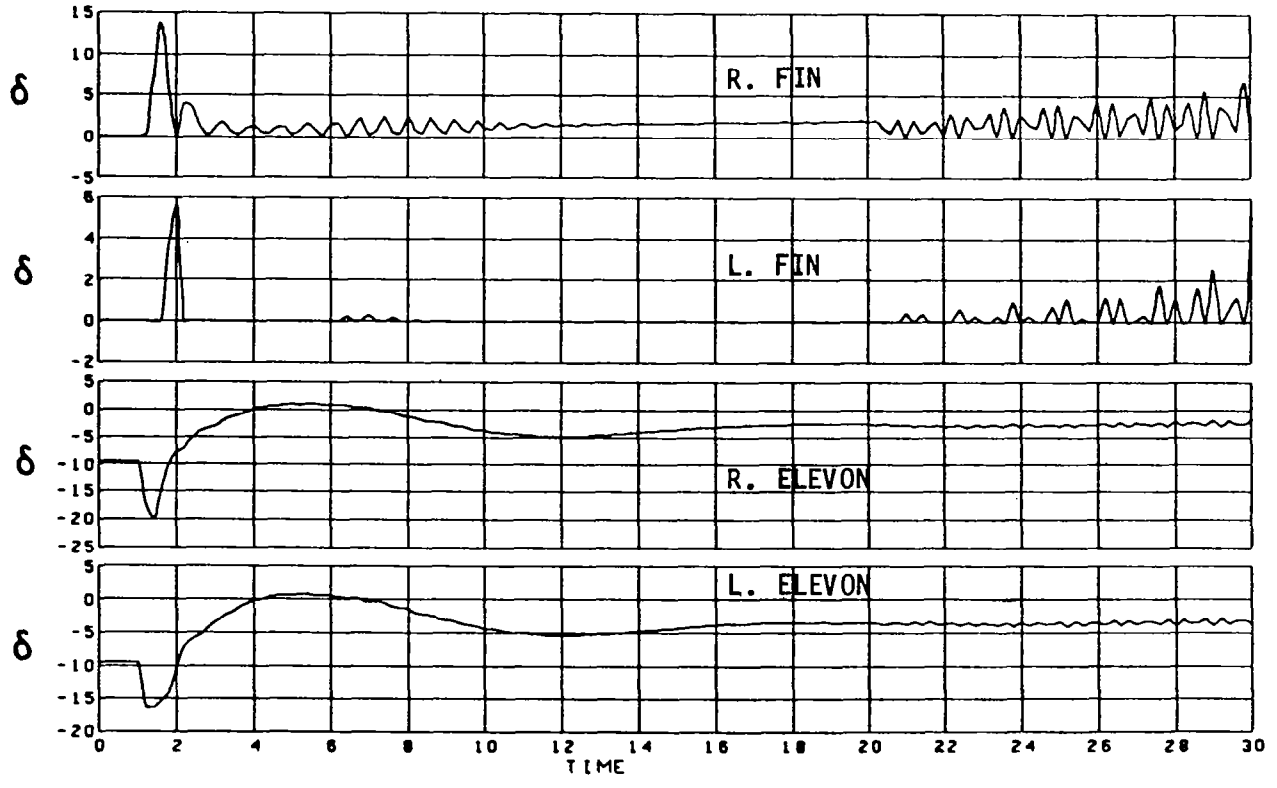CONTROL SURFACE DEFLECTION (DEG)
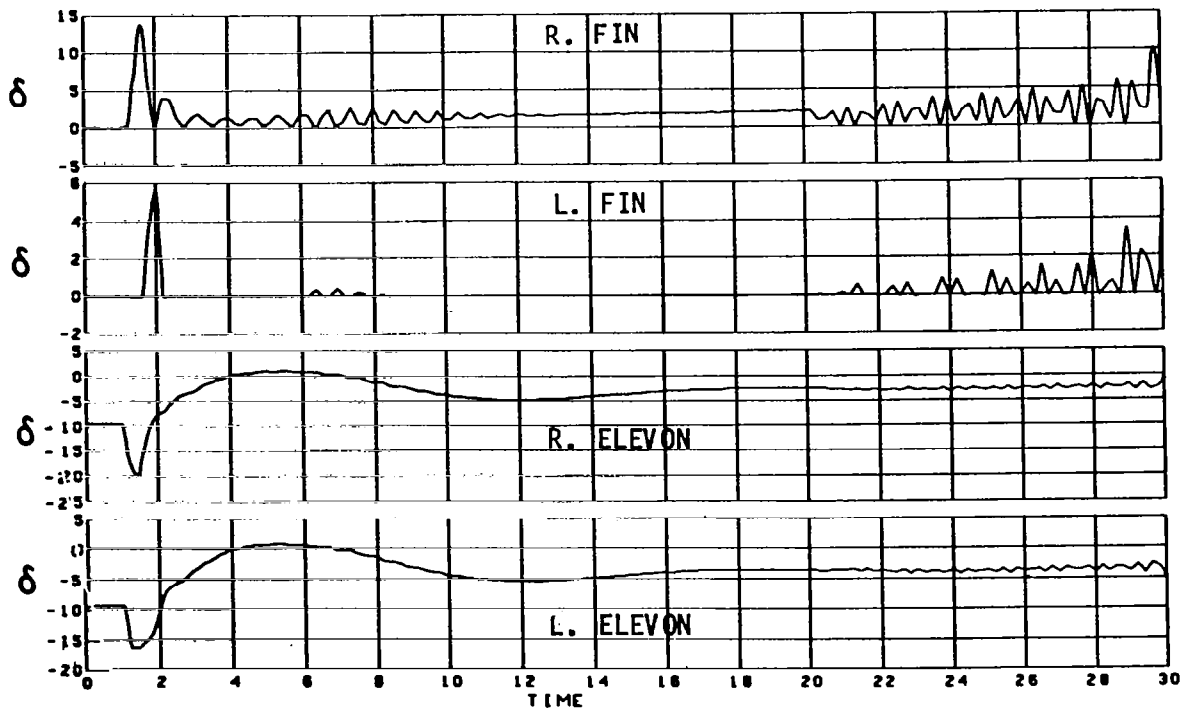
Figure 51: Double Size Tip-Fin Configuration M = 3.5
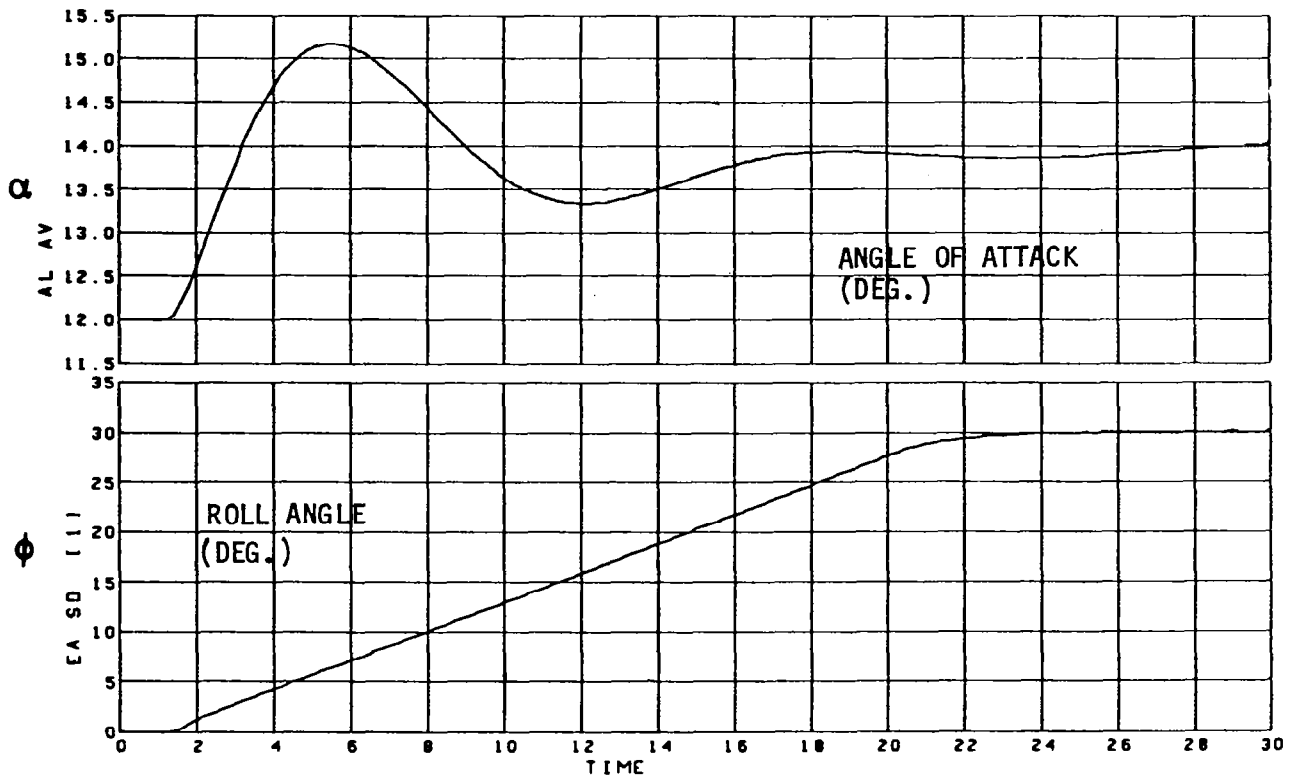
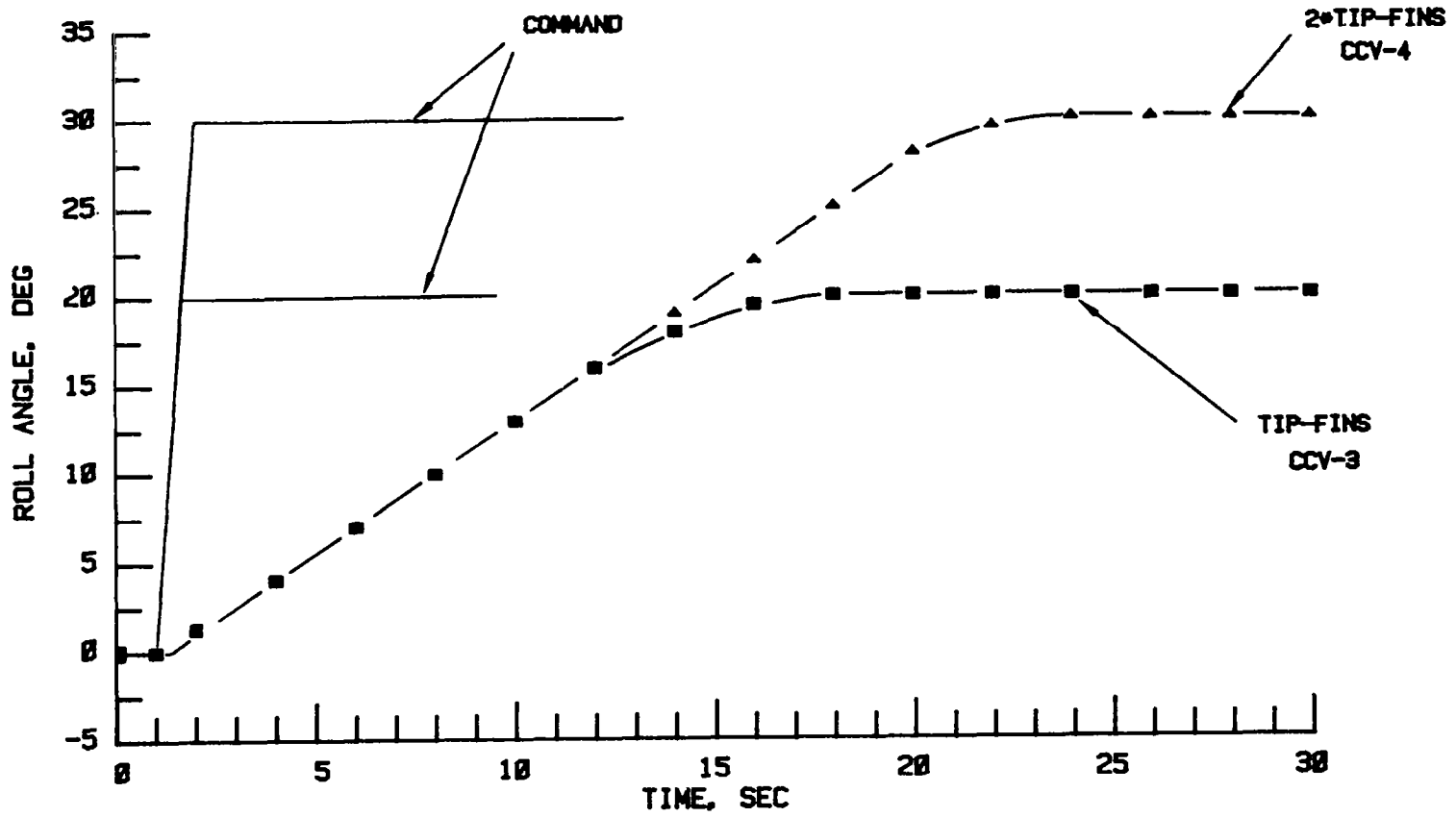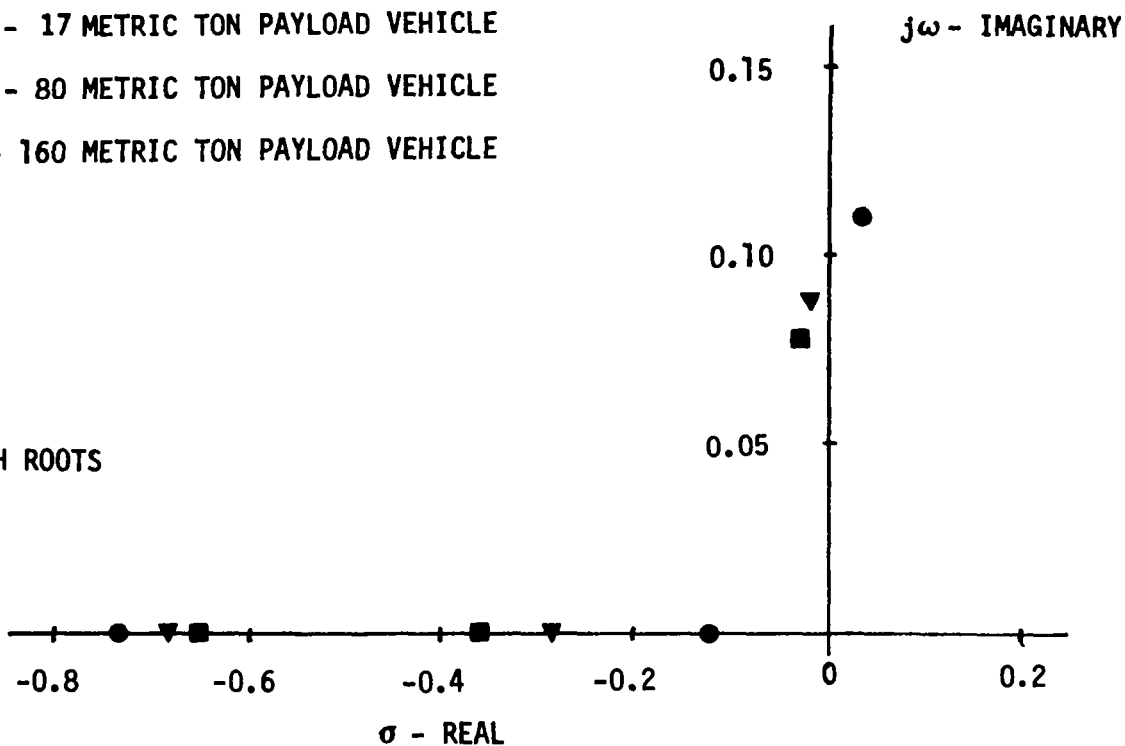Figure 52: Double Size Tip + Fin Small Vertical Tail Configuration M = 3.5

Figure 53: Effect of Tip-Fin Size on Roll

C. G. = 0.725 L_B

● − 17 METRIC TON PAYLOAD VEHICLE

▼ − 80 METRIC TON PAYLOAD VEHICLE

■ − 160 METRIC TON PAYLOAD VEHICLE

jω − IMAGINARY

0.15

0.10

0.05

PITCH ROOTS

-0.8   -0.6   -0.4   -0.2   0   0.2

σ − REAL

jω − IMAGINARY

0.3

0.2

0.1

YAW-ROLL ROOTS

-0.8   -0.6   -0.4   -0.2   0   0.2

σ − REAL
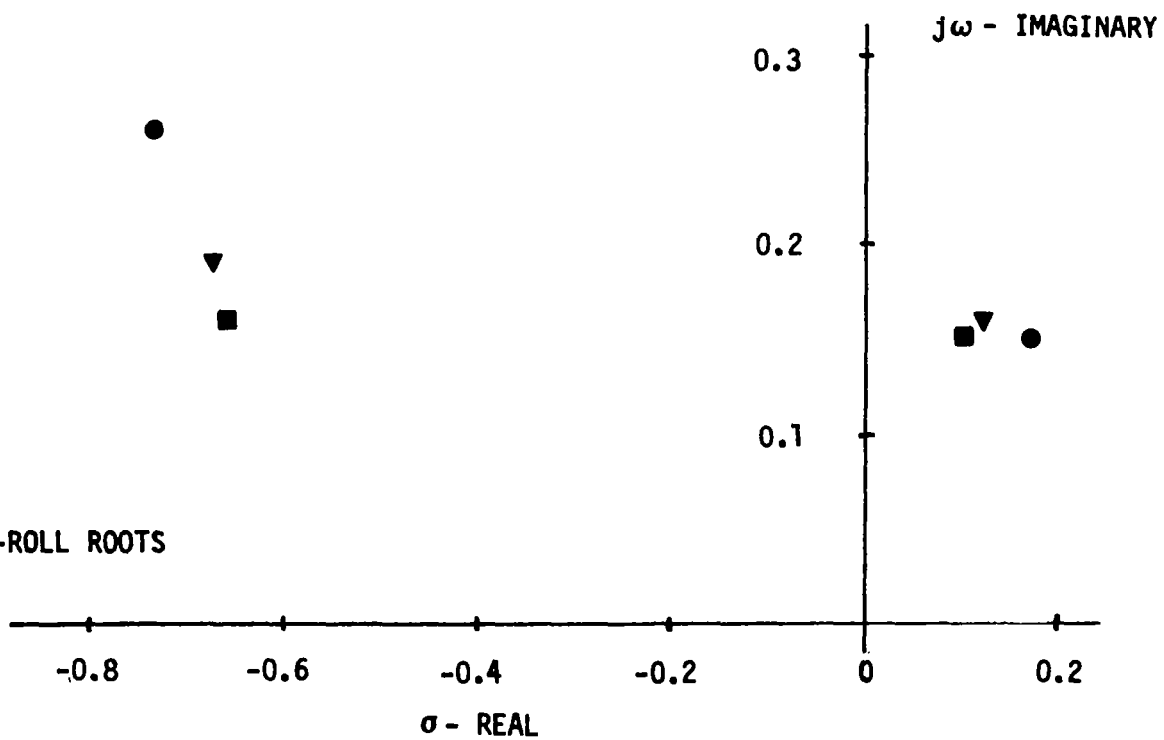
Figure 54:   Effect of Vehicle Size on Vehicle Dynamics

$$\Delta A_Z = 0.25 \qquad \Delta \phi = 30^0$$

Figure 55: Pitch and Roll Response — 80 Metric Ton Payload Vehicle
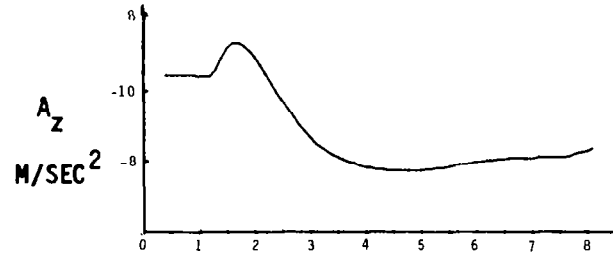
PITCH AND ROLL RESPONSE

160 METRIC TON PAYLOAD VEHICLE

C. G. = 0.715   MACH = 0.3

ΔA_Z = 0.25 $\Delta \phi$ = 30^0

A_Z
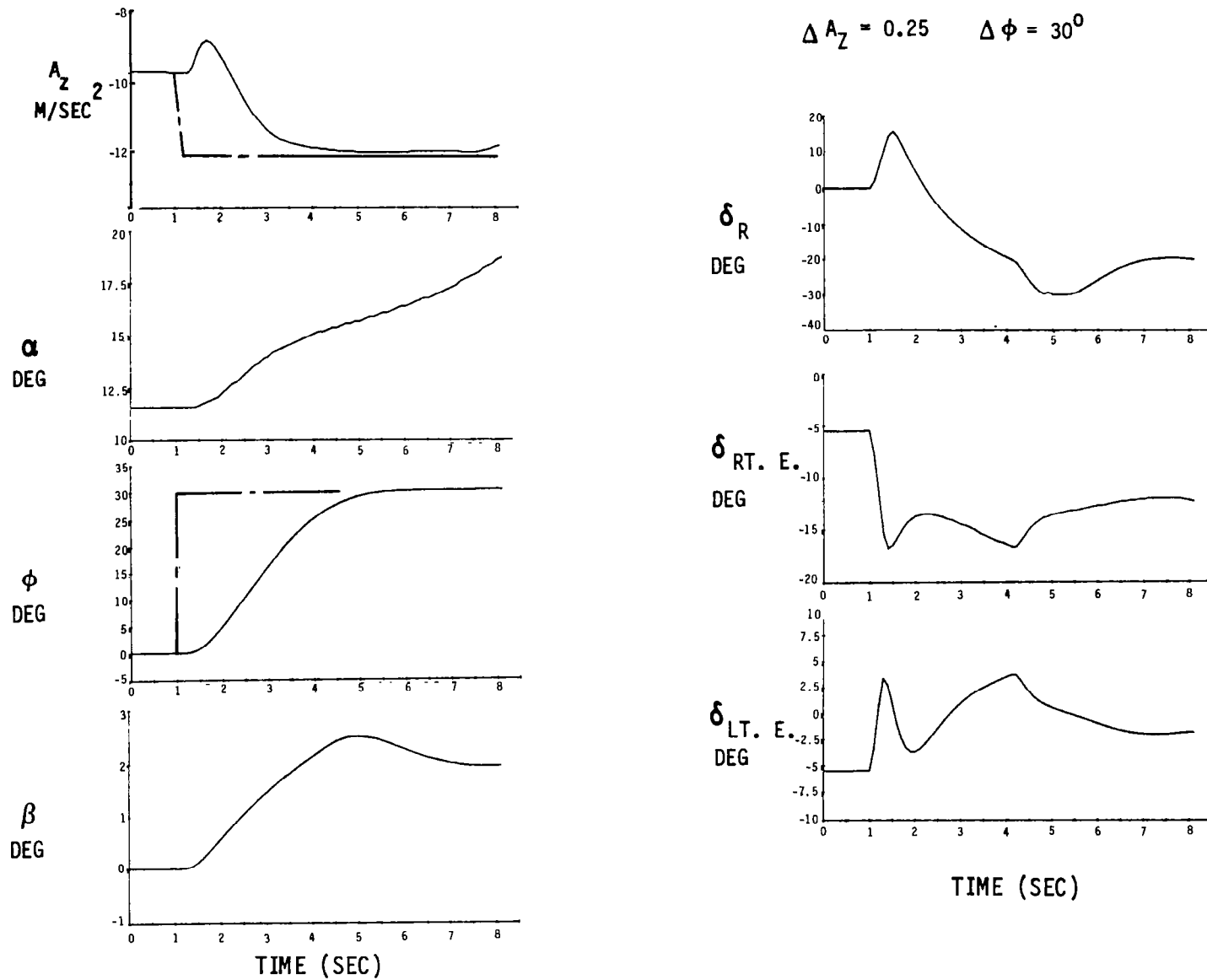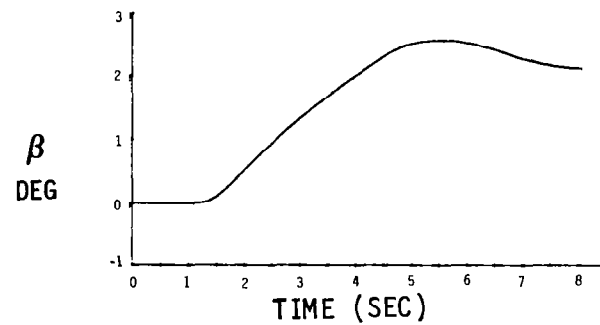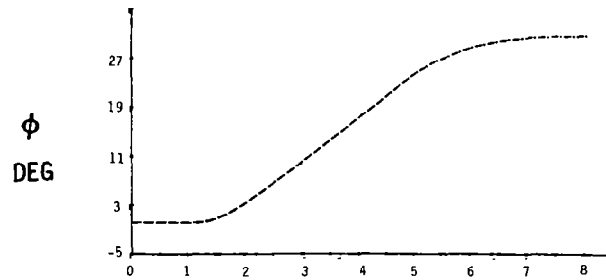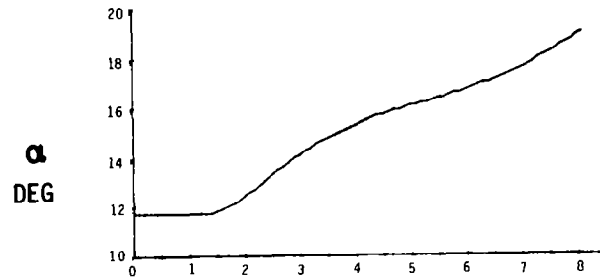M/SEC^2

8
-10
-8

0 1 2 3 4 5 6 7 8

α
DEG

20
18
16
14
12
10

0 1 2 3 4 5 6 7 8

ϕ
DEG

27
19
11
3
-5

0 1 2 3 4 5 6 7 8

β
DEG

3
2
1
0
-1

0 1 2 3 4 5 6 7 8

TIME (SEC)

δ_R
DEG

20
15
10
5
0
-5
-10
-15
-20
-25
-30
-35

0 1 2 3 4 5 6 7 8

$\delta_{RT. E.}$
DEG

5
2
-1
-4
-7
-10

0 1 2 3 4 5 6 7 8

$\delta_{LT. E.}$
DEG

5
2
-1
-4
-7
-10

0 1 2 3 4 5 6 7 8

TIME (SEC)
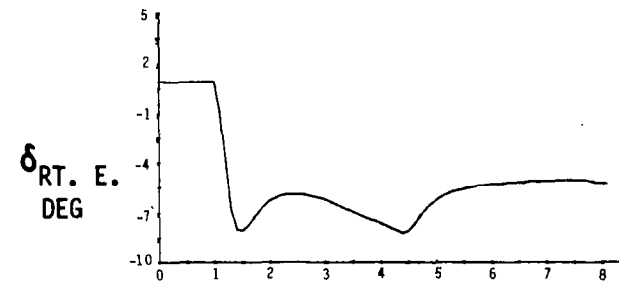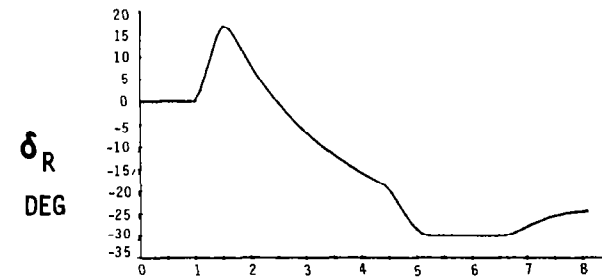
Figure 56:   Pitch and Roll Response — 160 Metric Ton Payload Vehicle
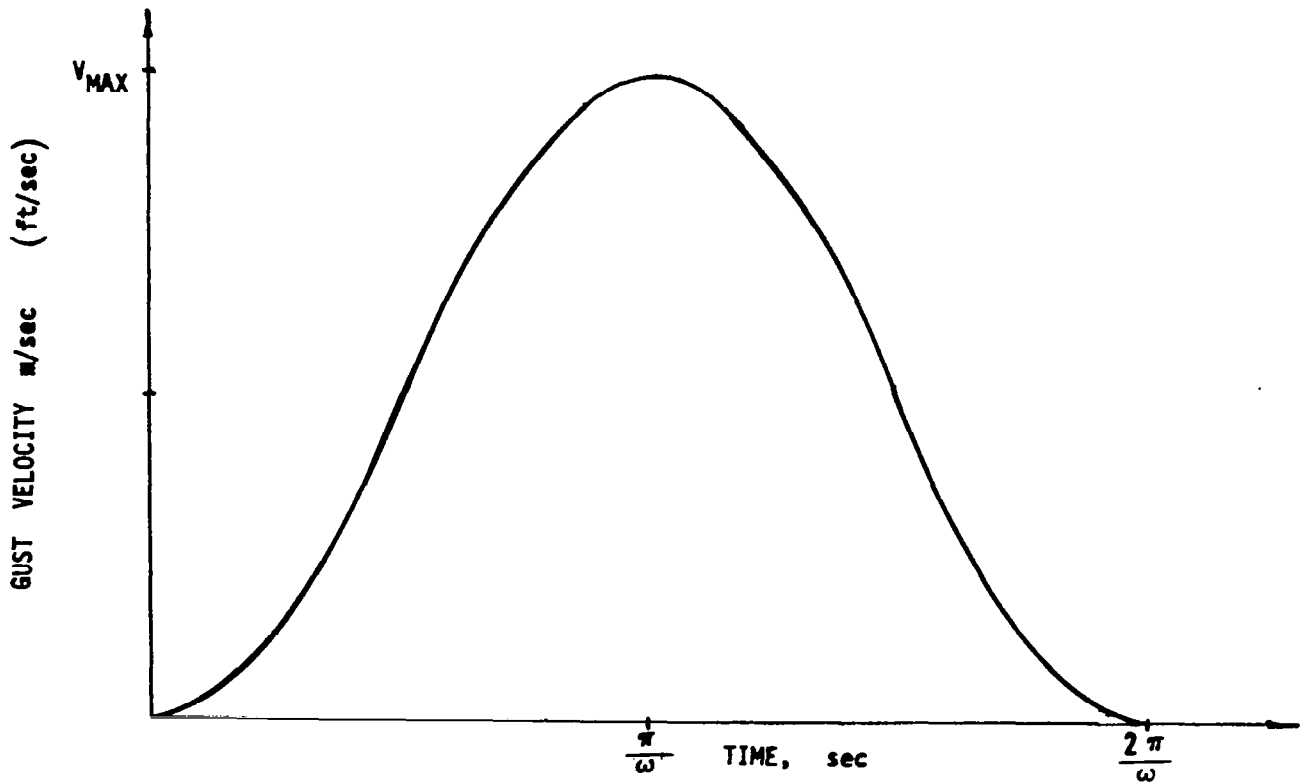
Figure 57:   Gust Form
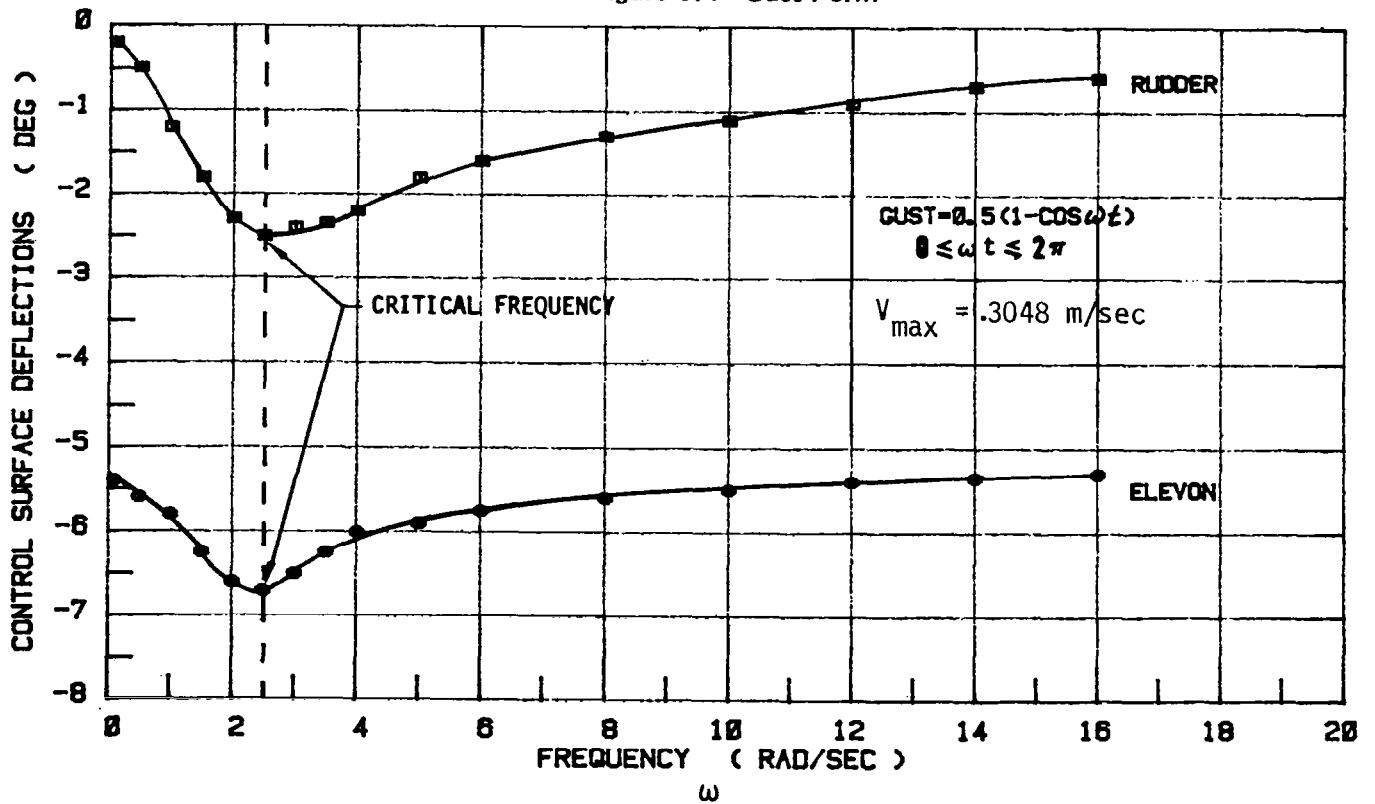
Figure 58:   Control Deflections with Gust

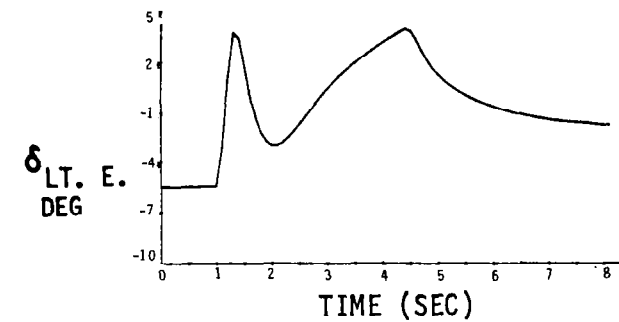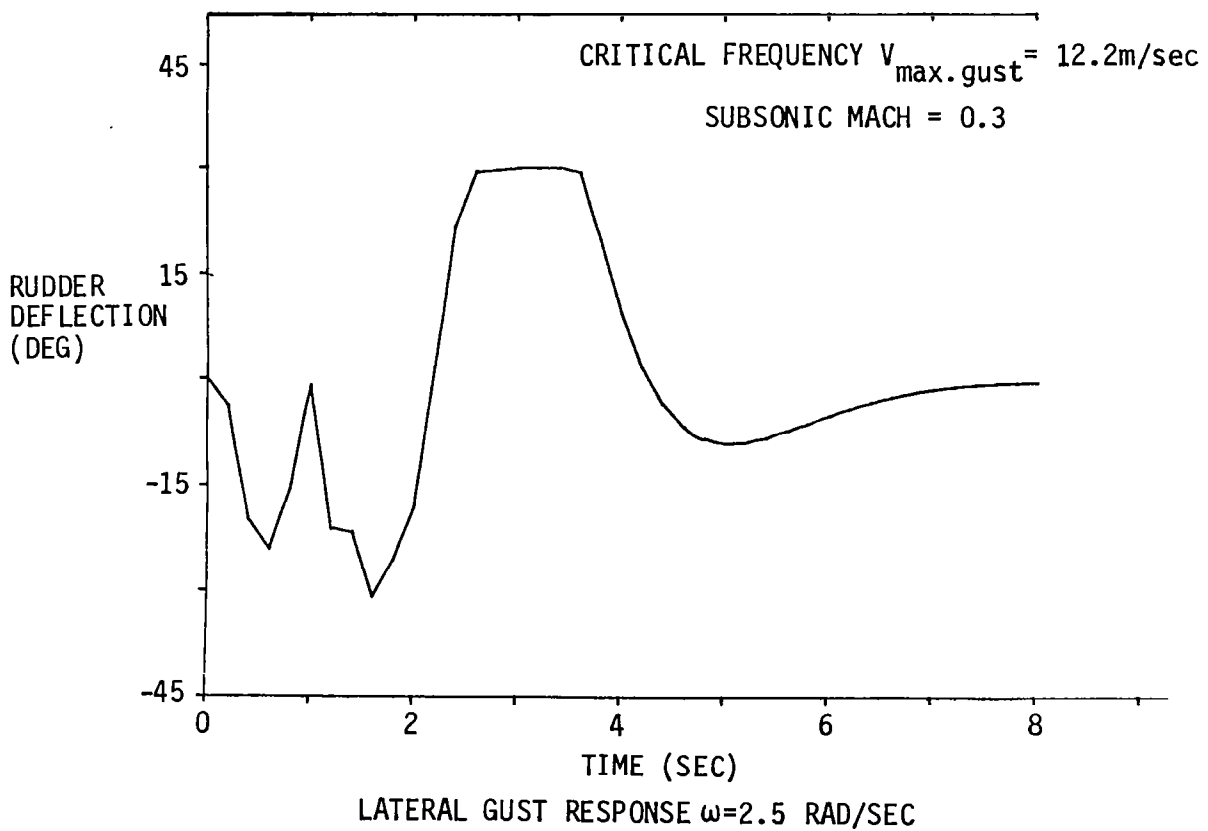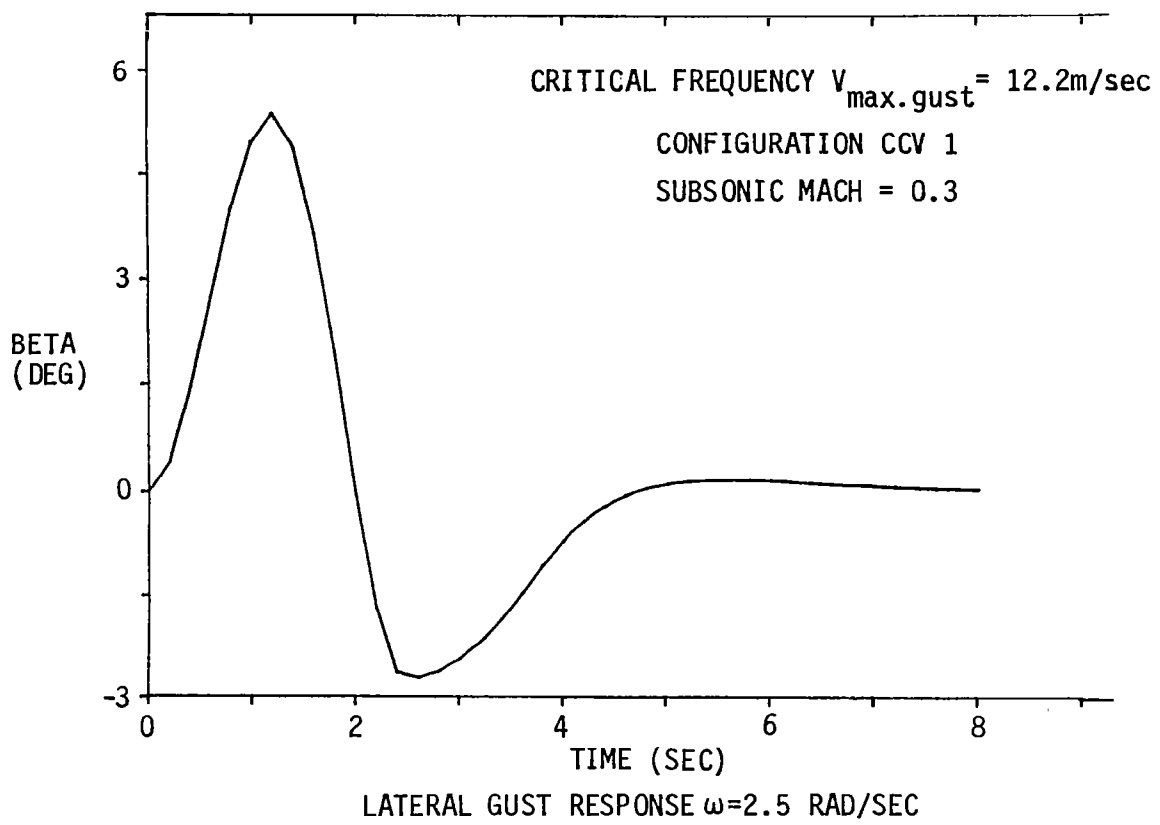Figure 59: Lateral Gust Response ω=2.5 Rad/Sec

VEHICLE RESPONSE TO LATERAL OFFSET
TESTING OF GROUND TRACK HOLD MODE
TIP-FIN CONFIGURATION CCV-3
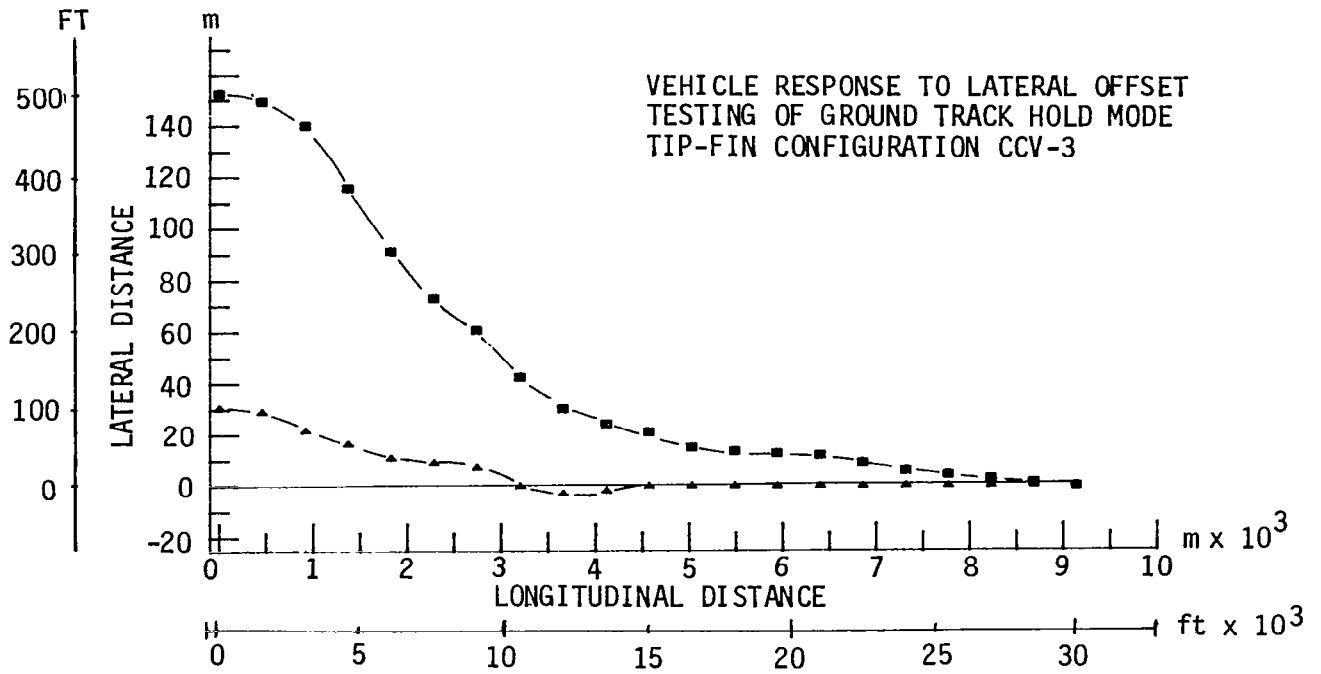
Figure 60: Approach Guidance Loop Response
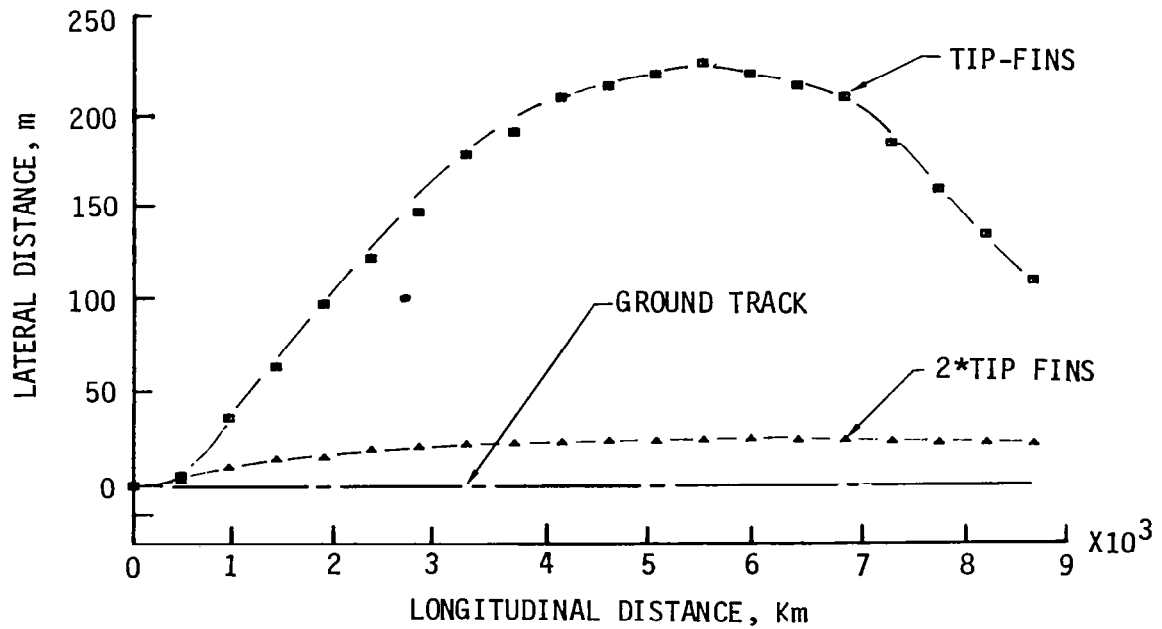
Figure 61: Lateral Drift with Crosswind — 4.6 m/sec (15 ft/sec)
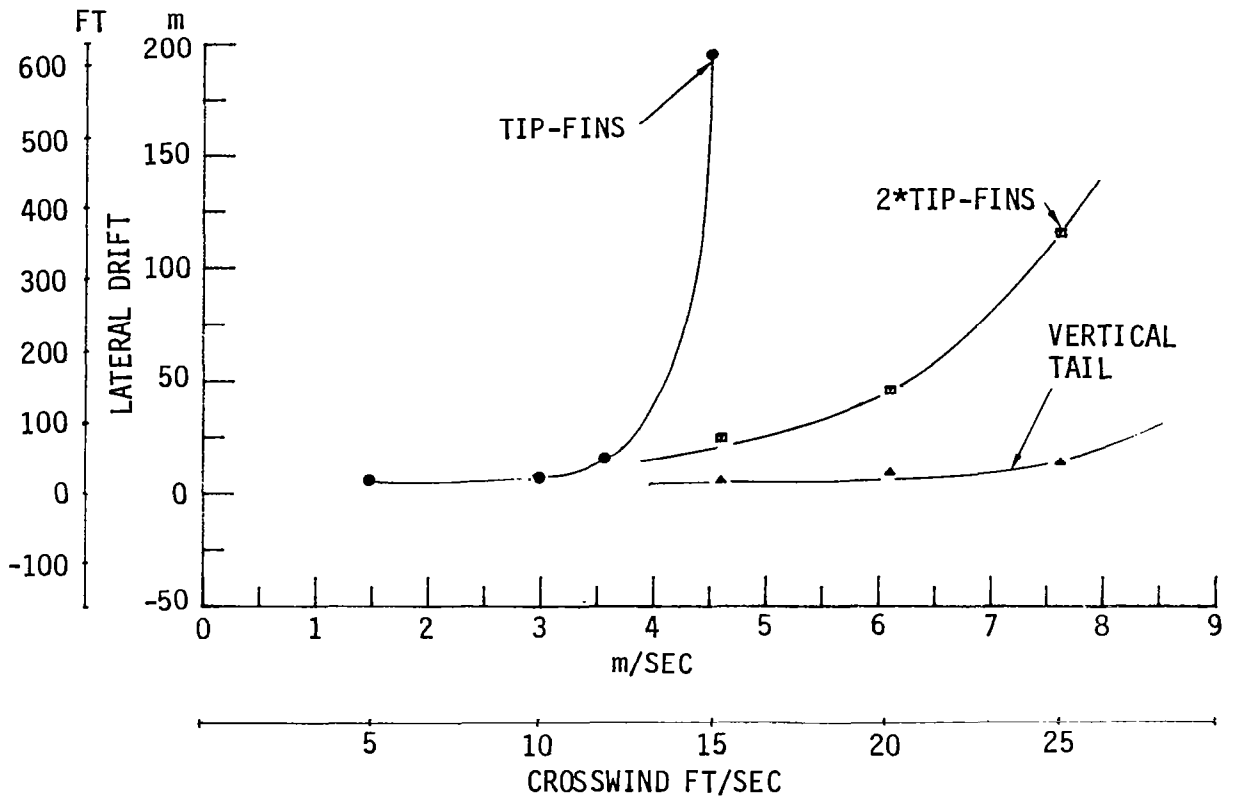
Figure 62: Maximum Drift on Approach
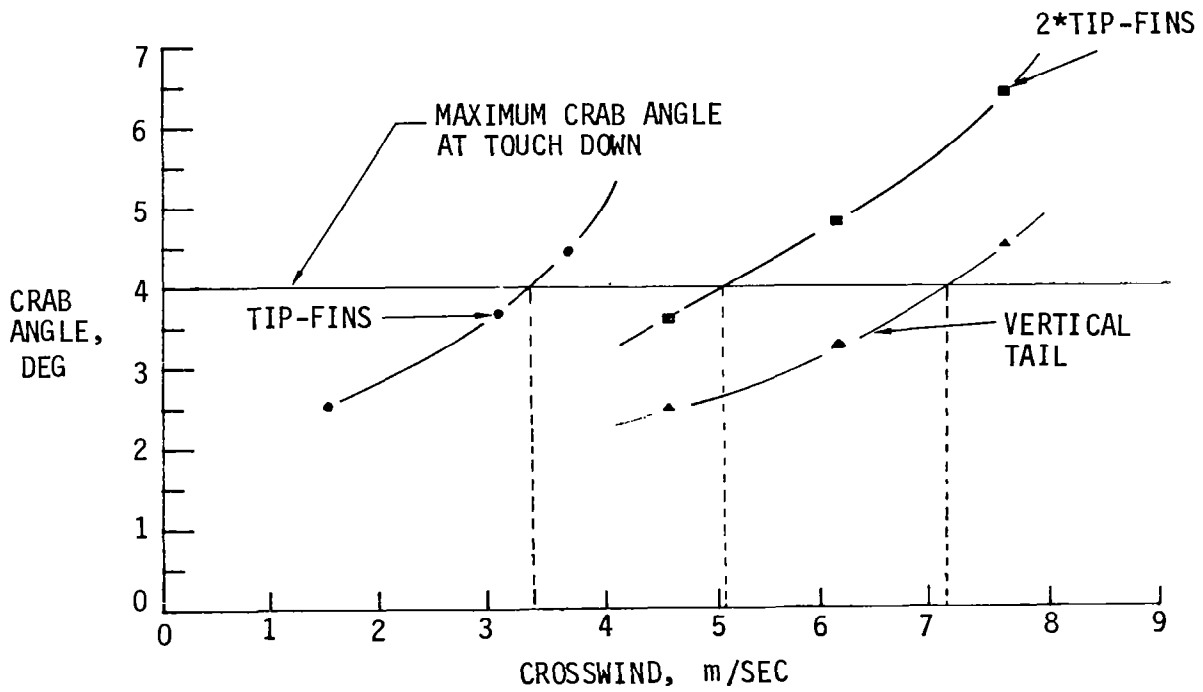
Figure 63: Maximum Crab Angle on Approach

80
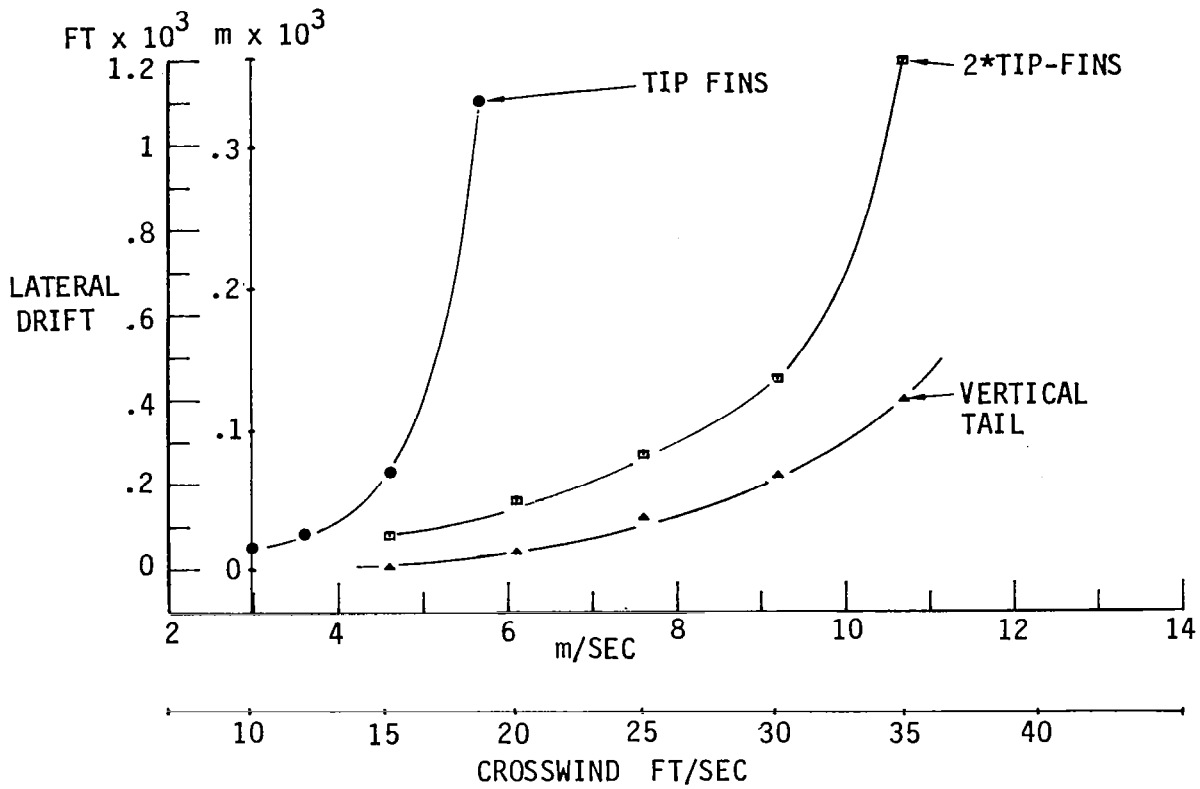
Figure 64: Maximum Drift on Landing

SINGLE RUDDER PANEL
2 DUAL TANDEM ACTUATORS
4 SYSTEMS
4 ACCUMULATORS

4 ELEVON PANELS
2 LEFT & 2 RIGHT
2 DUAL TANDEM
ACTUATORS PER PANEL
4 SYSTEMS PER PANEL
4 ACCUMULATORS

SINGLE BODY FLAP
4 MOTOR DRIVEN HINGES
1 SYSTEM PER MOTOR

4 APU LOCATED IN
INTERTANK BAY
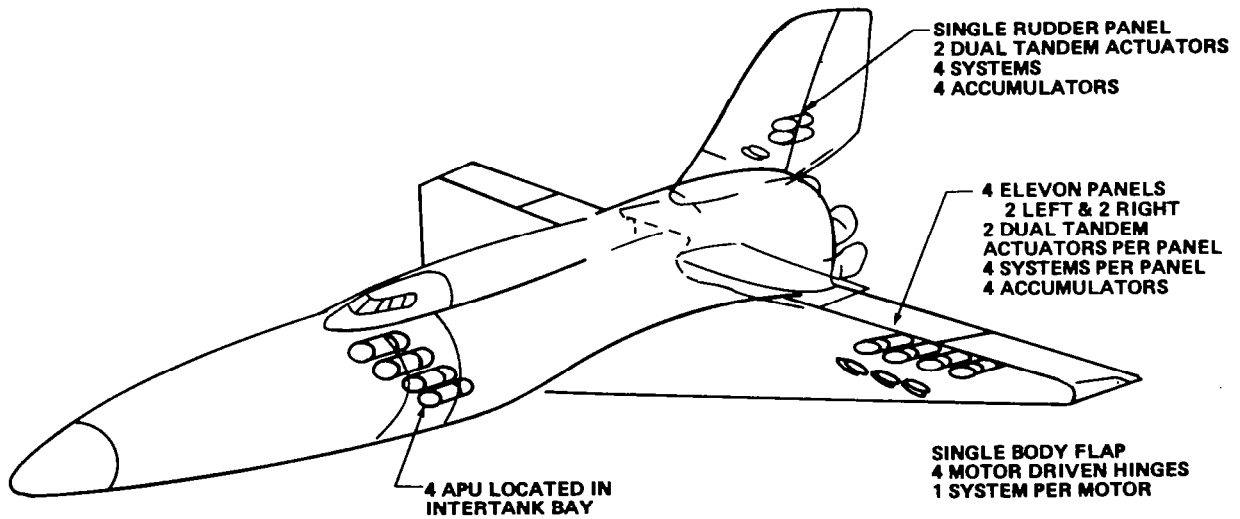
TVC WEIGHTS, POWER & DUTY
CYCLE RATIOED FROM SHUTTLE
237 KW, 34 KW-HR

Figure 65: Control System Aerodynamic Surfaces

1. NO SINGLE FAILURE WILL REDUCE CONTROL CAPABILITY BELOW MINIMUM CONTROL REQUIREMENTS.

2. NO DOUBLE FAILURE WILL CREATE AN UNCONTROLLABLE SITUATION.

   1 AND 2 TRANSLATE TO "FAIL OPERATIONAL - FAIL SAFE".

3. SECONDARY POWER, HYDRAULIC AND ELECTRICAL, COMPUTATION, AND SIGNAL PATHS ARE ALL TO BE CONSIDERED AS PART OF BASIC LOOP AND THEREFORE SUBJECT TO REDUNDANCY.

4. JAMMED ACTUATORS OR SURFACES ARE EXCLUDED BECAUSE OF THE REMOTE PROBABILITY OF THIS OCCURRENCE.

5. SECONDARY OR BACKUP SYSTEMS SHALL BE FULL TIME - NO DISCONNECT/ENGAGE TRANSIENTS TO BE CONSIDERED.

6. SURFACES SHALL BE FLUTTER FREE THROUGH ACTUATOR DAMPING - NO BALANCE WTS.

Figure 66:   CCV Control System Group Rules

CONTROL SYSTEM IS AS DEFINED IN NASA CR-2723 (REF. 1).   FOUR ELEVON PANELS ACTUATED BY TWO DUAL TANDEM ACTUATORS PER PANEL. TWO RUDDER PANELS POWERED BY TWO DUAL TANDEM ACTUATORS PER PANEL.   FOUR HYDRAULIC SYSTEMS POWERED BY FOUR AUXILIARY POWER UNITS.

DUTY CYCLES AS SHOWN ON TABLE 7 OF CR-2723.

ELEVON EQUIVALENT SUMMARIZED = .1901 HR   AT 14.82°/SEC.

RUDDER EQUIVALENT SUMMARIZED = .1619 HR   AT 4.25°/SEC.

WEIGHT FACTORS

    HYD. SYST. + APU = 1.04 X PK KW = kg

    FUEL TANKS + FUEL + 2.52 X KW HRS = kg

    HYD LINES - RUDDER = .69 X PK KW = kg

                ELEVON = 1.41 X PK KW = kg

    TVC RATIOED FROM SHUTTLE   BODY FLAP

        237 KW PK; 34 KW-HR   102.7 KW PK; 0 KW-HR

                                                  WT. = 192 kg

Figure 67:   CCV Control System Definition

| SURF. RATE | RUDDER | | | kW HOUR | ELEVON DEFL. DEG. | ELEVON H/M Nm/1 SIDE | kW PEAK BOTH/SIDES | kW HOUR BOTH/SIDES |
	DEFL. DEG.	H/M Nm	kW PEAK					
°/SEC								
10	± 25	62580	19	1.3	+10 -30	137500	83	23
15	± 25	135500	61	2.8		152100	137	26
20	± 25	187900	113	3.9		878900	1056	149
40	± 25	255300	307	5.3		879100	2113	149
100	± 25	210200	632	4.3	+10 -30	879100	5283	149

Figure 68: Power Requirements Control Surfaces

CONTROL SURFACE DISPLACEMENT RATE	ACTUATOR WT-kg RUDDER ELEVON BODY FLAP	LINE WT. kg	kW/kW HR	HYD SYST. AND APU kg	APU FUEL & TANK kg	Σ WT - kg C. G. STA. m	% ENTRY WT.
10°/SEC.	46 160 250	23 207 190	441/59	820	265	1970 / 57.5	(1.19)
15°/SEC.	100 180 250	77 345 190	538/63	1000	280	2430 / 57.6	(1.47)
20°/SEC.	139 1040 250	140 2660 190	1509/187	2800	841	8060 / 51.4	(4.7)
40°/SEC.	190 1040 250	380 5320 190	2759/188	5120	850	13340 / 57.4	(7.6)
100°/SEC.	160 1040 250	780 13300 190	6254/187	13110	840	28200 / 57.3	(14.7)
VEHICLE STATION	68/62/66	59		55 57/50	50		

Figure 69: Element Weight Flight Control System
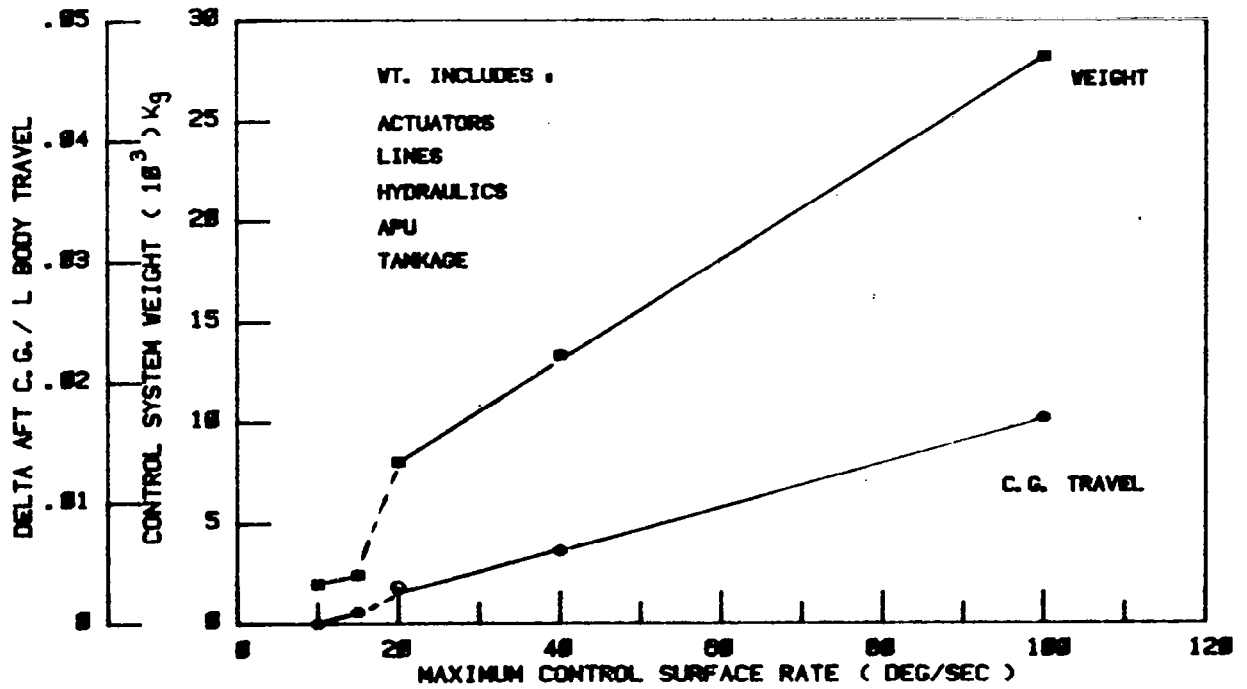
Figure 70: Control Rate /Weight Trade

	DEFLECTION DEGREES	H/M Nm	RATE °/SEC	kW PEAK PER SIDE	kW HOUR BOTH SIDES
RUDDER	($\pm$ 25)	255300	(40)	(550)	(9.4)
TIP FIN RUDDER	0^0	+3620	40	173	6.0
	+ 60^0	-80600			
ELEVON	($^+_-$ $^{10}_{30}$)	879000	(40)	(1890)	(270)
	+ 10	+1026000	40	2200	3.0
	- 30	- 372000			
BODY FLAP (Ref. 1)		- 570000			

(   )   Configuration using Central Fin and Rudder.

Figure 71: Operational Requirements — Aerodynamic Control Surfaces

	ACTUATOR WT. kg	LINE WT. kg	kW/kW HOUR	HYD SYST & APU kg	APU FUEL & TANKAGE kg	WT./C. G. STA. kg/m
CENTER BODY						
RUDDER	190	380	2760/189	5120	850	13340
ELEVON	1040	5320				
BODY FLAP	250	190				57.4
TIP FIN						
RUDDER (4.2 m^2)	143	560	2647/211	4940	950	14500
ELEVON	1220	6200				
BODY FLAP	250	190				57
TIP FIN (8.4 m^2)						
RUDDER	290	1120	2854/215	5300	966	15530
ELEVON	1220	6200				
BODY FLAP	250	190				57
STATION						
RUDDER	68					
TIP FIN	62	59		55	50	
ELEVON	62					
BODY FLAP	66					

Figure 72: Weight — Aerodynamic Control System
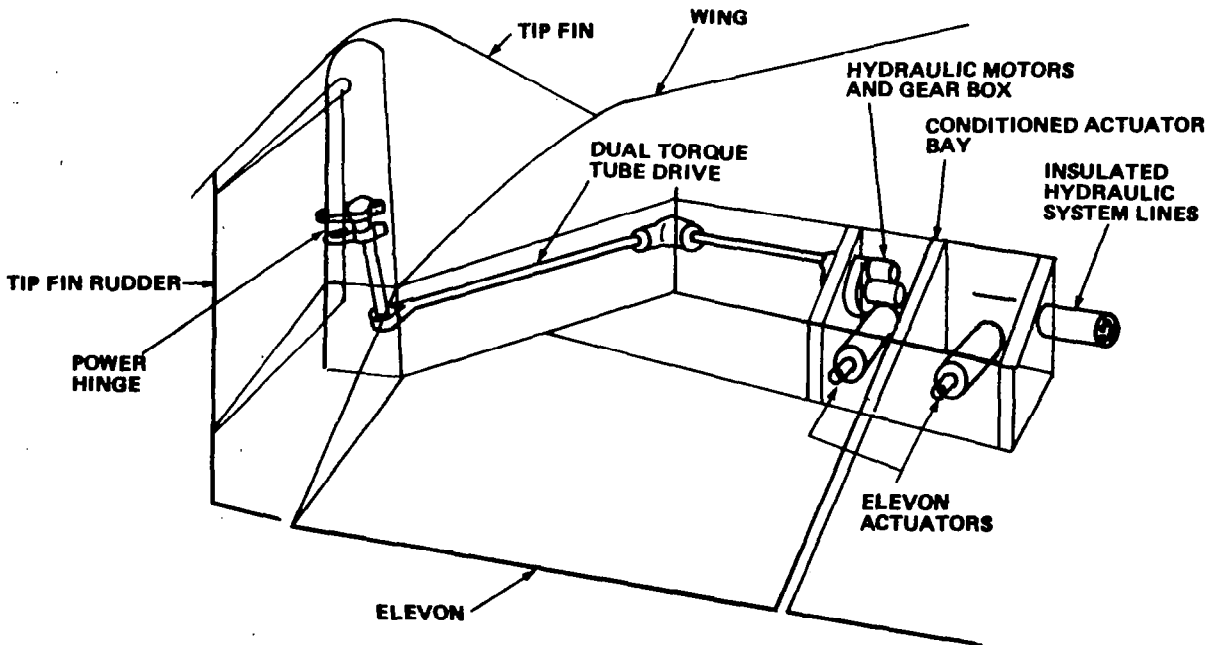
Figure 73: Motor and Drive System — Fin-Wing Tip Installation

DELETED	WT. (kg)	STATION (m)
RUDDER ACTUATORS	190	68
LINE WEIGHT	380	59
HYD SYST & APU	570	55
APU FUEL & TANKAGE	15	50
STRUCTURE FIN & RUDDER	2120	68
	3280	64

TIP FIN
. SURFACE
. RUDDER

	CENTRAL POWER SUPPLY		MOTOR & SHAFT	
	WT. (kg)	STA. (m)	WT. (kg)	STA. (m)
ACTUATORS	140	62	70	60
LINE WEIGHT	560	59	490	59
HYD SYST & APU	360	55	360	55
APU FUEL & TANKAGE	15	50	15	50
STRUCTURE	1810	62	1810	62
	2900	60	2750	60

Figure 74: Weight — Tip Fin (4.2 m^2 Rudder)

TIP FIN

. SURFACE = 18 m^2
  RUDDER = 84 m^2

	CENTRAL POWER SUPPLY		MOTOR & SHAFT	
	WT. (kg)	STA. (m)	WT. (kg)	STA. (m)
ACTUATORS	290	62	130	60
LINE WEIGHT	1120	59	970	59
HYD SYST & APU	720	55	720	55
APU FUEL & TANKAGE	30	50	30	50
STRUCTURE ▷	3540	62	3540	62
	5700	60	5400	60

▷ WING FLUTTER NOT COVERED

Figure 75: Weight — Growth Tip Fin (8..4 m^2 Rudder)
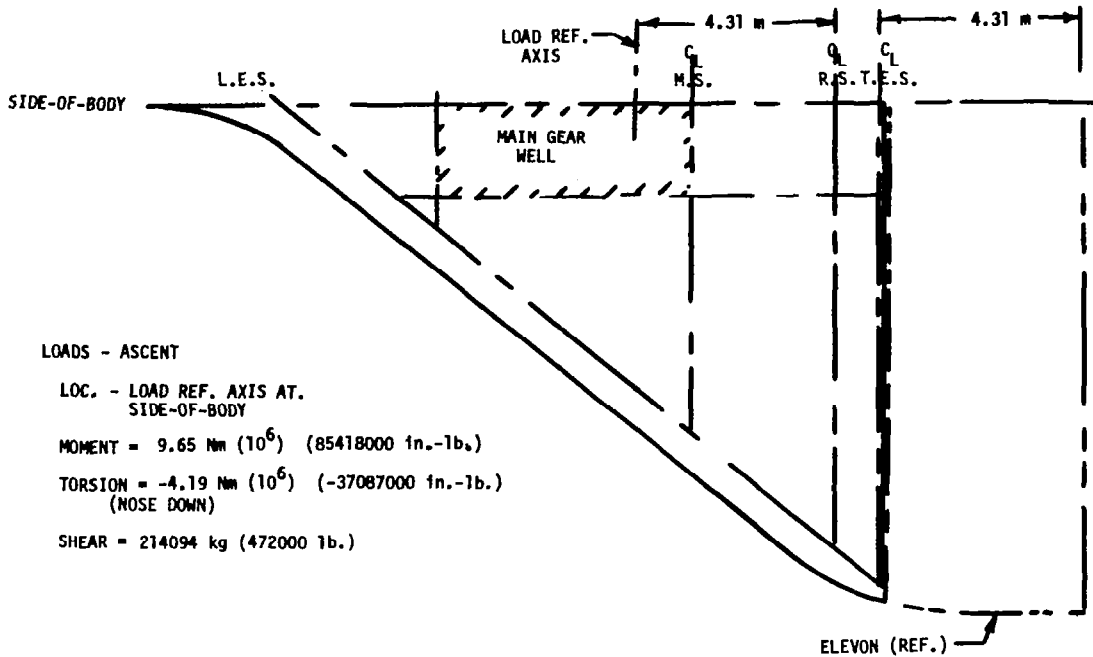
Figure 76: Wing — Control Configured Design

Figure 77: Aft Wing Box

TITANIUM
HONEYCOMB
WT. = 6.54 kg/m^2

RIB CHD.
TITANIUM
WT. = 1.95 kg/m^2

RIB TRUSS
(TUBE - B/AL)
WT. = 1.67 kg/m^2

C$_L$
MS

MAIN GEAR
WELL

.51 m

TYP. RIB
SPACING
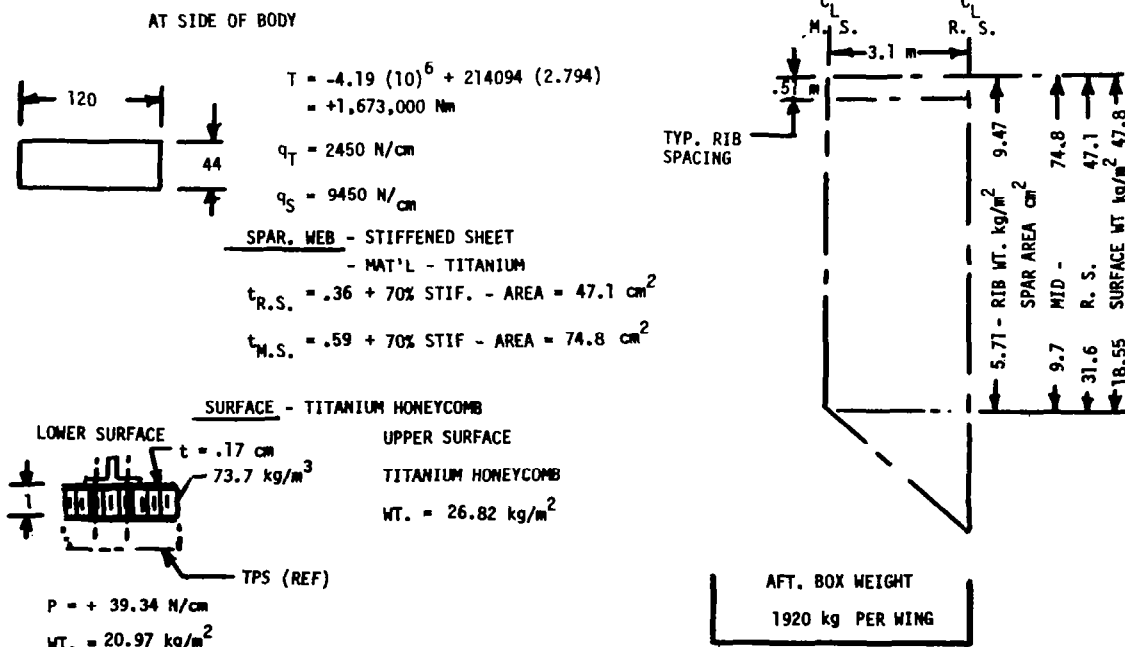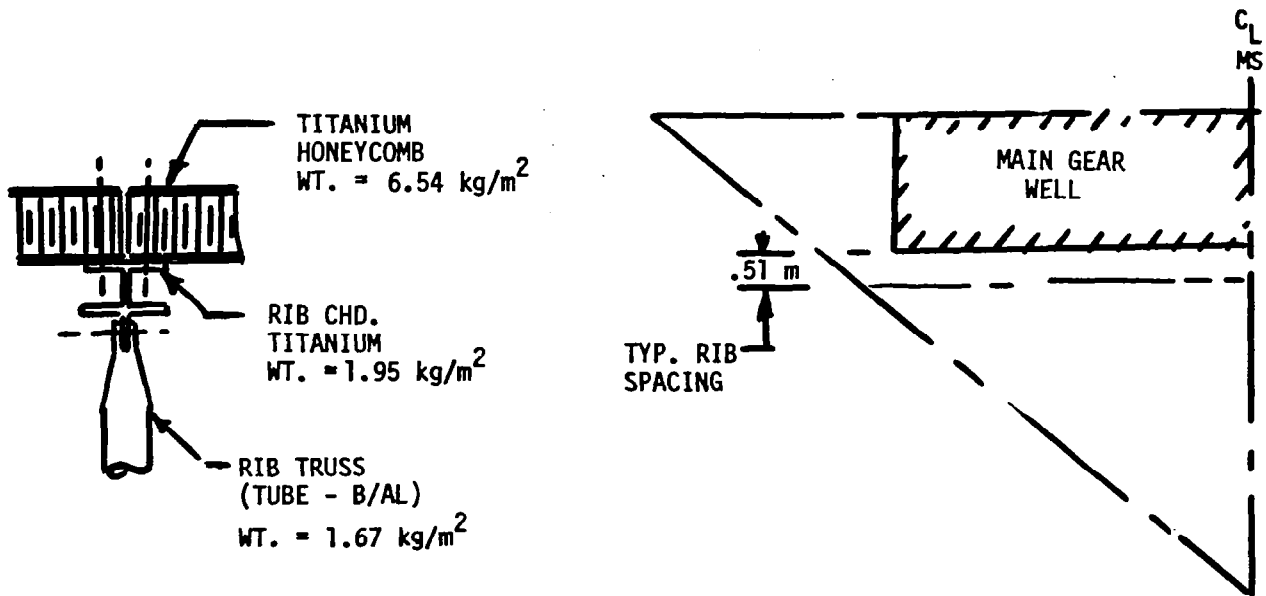
TYPICAL STRUCTURE - FWD WING

WT = (6.54 + 1.95 + 1.67) 1.05 = 10.67 kg/m^2

STRUCTURE WT. = 10.67(2) (38) = 816 kg/SIDE

Figure 78:   Forward Wing

AFT WING BOX	3828
TRAILING-EDGE SECTION	445
FWD. WING ▷	1633
LEADING EDGE AND LEADING- EDGE SPAR	3832
	9739 kg (21470 lb.) ▷

WING THERMAL PROTECTION
SYSTEM (INSULATED
METAL HEAT SHIELD SYS.)   2512 kg (5540 lb.)

▷   MAIN GEAR WELL NOT INCLUDED

Figure 79:   Wing Weight

HINGE MOMENT: .44 $(10)^6$ Nm LIMIT @ M = 1.2
STRUCT. TEMP.: 589 K
AVERAGE SURF. PRES: .834 N/cm² LIMIT

- ACTUATOR CAP. = $\frac{4}{3}$ (.44 $(10)^6$) = .59 $(10)^6$ Nm

- ACTUATOR LD. = $\frac{.59(10)^6}{355}$ = 17.0 $(10)^5$ N

- LOCAL ACTUATOR & HINGE ATTACH
  ULT. LD = 2.5 (ACT. LD)

- ACT. SUPT. FTG ULT. LD = 1.5(1.2) (ACT. LD)
- DISTRIBUTION RIB ULT. LD = 1.5 (ACT. LD)
- ELEVON STRU. ULT. LD = 1.5 (LIMIT)

DIMENSIONS IN cm
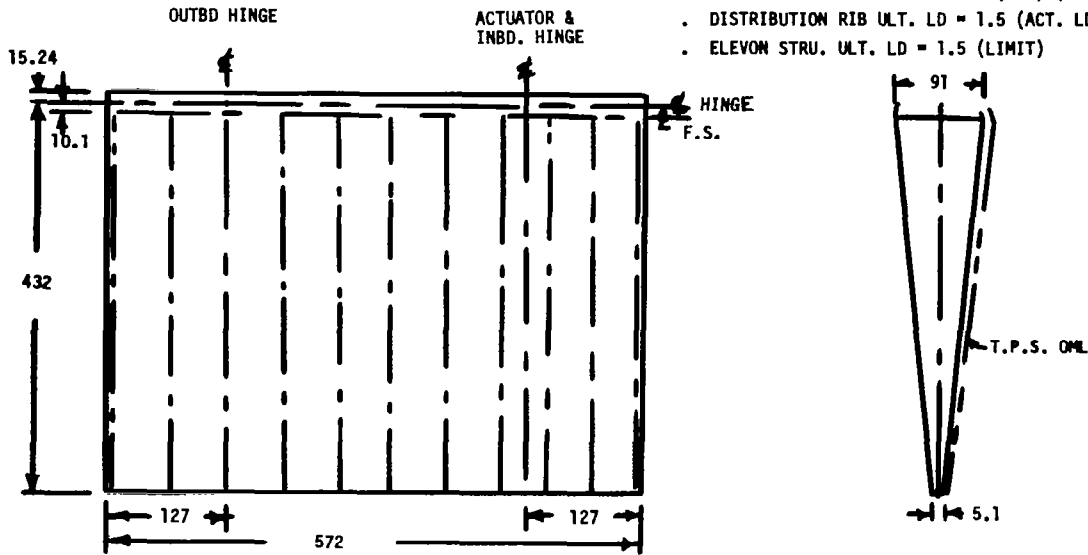
Figure 80:   Elevon — Control Configured Vehicle

HINGE MOM. ULT = 1.5 (.44 $(10)^6$)
= .66 $(10)^6$ N
AVE SURF. PRES. = 1.5 (8.34) = 12.51 N/m²

SURFACE q_{MAX} = $\frac{.66 (10)^6}{2 (4.22)}$ (.05 + .91) ($\frac{4.44}{5.72}$)

= 1260 N/cm

DIMENSIONS cm
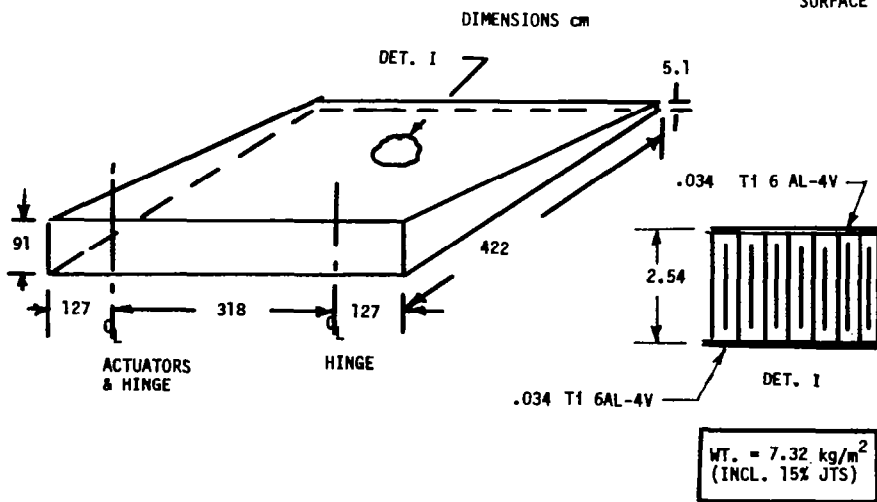
4-15 6AL-4V H/C CORF
(57.7 kg/m³)

ALUM. BRAZE
(.038 cm ALUM.)

f_s = $\frac{1260}{(.036)}$ = 17500 N/cm²

M_{ULT} = $\frac{(63.5) (.834) 1.5}{12}$
= 420 N/cm

f_b = $\frac{420}{.036 (2.54)}$ = 4600 N/cm²

$F_{c_y 589°K}$ = 57200 N/cm²

WT. = 7.32 kg/m²
(INCL. 15% JTS)

.034 T1 6 AL-4V

.034 T1 6AL-4V

DET. I

Figure 81:   Elevon Structure

89

Figure 82 content

ACTUATOR RIB $P_U = P_L = 480000$ N

$q = 805$ N/cm

CHORD: Ti 6AL - 4V

AREA @ F.S. = 9.7 cm^2

R.S. = 1.16 cm^2

$F_C = 55000$ N/cm^2

WEB: T_1 6AL-4 CORRUG

$t = .081$ cm

$f_s = \frac{805}{.081} = 9940$ N/cm^2

$F_{S_{589 K}} \cong 12400$ N/cm^2

$\bar{t} = (.081)(1.21)^*(1.1)^{**}$

$= .108$ cm

RIB WT. = 34 kg

2 RIB/ELEVON

WEIGHT (WETTED AREA) = 1.37 kg/m^2

DIMENSIONS cm

FRONT SPAR

$P = 300(1.8) = 540$ N/cm

3

127   318   127

159

R_1 R_2

$R_1 = R_2 = 154790$ N

$M_3 = 29000$ Nm

$M_1 = 44000$ Nm

AT. PT 1

6.4

86   t = .203
STAB. BY
WEB &
SURF. H/C

WT. = 39.1 kg

WEIGHT/(WETTED) AREA = .83 kg/m^2

* EFF. LT

** JOINTS

$f_b = \frac{44000}{86(6.4)(.203)} = 39400$ N/cm^2

@ b/t = 10   T = 589 K

$F_{cc} \cong 41400$ N/cm^2

$q = 1000 + 350 = 1350$ N/cm
INBD (1)

USE q_{ave} SPAR = 960 N/cm

CORRUG. WEB t = .081 cm

$q_{ALLOW_{589 K}} = 1000$ N/cm

Figure 82: Elevon Structure

Figure 83 content

TYPICAL RIB   LD = 1.8(44) = 79 N/cm

$R_1 = 79(432) = 34100$ N

T = 34100(216) = 7,365,600 N/cm

$q_{DIST} = \frac{7365600}{2 \cdot \frac{91 + 5.1}{2} \cdot 432} = 175$ N/cm

91.4 cm

②④⑥

①③⑤

35.6 cmTYP.

R_1

MEM. 2-3

5.1 cm

.152 cm

2.54 cm   .152 cm

MEM. 2-4   T1-6 AL-4V

V = 34100 - 91(175) + 175(2)$\frac{17.8}{432}$(43.2) - 17.8(79)

= 17400 NTEN

USE .9(17400) FOR COMP. DES:.

TUBE 5.08 cm D.. X .051 cm WALL

$F_{COL} = 23400$ N/cm^2

$f_c = 21400$ N/cm^2

MEM. 3-4

V = 17900 N

TUBE 5.08 cm D X .051 cm WALL

$F_{COL} = 27000$ N/cm^2

$f_c = 23400$ N/cm^2

WEIGHT = 1.71 kg/m^{2}ELEVON WETTED AREA

$M = \frac{79(35.6)^2}{12} = 8243$ N cm

$P = 17400\left(\frac{35.6}{91.4}\right) + \frac{35.6}{2}(175) = 9900$ N

$f_c = \frac{8243(3)}{(2.54)^2(.152)} + \frac{9900}{1.16}$

$= 25200 + 8500$

$= 33700$ N/cm^2

$F_{cc} = 33240$ N/cm^2

Figure 83: Elevon Structure

90

OUTBD
HINGE FTG

ACTUATOR/HINGE
FTG. - ELEVON

ACTUATOR/HINGE SUPPORT FTG

91 | 61

2.5 DIA

R =169000 N

→10.2|←
|←15.9→|

28

88

36

7.6 DIA

C_L ACTUATOR
P = ± 850000 N (1.8)

R = 820000 N (1.8)

R = ± 477000 N

→|10.2|←
|←15.2→|

DIMENSIONS IN cm

C_L ACTUATOR
P = ± 850000 N (1.8)

± 477000 N

±544000 N

MAT'L: TI 6AL-4V

WEIGHT = 3.2 kg

MAT'L TI 6AL-4V

WEIGHT 38 kg/FTG
(2/ELEVON)

MAT'L TIT. 6AL-4V

INBD   OUTBD

WEIGHT =120 kg/FTG   WEIGHT =36 kg/FTG
(2/ELEVON)

TOTAL FTG WT/ELEVON = 355 kg
WT = 7.08 kg/m² WETTED AREA

Figure 84: Elevon Hinge and Actuator Fittings

ITEM	Unit Wt. (Wet Area)		Total Wt. (Elevon - 265 ft²)	
	kg/m²	#/ft²	kg	lb.
Honeycomb Panels	7.32	(1.5)	360	(800)
Typical Rib	1.71	(.35)	83	(184)
Front Spar	.83	(.17)	39	(86)
Actuator Ribs (2)	1.34	(.28)	60	(150)
Leading Edge Upper	.36	(.073)	18	(39)
Leading Edge Lower (Incl. TPS)	1.32	(.27)	65	(142)
Trailing Edge Spar	.15	(.03)	6	(14)
Outboard Hinge Fitting (1)	.07	(.015)	3	(7)
Outboard Hinge Fitting Supt. (1)	.73	(.15)	36	(80)
Actuator and Inboard Hinge, (2) Fitting	1.51	(.31)	75	(166)
Inboard Act. and Hinge Support (2)	4.88	(1.00)	240	(528)
	20.22 kg/m²	(4.15)	990 kg	(2096)
TPS Bottom Surface	26.85 kg/m²	(5.5#/ft²)	660 kg	(1450)
Outboard & Inboard Rib Covers	26.85 kg/m²	(5.5#/ft²)	120 kg	(258)
Weight/Elevon Seg. =			1770 kg	(3904)
Weight Per Airplane = 4 (1770) =			7080 kg	(15616)

Figure 85: Elevon — Weight Summary

Elevon Area = 98.5 m^2 (1060 ft^2)
No. of Segments = 4
T. P. S. Wt. = 26.9 kg/m^2 (5.5 #/ft^2)
Max. Surface Temp. = 1760 K (2700°F)
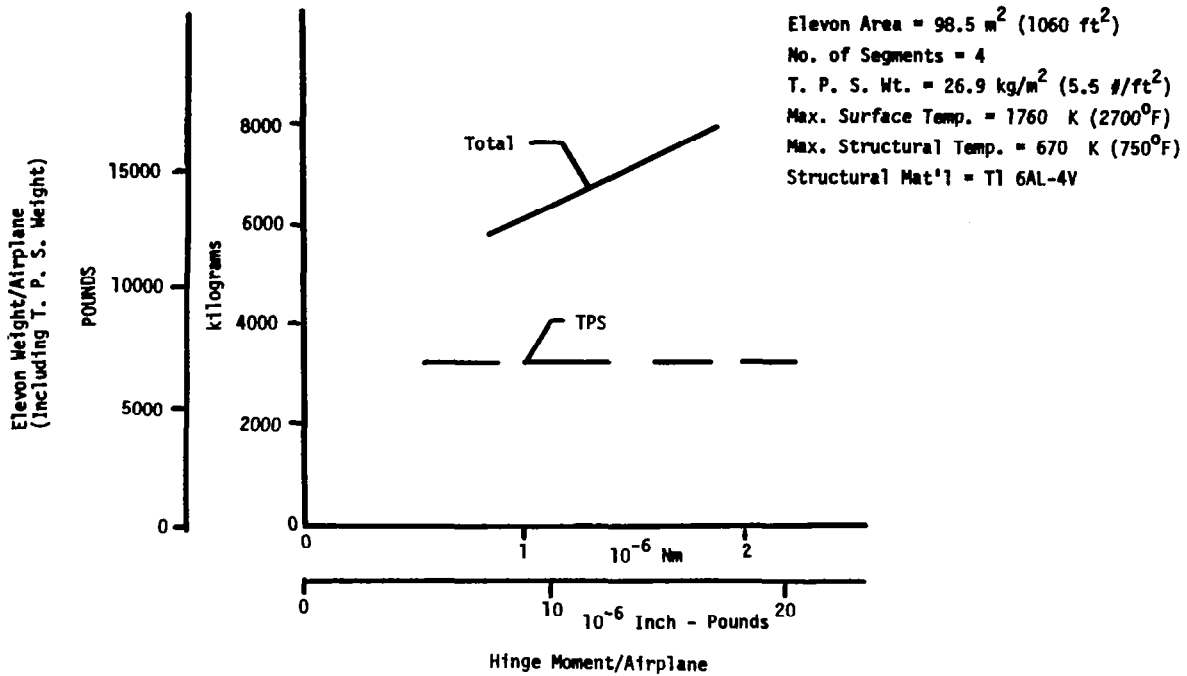Max. Structural Temp. = 670 K (750°F)
Structural Mat'l = Ti 6AL-4V

Figure 86: Elevon Weight

Critical Loads - V_D, 6095 to 9144 m Alt., 10° Yaw, 15° Rudder

Displ. (Ref. X-20 Tip Fin Pressures)

- Fin Surface Pressure   6224 N/m^2 (130 psf) Limit
- Rudder Surface Pressure   22647 N/m^2 (473 psf) Limit
- Vent Pressure   63.7 N/m^2 (1.33 psf) Limit

NOTE: Rolling Maneuvers May Result In Slightly Higher Loads
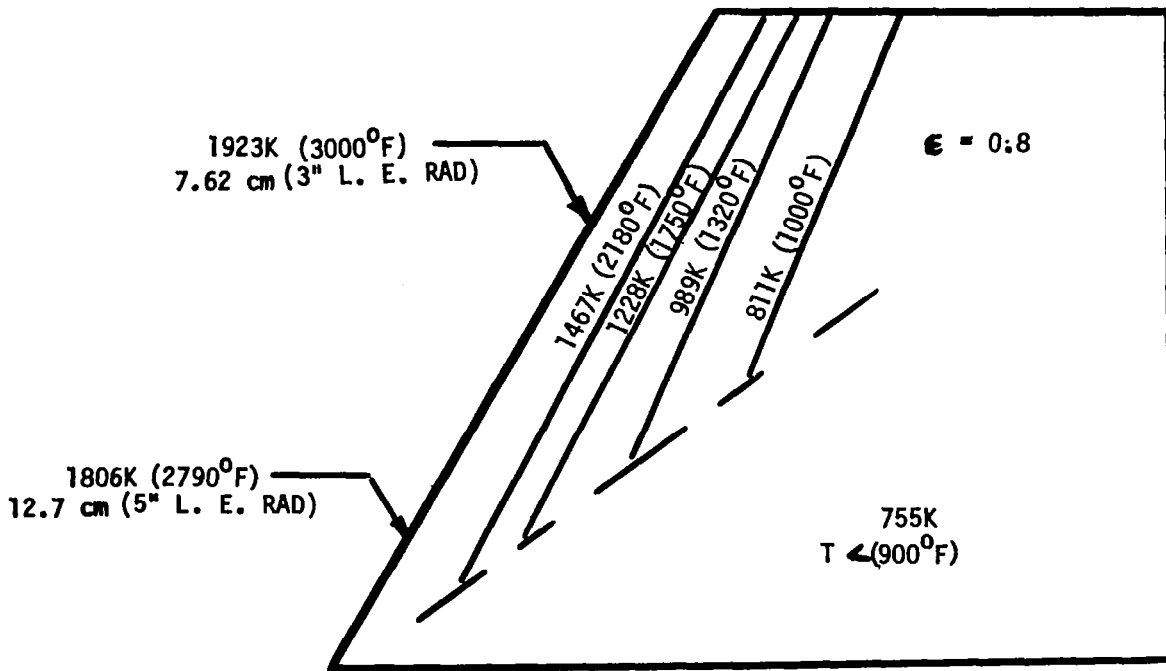
Figure 87: Design Loads

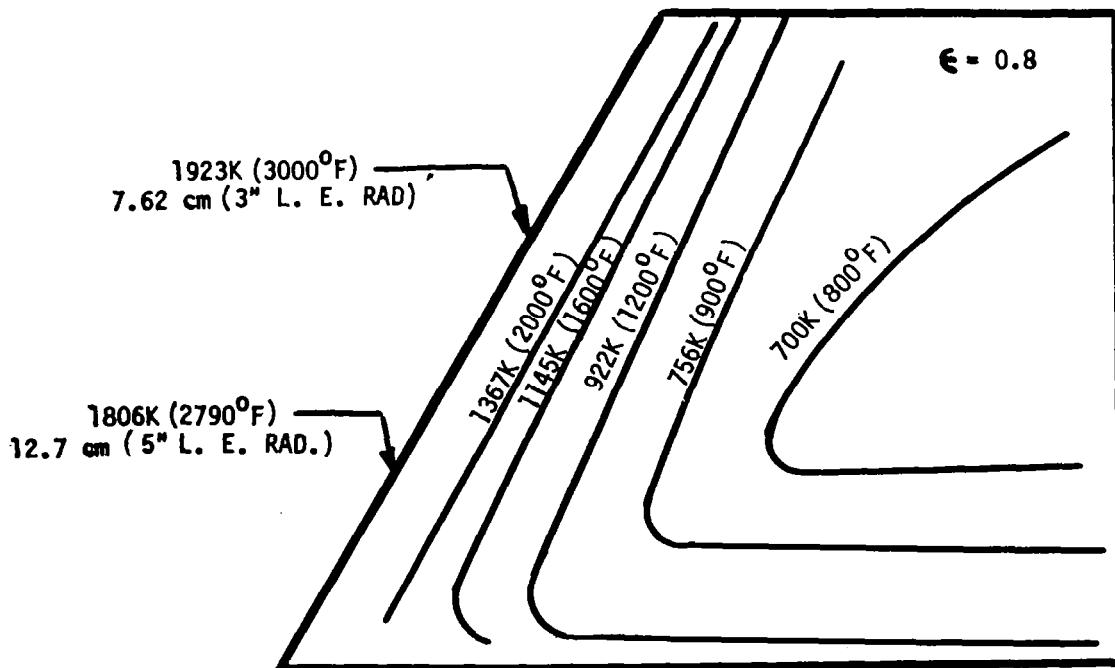*Figure 88: Isotherms — Fin Inboard — Wing Tip Installation*

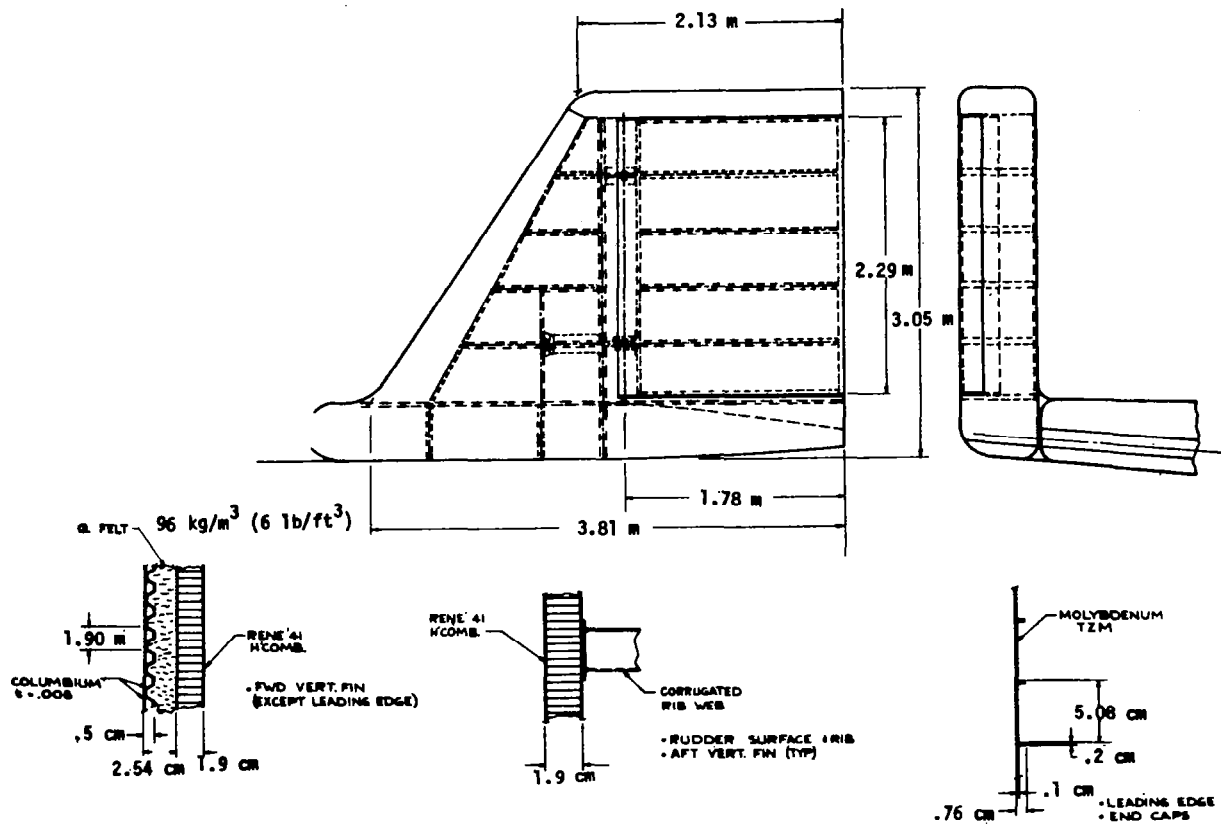*Figure 89: Isotherms — Fin Outboard — Wing Tip Installation*

93

Figure 90: Structural Concept — Wing Tip Fin

All Dimension Meters
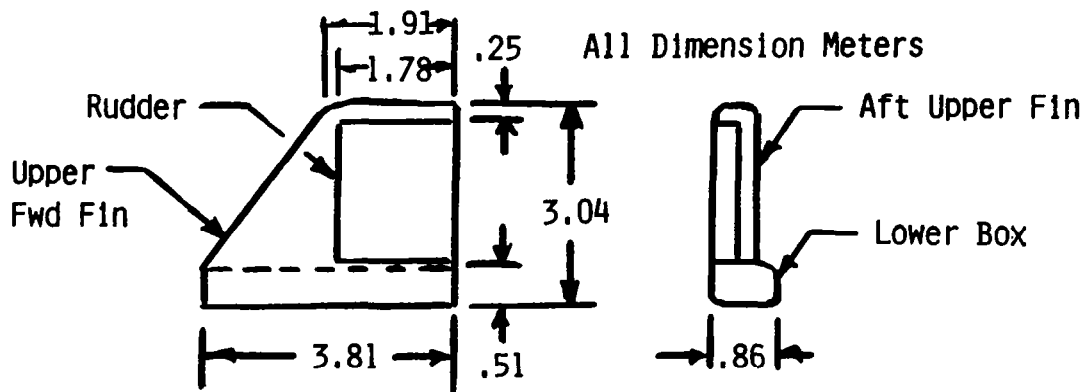
	MASS
Fin Tie To Wing	81.6
Rudder	127.9
Aft Upper Fin	124.3
Lower Box (Incl. L. E.)	339.3
Upper Forward Fin	235.0

908.1 kg (2002 lb) PER SIDE

Figure 91: Mass Summary — CCV Tip Fin

ITEM	WEIGHT SIZED FOR C. G. @ 72.5% B. L.		C. G. BODY STATION	$I_{0_{COMP.}}$ $kg\ m^2 \cdot 10^{-6}$	CENTER OF GRAVITY B. S./L_B
	kg	lb.	m		m/%
Wing and Elevon	13250	(29,217)	18.2	.21	
Tail	1815	(4,004)	18.9	-	
Body ▷	66270	(146,100)	14.6	15.42	▷ Body & Body Flap
Induced Env. Prot. ▷	14330	(31,600)	15.0	4.3	▷ Body, Wing, Body Flap & Elevon
Landing Docking	4540	(10,000)	15.5		
Propulsion	34600	(76,305)	19.4	-	
Prime Power	1470	(3,241)	15.1	-	
Electrical	1260	(2,770)	13.5	-	
Hydraulic	10700	(23,538)	17.7	-	
Control Surface	1540	(3,392)	19.7	-	
Avionics	1310	(2,880)	9.4	-	
Environment Control	1500	(3,300)	9.4	-	
Personnel Provisions	360	(797)	9.4	-	
Growth	11830	(26,085)	15.3	1.94	
Dry Weight	164800	(363,230)	16.2	21.87	16.1/79.2
Personnel	260	(580)	9.4		
Cargo	10100	(22,270)	13.5		
ACPS	40	(90)	9.3		
Residuals	11400	(25,100)	15.9		
Landing Wt.	186500	(411,260)	-		15.9/77.9
ACPS Prop.	2720	(6,050)	9.3		
Entry Wt.	197100	(434,470)			15.8/77.5
Reserve Fluids	11430	(25,146)			
Inflight Losses	700	(1,530)	15.1		
Ascent Propellent	1270050	(2,800,000)	16.2	122.83	16.2/79.4
GLOW	1471200	(3,243,500)			

Figure 92: Weight Statement — Control Configured Design with Wing Tip Fins

M = 0.3   ALTITUDE = SEA LEVEL   C. G./L = 0.715

NASA W. T. DATA TEST # = 814   RUNS = 4, 8, 16, 20

DATA: C_N, C_A, C_m, C_{Y_β}, C_{n_β}, C_{l_β}

Control Power: (Per Deg)

	(SIDE)	(YAW)	(ROLL)
RUDDER:	$C_{Y_{\delta_R}}$ = .0029	$C_{n_{\delta_R}}$ = -.00135	$C_{l_{\delta_R}}$ = .0007
AILERON:	$C_{Y_{\delta_A}}$ = -.0025	$C_{n_{\delta_A}}$ = .00001	$C_{l_{\delta_A}}$ = .0030

Rotary Derivative: (Per Radian)

$$C_{m_q} = -2.0 \quad C_{n_p} = .08 \quad C_{l_p} = -.30$$

$$C_{n_r} = -.30 \quad C_{l_r} = .15$$

Hinge Moment: (Per Deg)

ELEVON: $C_{h_{\delta_e}}$ = -.0068 $C_{h_{\delta_\alpha}}$ = -.0076

RUDDER: $C_{h_{\delta_R}}$ = -.010 $C_{h_{\delta_\beta}}$ = .005

BODY FLAP: $\delta_{B.F.}$ = 0 (DEG) $C_{h_{\delta_\alpha}}$ = -.003

Figure 93: Baseline Configuration Aerodynamic Data

DESIGN POINT # = 2

M = 0.6   ALTITUDE = 9500 m   C. G./L = 0.715

ALPHA = 10 (Deg)   ROLL = 0 (Deg)

NASA W. T. DATA TEST # - 814   RUNS = 3, 7, 15, 19

DATA: C_N, C_A, C_m, C_{Y_β}, C_{n_β}, C_{l_β}

Control Power: (Per Deg)

(SIDE)   (YAW)   (ROLL)

RUDDER: $C_{Y_{\delta_R}}$ = .0030 $C_{n_{\delta_R}}$ = -.0015 $C_{l_{\delta_R}}$ = .0008

AILERON: $C_{Y_{\delta_A}}$ = -.0001 $C_{n_{\delta_A}}$ = -.00002 $C_{l_{\delta_A}}$ = .0026

Rotary Derivative: (Per Radian)

C_{m_q} = -3.4 C_{n_p} = .07 C_{l_p} = -.25

C_{n_r} = -.50 C_{l_r} = .20

Hinge Moment: (Per Deg)

ELEVON: $C_{h_{\delta_e}}$ = -.0080 $C_{h_{\delta_\alpha}}$ = -.0080

RUDDER: $C_{h_{\delta_R}}$ = -.012 $C_{h_{\delta_\beta}}$ = .0070

BODY FLAP: $\delta_{B. F.}$ = 0 (Deg) $C_{h_{\delta_\alpha}}$ = -.005

Figure 94: Baseline Configuration Aerodynamic Data

M = 1.2   ALTITUDE = 15800 m   C. G./L = 0.715

ALPHA = 7 (Deg)   ROLL = 0 (Deg)

NASA W. T. DATA TEST # = 814   RUNS = 1, 5, 13, 17 (Note: Adjusted for
                                                                                    B. F. -14 Deg)

DATA: C_N, C_A, C_m, C_{Y_β}, C_{n_β}, C_{l_β}

Control Power (Per Deg)

	(SIDE)	(YAW)	(ROLL)
RUDDER:	$C_{Y_{\delta_R}}$ = .0017	$C_{n_{\delta_R}}$ = -.0009	$C_{l_{\delta_R}}$ = .0005
AILERON:	$C_{Y_{\delta_A}}$ = .0005	$C_{n_{\delta_A}}$ = .0010	$C_{l_{\delta_A}}$ = .0030

Rotary Derivative: (Per Radian)

C_{m_q} = -1.5 C_{n_p} = .10 C_{l_p} = -.30

C_{n_r} = -.30 C_{l_r} = .16

Hinge Moment: (Per Deg)

ELEVON: $C_{h_{\delta_e}}$ = -.017 $C_{h_{\delta_\alpha}}$ = -.010

RUDDER: $C_{h_{\delta_R}}$ = -.017 $C_{h_{\delta_\beta}}$ = .018

BODY FLAP: $\delta_{B. F.}$ = -14 (Deg) $C_{h_{\delta_\alpha}}$ = -.0012

Figure 95: Baseline Configuration Aerodynamic Data

DESIGN POINT # = 4

M = 3.5   ALTITUDE = 30500 m   C. G./L = 0.715

ALPHA = 12 (Deg)   ROLL = 0 (Deg)

NASA W. T. DATA TEST # = UPWT 1235   RUNS = 15, 20, 23, 47, 52

DATA: C_N, C_A, C_m, C_{Y_β}, C_{n_β}, C_{l_β}

Control Power: (Per Deg)

(SIDE)	(YAW)	(ROLL)

RUDDER: $C_{Y_{\delta_R}}$ = .00015 $C_{n_{\delta_R}}$ = -.00018 $C_{l_{\delta_R}}$ = .00008

AILERON: $C_{Y_{\delta_A}}$ = .0010 $C_{n_{\delta_A}}$ = -.0005 $C_{l_{\delta_A}}$ = .0012

Rotary Derivative: (Per Radian)

C_{m_q} = -1.9 C_{n_p} = .04 C_{l_p} = -.20

C_{n_r} = -.5 C_{l_r} = .05

Hinge Moment: (Per Deg)

ELEVON: $C_{h_{\delta_e}}$ = -.012 $C_{h_{\delta_\alpha}}$ = -.003

RUDDER: $C_{h_{\delta_R}}$ = -.01 $C_{h_{\delta_\beta}}$ = .019

BODY FLAP: $\delta_{B. F.}$ = 0 (Deg) $C_{h_{\delta_\alpha}}$ = -.020

Figure 96:   Baseline Configuration Aerodynamic Data

M = 8   ALTITUDE = 52600 m   C. G./L = 0.715

ALPHA = 36 (Deg)   ROLL = 0 (Deg)

NASA W. T. DATA TEST # = Based upon LRC Helium (M = 20.3) Facility and Computer
Calculated Results ("Hyperez"). See Figure

DATA: C_N, C_A, C_m, C_{Y_β}, C_{n_β}, C_{l_β}

Control Power: (Per Deg)

	(SIDE)	(YAW)	(ROLL)
RUDDER:	$C_{Y_{\delta_R}}$ = .00002	$C_{n_{\delta_R}}$ = -.00003	$C_{l_{\delta_R}}$ = 0.0
AILERON:	$C_{Y_{\delta_A}}$ = .0003	$C_{n_{\delta_A}}$ = -.0005	$C_{l_{\delta_A}}$ = .0015

Rotary Derivative: (Per Radian)

C_{m_q} = -3 C_{n_p} = -.023 C_{l_r} = -.24

C_{n_r} = -.39 C_{l_r} = -.055

Hinge Moment: (Per Deg)

ELEVON: $C_{h_{\delta_e}}$ = -.015 $C_{h_{\delta_a}}$ = -.015

RUDDER: $C_{h_{\delta_R}}$ = 0.0 $C_{h_{\delta_\beta}}$ = 0.0

BODY FLAP: $\delta_{B.F.}$ = 16 (Deg) $C_{h_{\delta_a}}$ = -.018

Figure 97: Baseline Configuration Aerodynamic Data
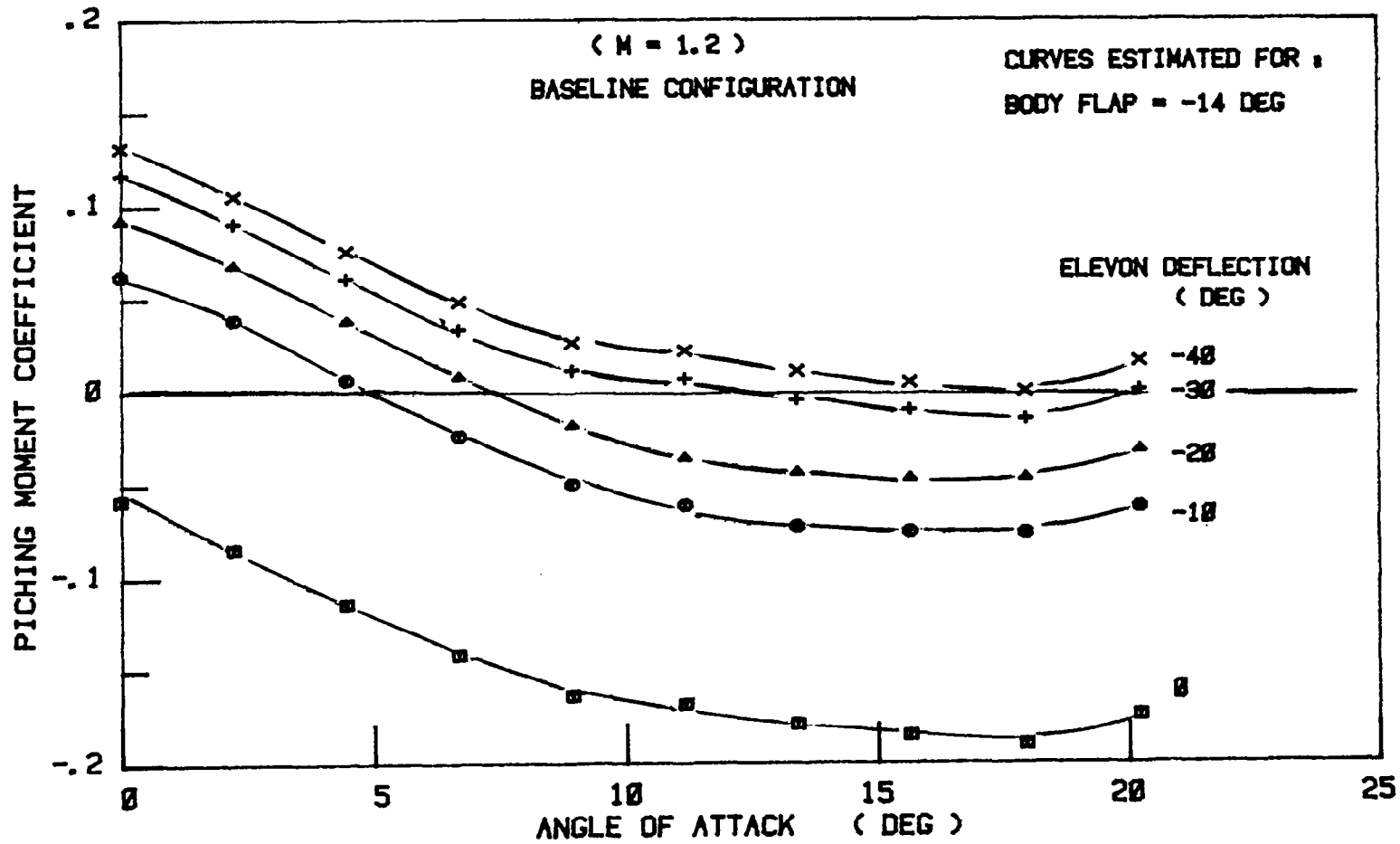
Figure 98: Transonic Pitching Moments

MACH	C_{L_δ}	δ^0	C_{D_0}	dC_D/dC_L^2	C_{m_δ}	C_{m_0}	$C_{m_{\delta_e}}$	$C_{L_{\delta_e}}$	$C_{D_{\delta_\alpha}}$
0→.6	.050	-1.0^0	.055	.26	0	-.07	-.012	.018	.002
.9	.050	-1.0	.060	.28	0	-.07	-.011	.015	.002
1.0	.053	-1.1	.085	.29	-.001	-.08	-.011	.014	.002
1.2	.058	-1.4	.125	.32	-.006	-.10	-.010	.011	.003
1.5	.050	-1.3	.120	.38	-.003	-.10	-.009	.008	.002
2.0	.040	-0.8	.107	.46	+.001	-.11	-.005	.005	.001
4.0	.029	+0.8	.075	.61	.008	-.08	-.002	.001	.001

(PER DEGREE)

MACH	C_{n_β}	C_{l_β}	C_{Y_β}
0→.6	-.0018	-.0008	-.020
.9	-.0019	-.0009	-.020
1.0	-.0018	-.0009	-.020
1.2	-.0010	-.0008	-.021
1.5	-.0025	-.0007	-.020
2.0	-.0035	-.0005	-.019
4.0	-.0040	-.0001	-.018

Note: For Low δ's $(0^0 \rightarrow 5^0)$

Pitch, Lateral/Directional Derivatives based upon W. T. Data

where,

$$C_D = C_{D_0} + \frac{dC_D}{dC_L^2} C_L^2$$

$$C_L = C_{L_\alpha}(\alpha - \alpha_0)$$

$$C_m = C_{m_0} + C_{m_\alpha}\alpha$$

Figure 99 - Linearized Aerodynamic Data for Ascent

C_m = Pitching Moment/$q_1 S\bar{c}$

Rotary Derivatives:

$$C_{m_q} = \frac{2 C_m}{2 (q\bar{c}/2V)} \text{ (Per Radian)}$$

$$C_{n_p} = \frac{2 C_n}{2 (pb/2V}$$

$$C_{n_r} = \frac{2 C_n}{2 (rb/2V)}$$

$$C_{1_p} = \frac{2 C_1}{2 (pb/2V)}$$

Hinge Moment:

$$HM = C_{h_\delta} \delta S_x \bar{C}_x q_1$$

where, S_x = Ref. Area Control Surface

$\bar{C}_x$ = Ref. Length Control Surface

For Elevon:

$$S_x = S_e = 46.6 \text{ m}^2 \quad \text{Per Side}$$

$$\bar{C}_x = \bar{C}_e = 4.3 \text{ m} \quad \text{Per Side}$$

For Rudder & Vert. Tail:

$$S_{VERT} = 83.6 \text{ m}^2$$

$$S_{Rud} = 32.5 \text{ m}^2$$

$$\bar{C}_{Rud} = 3 \text{ m}$$

For Body Flap:

$$S_{B.\,F.} = 72.8 \text{ m}^2$$

$$\bar{C}_{B.\,F.} = 4.57 \text{ m}$$

S = Ref. Wing Area = 557 m^2

$\bar{c}$ = MAC = 17.7 m

$q_1 = \rho/2 V^2$

V = Velocity

b = Ref. Span = 37.1 m

$p, q,$ = Angular Velocities about X, Y, Z Axis

Figure 100 - Ascent Aerodynamic Coefficient Definitions

ROTARY DERIVATIVES (Per Radian)	MACH NUMBER			
	0.3	1.2	3.5	8
C_{m_q}	-2	-1.5	-1.9	-3
C_{n_p}	.08	.10	.04	-.02
C_{n_r}	-.3	-.3	-.5	-.39
C_{l_p}	-.3	-.3	-.2	-.24
C_{l_r}	.15	.16	.05	.06
ALL CONTROL EFFECTIVE (Per Deg)				
$C_{Y_{\delta_R}}$	.0029	.0017	.00015	.00002
$C_{Y_{\delta_A}}$	-.0025	.0005	.0010	.0003
$C_{n_{\delta_R}}$	-.00135	-.0009	-.00018	-.00003
$C_{n_{\delta_A}}$	.00001	.0010	-.0005	-.0005
$C_{l_{\delta_R}}$	.0007	.0005	.00008	0.00
$C_{l_{\delta_A}}$	.0030	.0030	.0012	.0015
HINGE MOMENTS (Per Deg)				
$C_{h_{\delta_e}}$	-.0068	-.017	-.012	-.015
$C_{h_{\alpha_e}}$	-.0076	-.010	-.003	-.015
$C_{h_{\delta_R}}$	-.010	-.017	-.01	0.0
C_{h_β}	.005	.018	.019	0.0
$C_{h_{\alpha_{B.F.}}}$	-.005	-.00	-.02	-.018

Figure 101: Ascent Aerodynamic Coefficients

REFERENCE TIP-FIN CONFIGURATION

DESIGN POINT # = 2

M = 0.6   ALTITUDE = 9500 m   C. G./L = 0.715

ALPHA = 10   ROLL = 0 (Deg)

NASA W. T. DATA TEST # = 835 (8 ft)   RUNS = 3, 7, 11, 38

DATA: C_N, C_A, C_m, C_{Y_β}, C_{n_β}, C_{l_β}

Control Power: (Per Deg)

	(SIDE)	(YAW)	(ROLL)
RUDDER:	$C_{Y_{\delta_R}} = -.00033$	$C_{n_{\delta_R}} = .00025$	$C_{l_{\delta_R}} = -.00025$
AILERON:	$C_{Y_{\delta_A}} = -.0001$	$C_{n_{\delta_A}} = -.00002$	$C_{l_{\delta_A}} = .0026$

Rotary Derivative: (Per Radian)

$C_{m_q} = -3.5$ $C_{n_p} = .07$ $C_{l_p} = -.25$

$C_{n_r} = -.5$ $C_{l_r} = .2$

Hinge Moment: (Per Deg)

ELEVON: $C_{h_{\delta_e}} = -.008$ $C_{h_{\delta_\alpha}} = -.008$

RUDDER: $C_{h_{\delta_R}} = -.012$ $C_{h_{\delta_\beta}} = .0070$

BODY FLAP: $\delta_{B. F.} = 0$ (Deg) $C_{h_{\delta_\alpha}} = -.005$

Figure 102: Tip Fin Configuration Aerodynamic Data

REFERENCE TIP-FIN CONFIGURATION

DESIGN POINT # = 3

M = 1.2   ALTITUDE = 15800 m   C. G./L = 0.715

ALPHA = 7   ROLL = 0 (Deg)

NASA W. T. DATA TEST # = 835 (8 FT)   RUNS = 1, 5, 9, 36, 40

DATA: C_N, C_A, C_m, C_{Y_β}, C_{n_β}, C_{l_β} (Adjusted for B. F. Angle)

Control Power: (Per Deg)

	(SIDE)	(YAW)	(ROLL)
RUDDER:	$C_{Y_{\delta_R}}$ = -.00039	$C_{n_{\delta_R}}$ = .00025	$C_{l_{\delta_R}}$ = -.000025
AILERON:	$C_{Y_{\delta_A}}$ = .0005	$C_{n_{\delta_A}}$ = .0010	$C_{l_{\delta_A}}$ = .0030

Rotary Derivative: (Per Radian)

C_{m_q} = -1.5 C_{n_p} = .10 C_{l_p} = -.30

C_{n_r} = -.30 C_{l_r} = .16

Hinge Moment: (Per Deg)

ELEVON: $C_{h_{\delta_e}}$ = -.017 $C_{h_{\delta_\alpha}}$ = -.010

RUDDER: $C_{h_{\delta_R}}$ = -.017 $C_{h_{\delta_\beta}}$ = .018

BODY FLAP $\delta_{B.\,F.}$ = -14   (Deg) $C_{h_{\delta_\alpha}}$ =

Figure 103 - Tip-Fin Configuration Aerodynamic Data

REFERENCE TIP-FIN CONFIGURATION

DESIGN POINT # = 4

M = 3.5   ALTITUDE = 30500 m   C. G./L = 0.715

ALPHA = 12   ROLL = 0   (DEG)

NASA W. T. DATA TEST # = 1255 (UPWT)   RUNS = 5, 13, 21, 29

DATA: C_N, C_A, C_m, C_{Y_β}, C_{n_β}, C_{l_β}

Control Power: (Per Deg)

	(SIDE)	(YAW)	(ROLL)
RUDDER:	$C_{Y_{\delta_R}}$ = .00028	$C_{n_{\delta_R}}$ = .0002	$C_{l_{\delta_R}}$ = .00020
AILERON:	$C_{Y_{\delta_A}}$ = .0010	$C_{n_{\delta_A}}$ = -.0005	$C_{l_{\delta_A}}$ = .0012

Rotary Derivative: (Per Radian)

C_{m_q} = -1.9 C_{n_p} = .04 C_{l_p} = -.2

C_{n_r} = -.05 C_{l_r} = .05

Hinge Moment: (Per Deg)

ELEVON: $C_{h_{\delta_e}}$ = -.012 $C_{h_{\delta_\alpha}}$ = -.007

RUDDER: $C_{h_{\delta_R}}$ = -01 $C_{h_{\delta_\beta}}$ = .019

BODY FLAP: $\delta_{B.F.}$ = 0 (Deg) $C_{h_{\delta_\alpha}}$ = -.02

Figure 104: Tip-Fin Configuration Aerodynamic Data

PITCH AUTOPILOT

$$K_E = 0.3 \quad K_I = 1 \quad K_q = 4$$
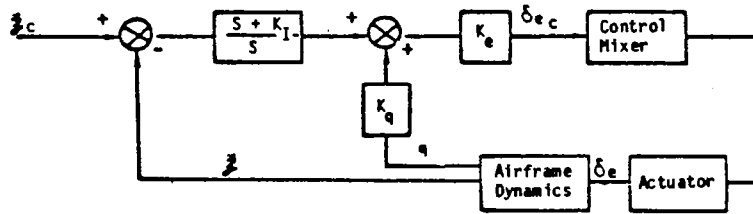
YAW - ROLL AUTOPILOT

$$K_A = 2 \quad K_{P_a} = -1$$

$$K_{r_r} = 1 \quad K_{Y_r} = -2$$

$$K_R = 16$$
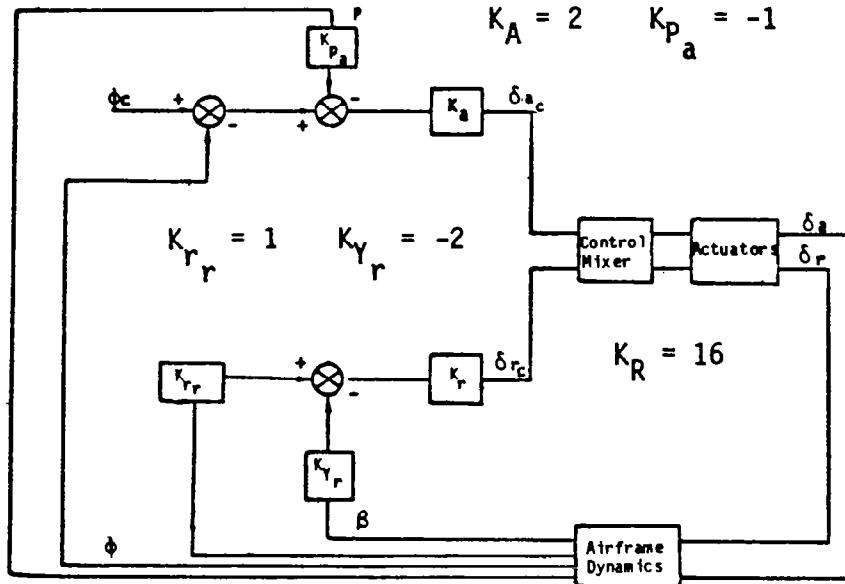
Figure 105:   Subsonic Mach = 0.3

108
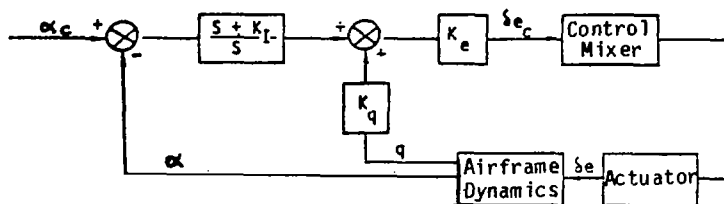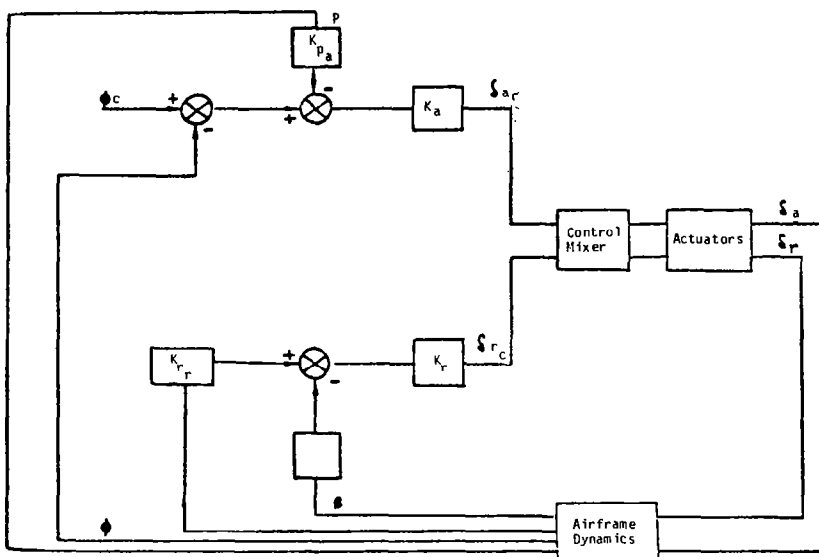
Figure 106: Pitch & Yaw-Roll Autopilots — Mach 1.2 D.P. 3
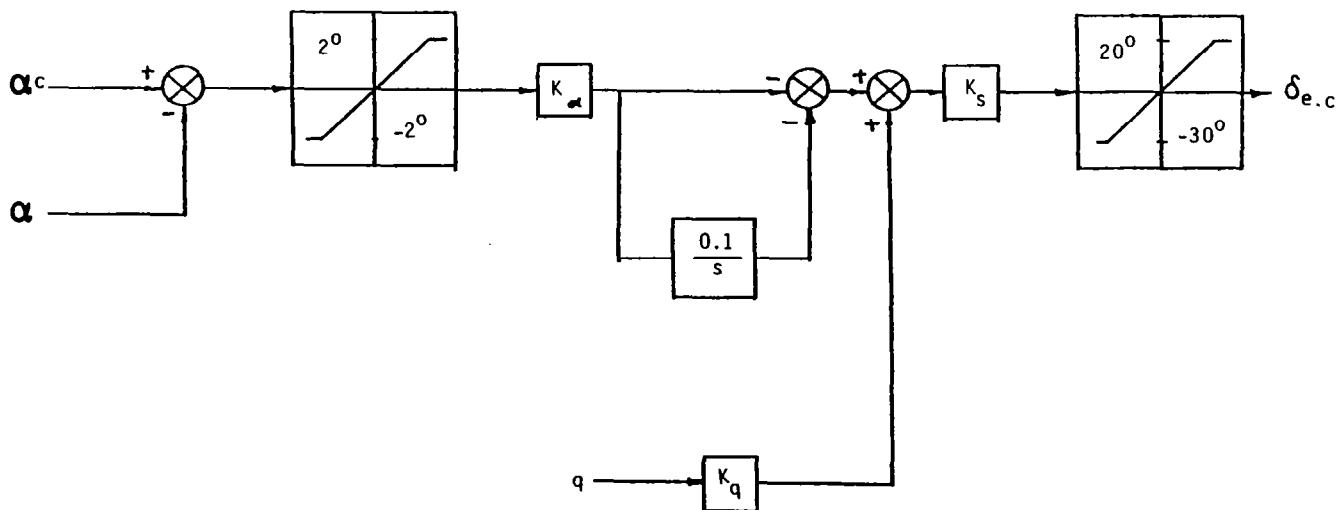
Figure 107: Pitch Autopilot Command Block Diagram — Mach 3,5 & 8 D.P. 4 & 5

ROLL AUTOPILOT
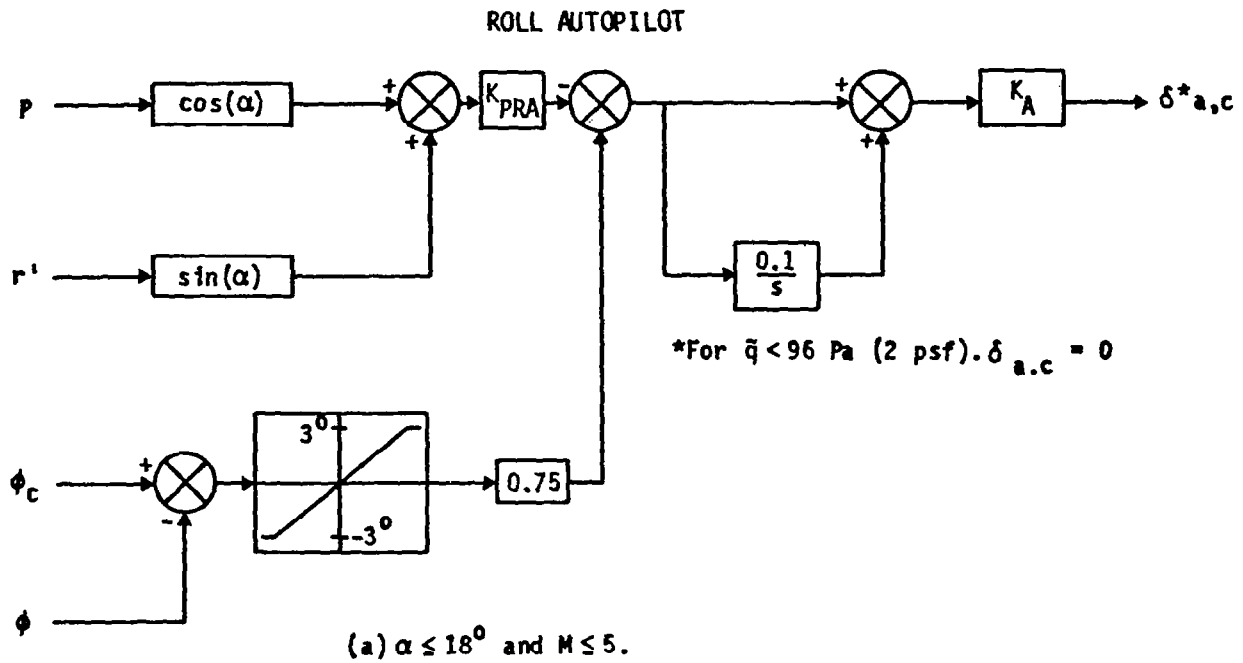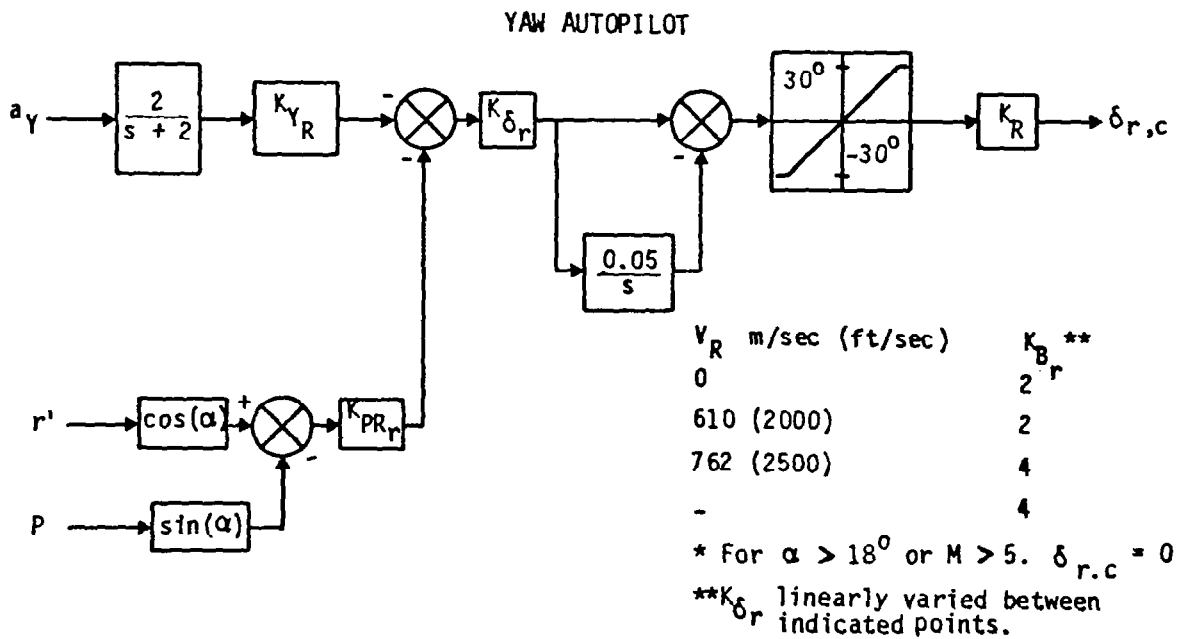

*For q̄ < 96 Pa (2 psf). δ_{a,c} = 0

(a) α ≤ 18° and M ≤ 5.

Figure 108: Roll Autopilot

YAW AUTOPILOT

V_R m/sec (ft/sec)	K_{δ_r} **
0	2
610 (2000)	2
762 (2500)	4
–	4

* For α > 18° or M > 5. δ_{r,c} = 0
**K_{δ_r} linearly varied between indicated points.

Figure 109: Yaw Autopilot D.P. 4 Mach = 3.5

110
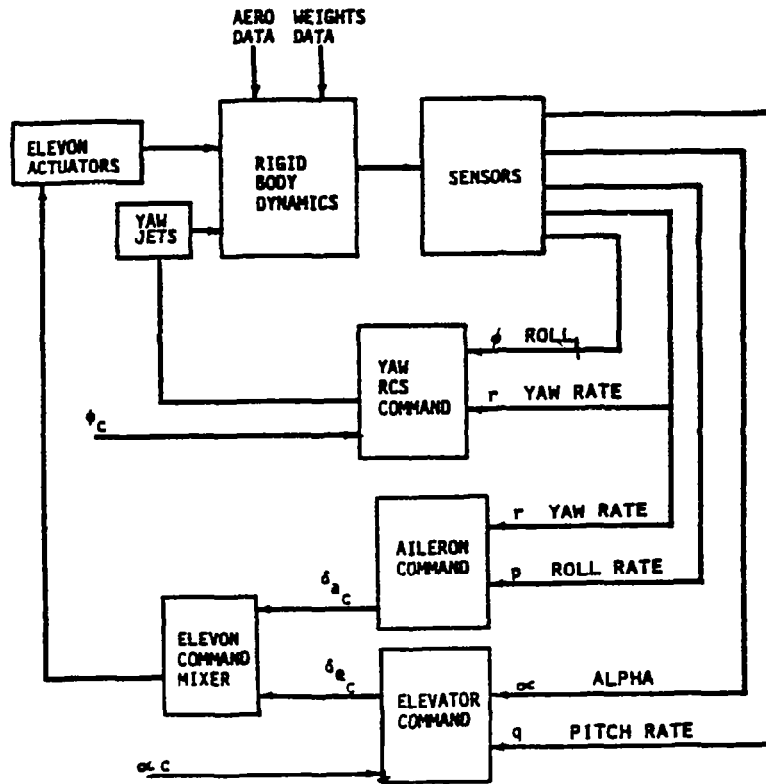
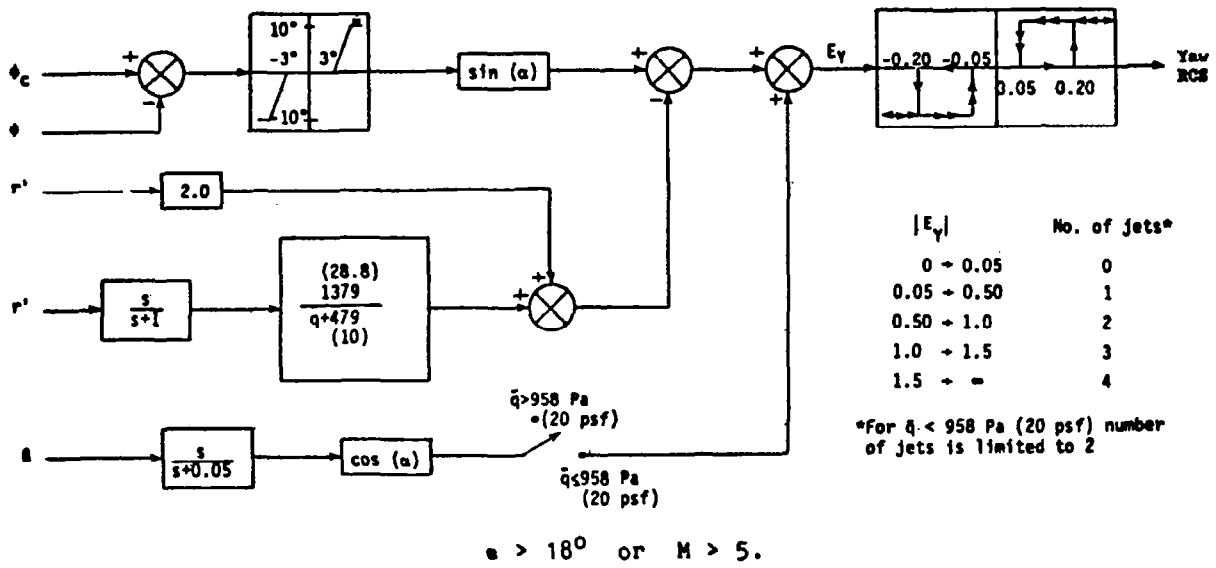Figure 110: Mach = 8 Hypersonic Simulation Configuration
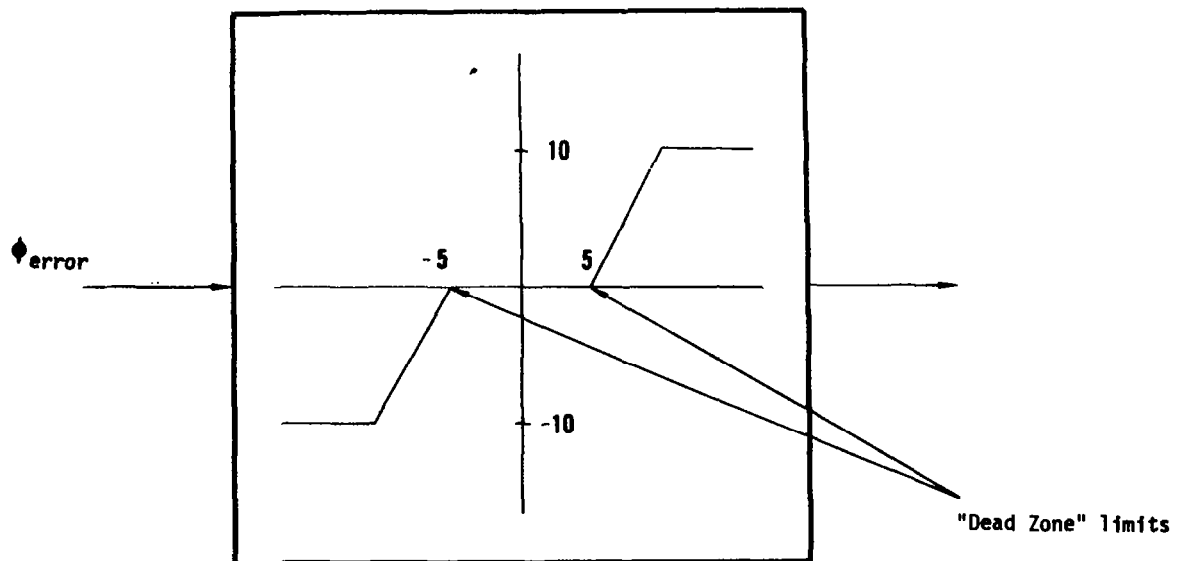
Figure 111: "Dead Zone"

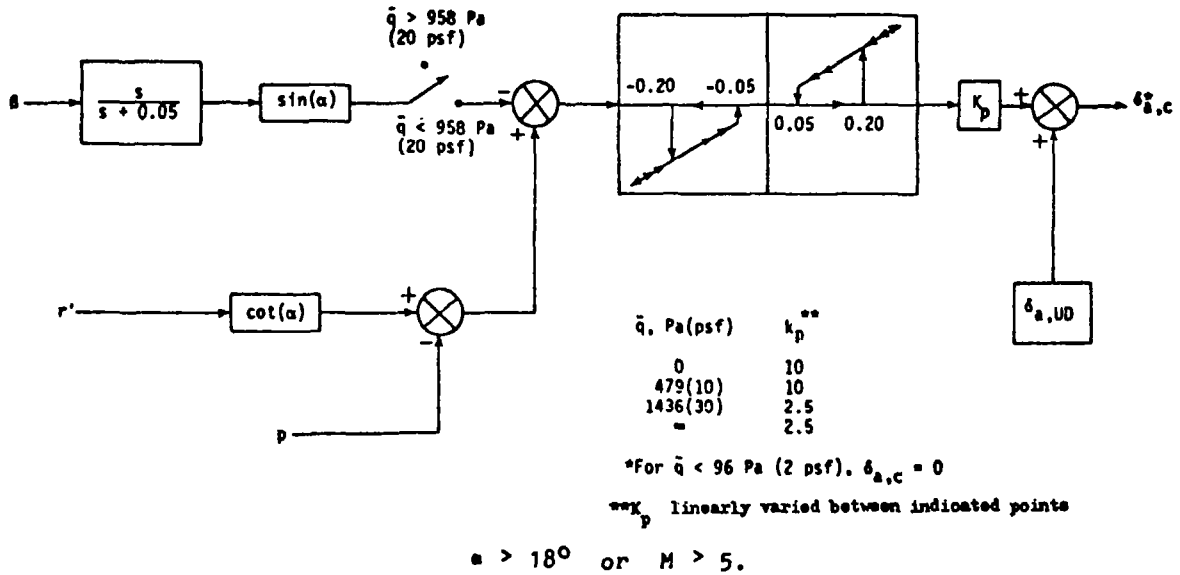Figure 112: Hypersonic Configuration CCV 1
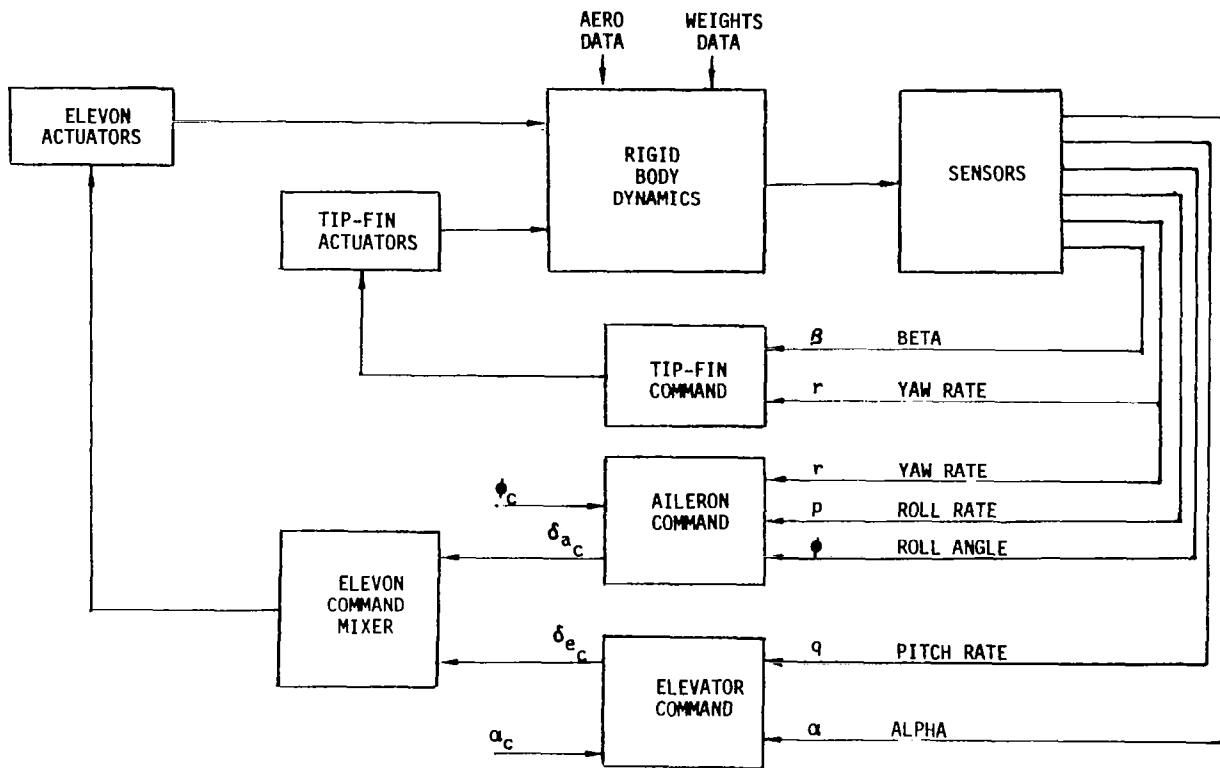

Figure 113: RCS & Aileron Command Blocks

Figure 114: Tip-Fin Simulation

Figure 115: Tip-Fin Command Block Diagram

RIGHT FIN COMMAND BLOCK

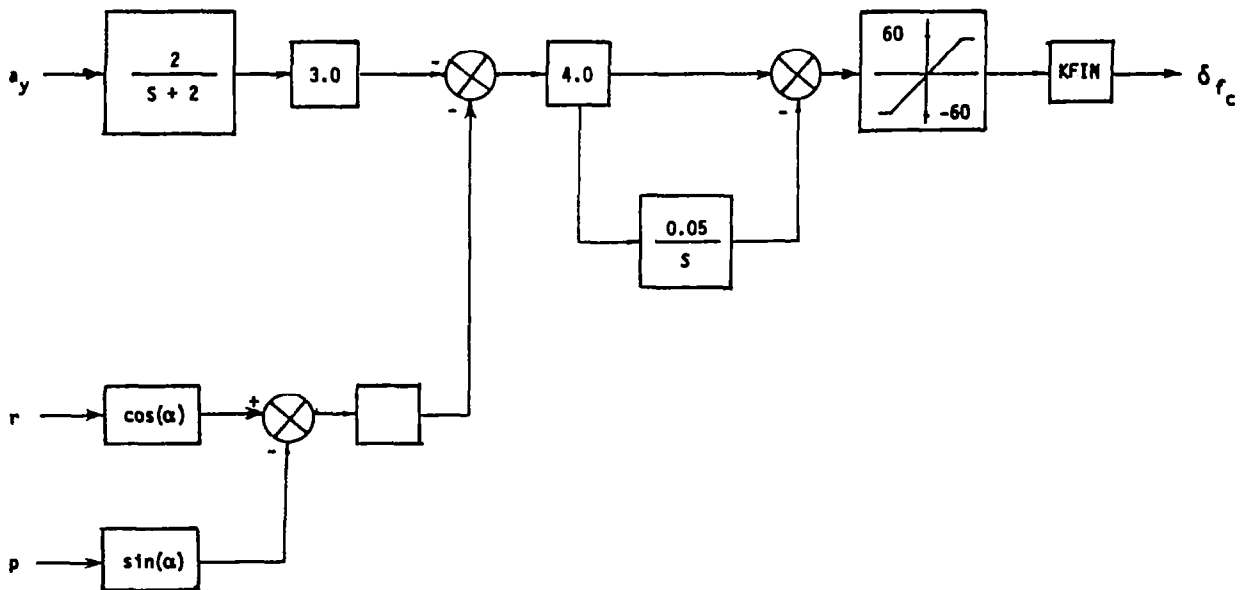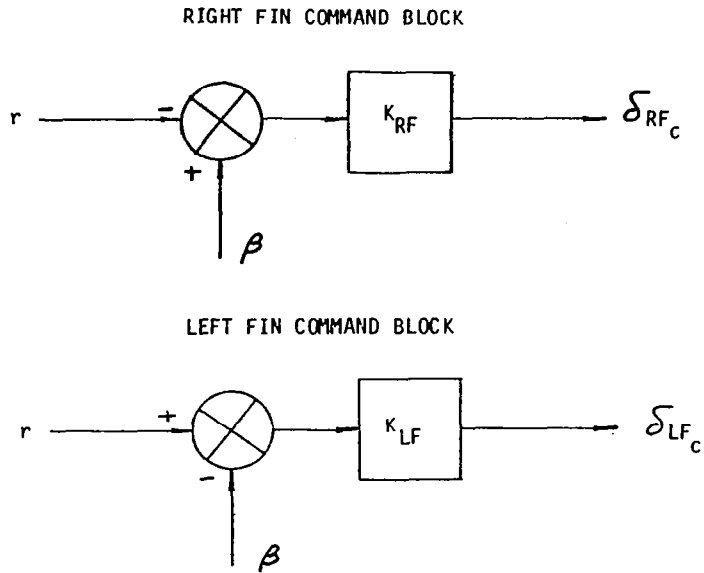LEFT FIN COMMAND BLOCK

Figure 116:   Tip Fin Command
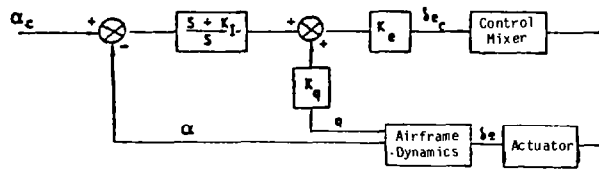
Figure 117: Pitch Autopilot

ROLL AUTOPILOT

d - lateral distance from
       runway centerline

V_d - lateral velocity

ψ - yaw angle

ϕ - roll angle
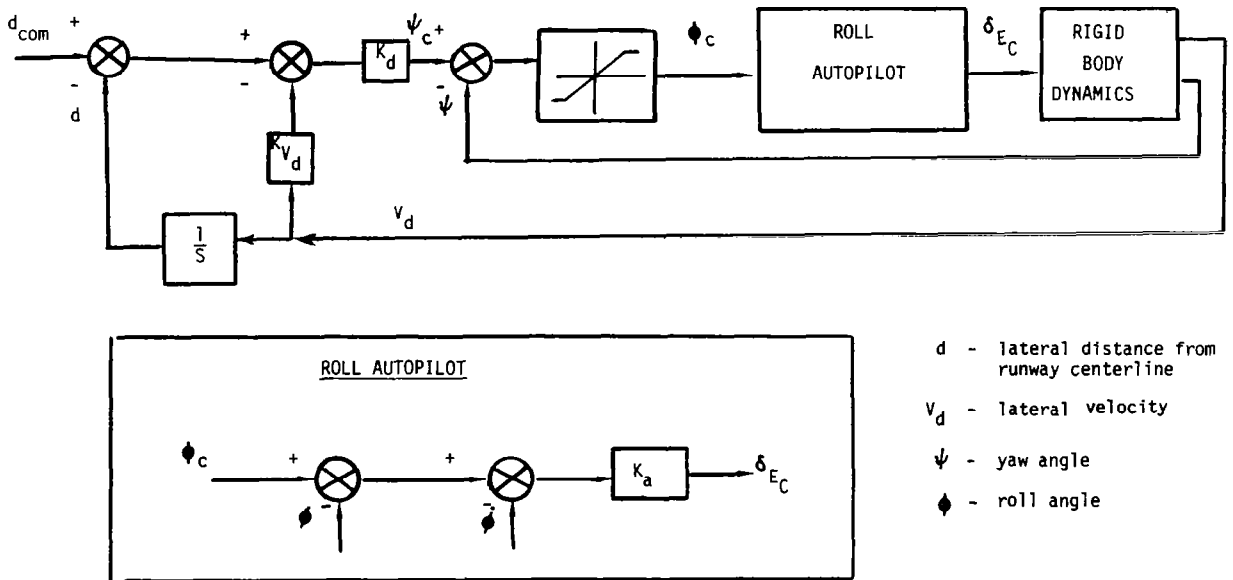
Figure 118:   Block Diagram for a Lateral Glide Slope Hold System

114

d — LATERAL DISPLACEMENT
ψ — VEHICLE HEADING
ψ REF — REFERENCE HEADING

LATERAL
BEAM

HOLD TO GROUND TRACK MODE
IS SIMILAR TO LATERAL BEAM
INTERCEPT AND HOLD MODE WITH

$\lambda \approx d$

AT APPROACH INITIATION
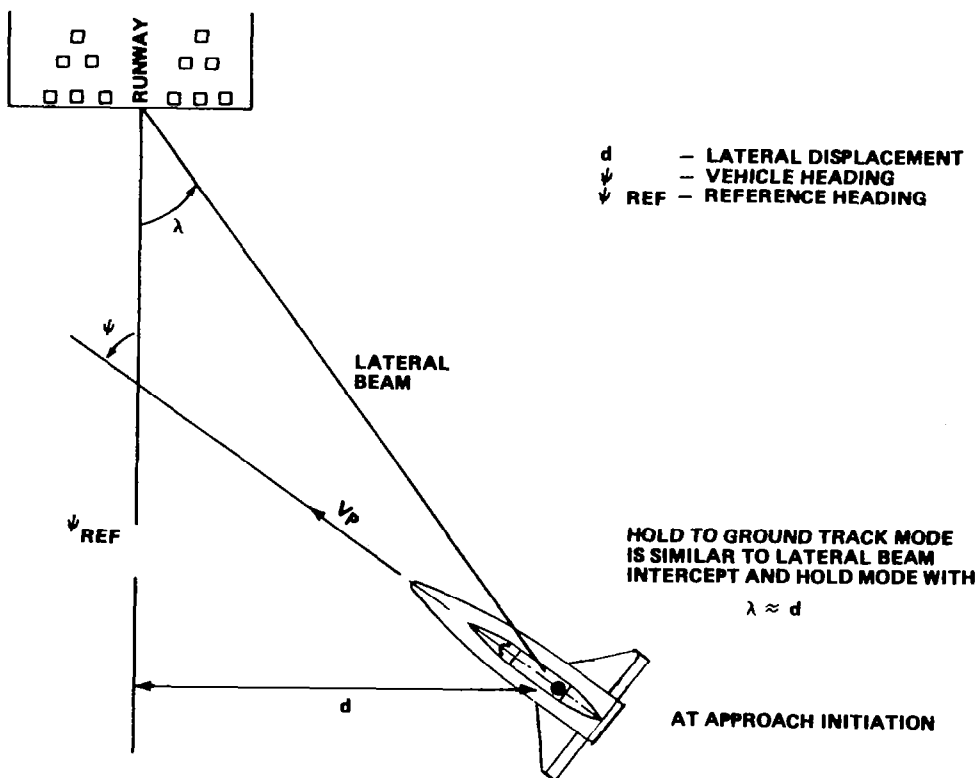
Figure 119: Geometry for Hold to Ground Track Mode

(JUST PRIOR TOUCHDOWN)

CROSSWIND

CRAB

GROUND TRACK

β
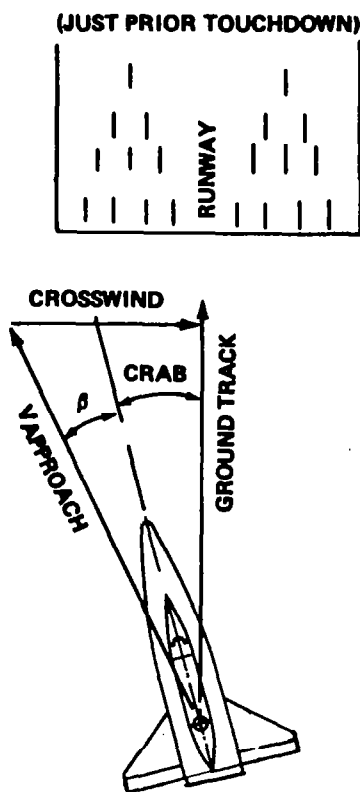
V APPROACH

Figure 120: Crab Angle Definition Final Approach

115

1: DECRAB 2: DEROLL 3: COMBINED 4: PREDICTIVE

T.D.

CRAB

CRAB = 0°

ANY CRAB

ROLL = 0°   ROLL   SOME ROLL   ROLL
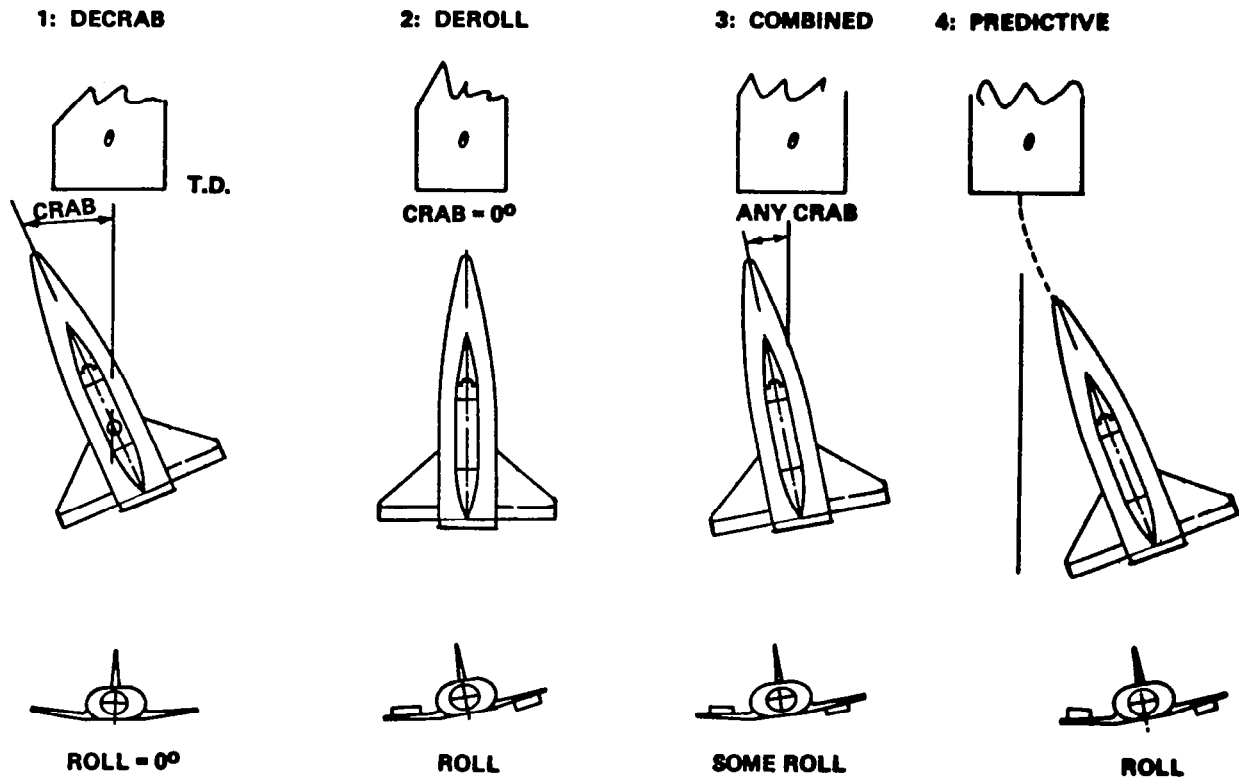
Figure 121: Runway Alignment Maneuver Options

CRAB
ANGLE

-4

+4

$+ \text{CRAB}_{\text{COM}}$

r

$+$

β

K_R

δ_{R_C}

r - Yaw Rate

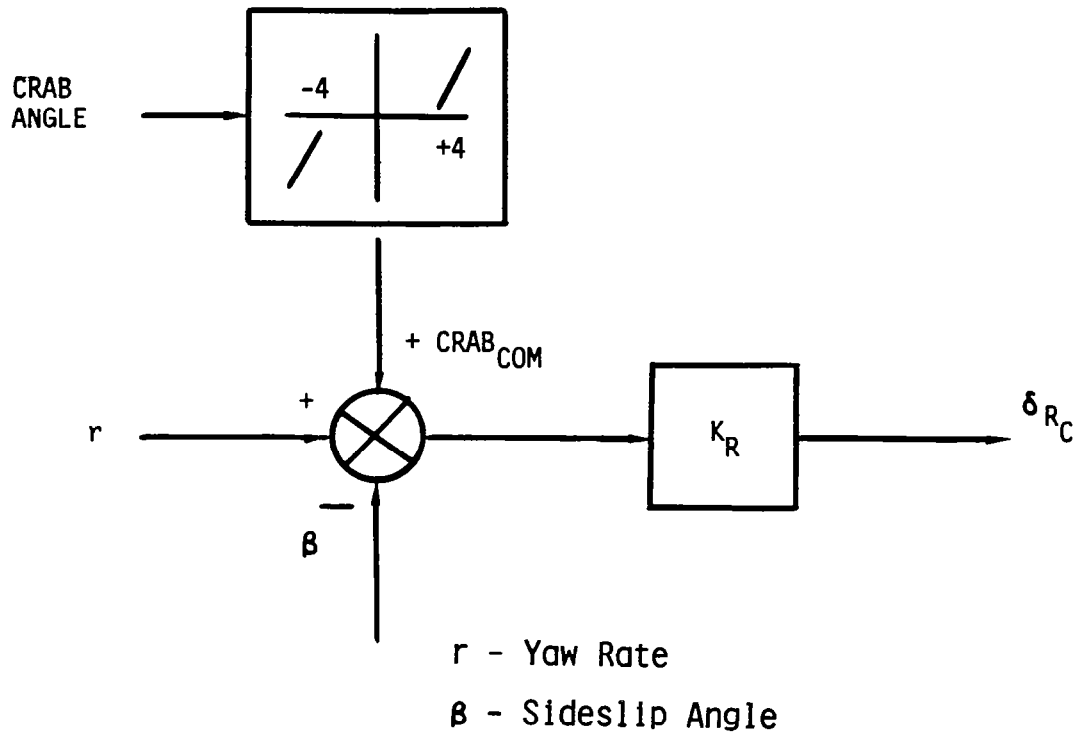β - Sideslip Angle

Figure 122: Yaw Autopilot with Crab Angle Command

116

1. Report No. NASA CR-3491	2. Government Accession No.	3. Recipient's Catalog No.
4. Title and Subtitle A STUDY OF FLIGHT CONTROL REQUIREMENTS FOR ADVANCED, WINGED, EARTH-TO-ORBIT VEHICLES WITH FAR-AFT CENTER-OF-GRAVITY LOCATIONS		5. Report Date February 1982
		6. Performing Organization Code
7. Author(s) Andrew K. Hepler, Howard Zeck, William H. Walker, and Alexander Polack		8. Performing Organization Report No.
		10. Work Unit No.
9. Performing Organization Name and Address Boeing Aerospace Company Kent, Washington 98031		
		11. Contract or Grant No. NAS1-16128
		13. Type of Report and Period Covered Contractor Report
12. Sponsoring Agency Name and Address National Aeronautics and Space Administration Washington, D. C. 20546		
		14. Sponsoring Agency Code

15. Supplementary Notes

Langley Technical Monitor: Delma C. Freeman, Jr.
Final Report

16. Abstract

This study is a follow-on to a previous Control Configured Design Approach (CCV) NASA study. The present study focuses on control requirements of CCV vehicles with far-aft center of gravity locations. The baseline system chosen to investigate is a fully reusable vertical take-off/horizontal landing single stage-to-orbit vehicle with mission requirements similar to that of the Space Shuttle vehicle. Evaluations were made to determine dynamic stability boundaries, time responses, trim control, operational center-of-gravity limits, and flight control subsystem design requirements. Study tasks included: a baseline vehicle analysis, an aft center of gravity study, a payload size study, and a technology assessment.

17. Key Words (Suggested by Author(s)) Control Configured Vehicles (CCV) Advanced Space Transportation Systems Vertical Take Off (VTO) Single Stage to Orbit (SSTO)	18. Distribution Statement Unclassified – Unlimited Subject Category 08

19. Security Classif. (of this report) Unclassified	20. Security Classif. (of this page) Unclassified	21. No. of Pages 121	22. Price A06